ITC

Geo-information Procedures for Water Accounting: A Case of The East Rapti River Basin, Nepal

Rajendra L. Shilpakar

February 2003

Geo-information Procedure for Water Accounting: A Case of The East Rapti River Basin, Nepal

by

Rajendra L. Shilpakar

Thesis submitted to the International Institute for Geo-information Science and Earth Observation in partial fulfilment of the requirements for the degree of Master of Science in,

Geo-information Science and Earth Observation,

Watershed Management, Conservation and River Basin Planning specialization.

Degree Assessment Board:

Ir. A.M. van Lieshout (Chairman), WRS Department, ITC
Dr. P. Droogers (External Examiner), Water Resources Consultant FutureWater
Prof. Dr. W.G.M. Bastiaanssen (Supervisor), WRS Department, ITC
Dr. A.S.M. Gieske (Member), WRS Department, ITC

INTERNATIONAL INSTITUTE FOR GEO-INFORMATION SCIENCE AND EARTH OBSERVATION
ENSCHEDE, THE NETHERLANDS

Disclaimer

This document describes work undertaken as part of a programme of study at the International Institute for Geo-information Science and Earth Observation. All views and opinions expressed therein remain the sole responsibility of the author, and do not necessarily represent those of the institute.

Abstract

Water accounting is a procedure, which classifies water balance components into water use categories and helps to generate understanding water depletion among different users in a river basin. Evaporative depletion is a key component in water accounting. The East Rapti river basin in Nepal has been selected as a case to demonstrate how remote sensing can be applied for water accounting. The Surface Energy Balance Algorithm for Land (SEBAL), complemented by a mountain radiation model can assess the evapotranspiration. A combination of supervised classification and band ratio method is applied to prepare a land cover map of the basin. By overlaying SEBAL derived ET with land cover map, monthly evaporative depletions for each land cover type are quantified. The agricultural land evaporates an average of 960 mm y^{-1} whereas a high ETa of 1029 mm y^{-1} is found in the forest. A high statistical relationship ($r^2 = 0.97$) between rainfall surplus and river runoff is found for the East Rapti river basin. A simple approach of rainfall surplus has been applied for estimating river runoff. The water balance on an annual basis is not closed. The water accounting analysis indicated that only 51% of the available water is depleted in the basin, while 49% is leaving the basin. As utilizable outflow takes place throughout the year, the basin is still an "open" basin. This indicates there is a high potential for further development of the water resources in the basin.

Key words: water accounting, remote sensing, SEBAL, evapotranspiration, rainfall surplus, depletion, outflow, East Rapti river basin

Acknowledgements

First of all, I wish to record my deepest and foremost gratefulness to my first supervisor Prof. Dr. Wim G. M. Bastiaanssen for his untiring and excellent guidance, supervision, invaluable suggestions, and critical reviews of my thesis.

My grateful thanks are due to my second supervisor Dr. Ambro Gieske for his constant support, regular supervision and invaluable suggestions.

It is my pleasure to thank the Government of the Netherlands and ITC in particular for offering me NFP fellowship to pursue my studies at ITC.

Part of this study is funded by IWMI through its project "Water Management for Agriculture and Environment – Park & People", I am pleased to extend my sincere thanks and gratitude to the team members of this project, in particular Dr. David Molden, Mr. Ian Makin and Dr. Dhruba Pant for their support and kind cooperation.

I express my special thanks and gratitude to my colleague Mr. Sudarshan Pandey of IWMI Nepal for his invaluable help.

Mr. Vijay S. Mishra of DOI, HMG/Nepal deserves my special thanks for his enormous support during field work. My gratitude goes to Dr. Divas B. Basnyat, TAHAL consulting engineers in Nepal, for his kind cooperation.

Many thanks goes to Mr. Khem B. Pathak and Mr. Ashok Shrestha of Narayani Lift Irrigation Office, Chitwan for their help during field data collection. Special thanks goes to all the staffs of Agriculture Service Centres in the East Chitwan area for assisting me in field data collection. I express my deepest appreciation to all the farmers who provided me the invaluable information. To all of you, I am very grateful.

I am thankful to the entire staff of the ITC with whom I had the privilege of working with during my studies. Special thanks goes to Ir. Arno van Lieshout for his help and kind cooperation during my studies at ITC. I wish to thank Ir. Gabriel Parodi, Ir. Remco Dost for their help during the field work preparation. Mr. Gerrit Polman deserved my special thanks for his technical support during my study at ITC. All my colleagues- who gave me a nice company during the study at ITC are also remembered.

Last but not least, my everlasting gratitude goes to my brothers, sister-in-law, sisters, wife, son, nieces and nephews, relatives and friends who always encourage me and wish my success.

Table of Contents

List of Figures

List of Tables

List of Figures

List of Tables

We need a Blue Revolution in agriculture that focuses on increasing productivity per unit of water – 'more crop per drop'.

- Kofi Annan

Chapter 1. Introduction

1.1. Background

Water is the vital resource for all life. To feed the ever-increasing population, more water is demanding for the irrigation to produce more food in the developing countries. A competition between water use groups has commenced in large parts of the world, and the water demand may exceed the water availability to feed thirsty crops (Seckler *et al.*, 1998). At the other hand, increasing global awareness in environment demanding more water to allocate for environmental uses. The recently established World Dialogue on Water for Food & Environmental Security stated "*achieving water security for the sustainable production of food and rural livelihoods while maintaining or improving the quality and biodiversity of the natural resources and eco-systems is one of the key challenges of the early 21st century*" (IWMI).

The tendency of increasing competition in using water from the river among various users has created conflicts among them. The efforts to improve water management at a particular hydrological domain demands understanding on how much water available, being used and depleted for various uses. The non-consumed component of applied irrigation water is not necessarily a "loss" to the total resource, but may, to a varying degree, be reusable (Allen *et al.*, 1997). Allen *et al.,* (1997) pointed out that a new methodology and new terms are needed to describe clearly the impact of any and all types of water use on actual physical losses of utilizable water from the affected hydrologic system. Water accounting is one of the tools to help generating the understanding among various users in a hydrological domain.

Water accounting is an art and procedure "to classify water balance components into water use categories that reflects the consequences of human intervention in the hydrologic cycle" (Molden, 1997). This classification would enable the analysis of water uses, depletion and productivity in a hydrological domain, which help to generate understanding among different users in the river basin. Molden *et al,.* (2001) applied these tools to four sub-basins in South Asia to identifies the quantities and productivity of various uses of water within a basin. The information were used to identify the water saving potential, and means of improving the productivity of the managed supplies.

In most cases the long term time series data required for analysing water accounting are not available and even available data are not reliable, mainly in the developing countries. Rapidly developing fast computers provides more opportunity to develop global data set and more global data sets are becoming available in the public domain, which provides good opportunity to simplify the water accounting procedure in regional scale. Lacroix *et al.,* (2000) successfully used such data set for hydrological modeling to assess basin water resources and to study alternative water allocations amongst competing demands. Recently the International Water Management Institute (IWMI) published global Water

and Climatic Atlas (IWMI, 2000). The IWMI database is currently the most extensive global climate database in terms of resolution, coverage and number of parameters. Droogers & Allen (2002) concluded that the IWMI dataset is considered to be an excellent source of information to compare different reference evapotranspiration (ETo) estimates, as the range in variation in climatological conditions is large, while the spatial resolution is much higher than other global datasets used in climate change studies.

One of the critical part in the water accounting process is the estimation of evaporation and transpiration (Molden, 1997). Traditionally, evapotranspiration is estimated based on the climatic parameters recorded in the representative station and extrapolated for the larger area or computed as residual term in water balance. New technologies and techniques of remote sensing show promise in improving estimates of evapotranspiration at different spatial scale and for separating process and non-process evaporation. Jackson *et al.* (1977) performed pioneering work on thermal infrared applications for a wheat mono-cropping system. Several new methods have been developed afterwards and a review on evapotranspiration algorithms using remotely sensed data is given by Kustas & Norman (1996). Surface Energy Balance Algorithm for Land (SEBAL) for heterogeneous terrain is one of the newest models in this field (Bastiaanssen *et al.*, 2000).

Nepal is known for its huge water resources potential. The surface water available in the country is estimated to be about 224.7 billion m^3 per annum. The per capita surface water availability is more than 9,580 m^3 per capita per annum which is many folds higher than the so called "water stress index" of 1,700 m^3 per capita per annum (Basnyat, 2001). The magnitude of annual water availability as presented above can be misleading, as there is high spatial and temporal variability in the water availability. The relationship between water availability and land use has to be quantitatively described which is not straightforward due to heterogeneity and complexity of hydrological processes in most of the catchments in the country. This study attempts to demonstrate that the remote sensing technique can be an effective way in providing key information on water availability and water use in agriculture and environmental system in various temporal and spatial scales. The East Rapti river basin is selected as a case study to demonstrate the methods.

A study carried out by IWMI Nepal (IWMI-Nepal, 2000b) in the East Rapti basin indicated that there are competitions among the water use sectors (e.g. agriculture and National park) in dry months. The same analysis also mentioned that the water consumed per unit area of cultivated crop is only 240 mm, which appears to be very low. This low figure may be due to the way in which evapotranspiration (ET) was computed. Crop evapotranspiration was estimated using standard technique Doorenbos & Pruitt (1977). The effective rainfall & potential evapotranspiration were computed for 10 days of the crop-growing season. For, non-irrigated crop, actual ET was taken equal to effective rainfall if the potential evapotranspiration is higher than the effective rainfall. The main drawback of this method is that it does not take into account the evapotranspiration from the soil moisture of root zone depth. This may be the main reason for the very low figure of evapotranspiration from crops. This indicates a new method is needed which can estimate ET accurately for the assessment of present water uses in the basin. This will be the key information for assessing the opportunity for further development of the water resources in the basin. This study attempts to apply remote sensing technique to overcome the problem. It can be regarded as the continuation of the study carried out by IWMI Nepal in 2000.

1.2. Objective

The main objective of this study is to develop a package of techniques that can assess the performance of present water uses in the East Rapti river basin using satellite imagery with minimum ground information. This study focuses on quantification of evaporative depletion by agriculture and environment (natural vegetation).

1.3. Water accounting framework

1.3.1. Water accounting components

Water accounting uses a 'water balance' approach to quantify the amount of water entering to the system and the amount leaving (depletions and outflows) from the system. The amounts leaving from the system are further classified in different water accounting components. The definitions, mathematical relationships of the terms uses for each components of water accounting provided in Molden (1997) and Molden & Sakthivadivel (1999) are listed below:

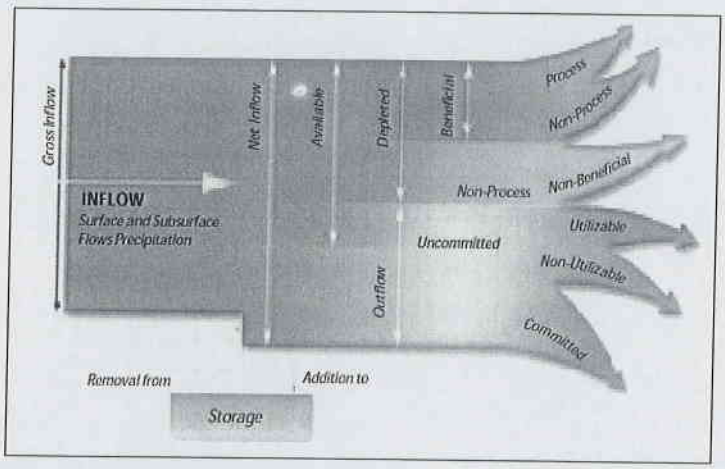

Figure 1.1: Graphical representation of water accounting components (IWMI)

Definitions

Gross inflow (GI) is the total amount of water entering into the water balance domain from precipitation, and surface and subsurface sources.

Net inflow (NI) is the gross inflow plus any changes in storage. If water is removed from the source over the water accounting time period, net inflow exceeded gross inflow; if water is added to storage, net inflow is lower than gross inflow.

Depletion (D) is a use or removal of water from a water basin that renders it unavailable or unsuitable for further use. The quantification of the water depletion is the primary concern of water accounting as interest is focused mostly on productivity and to derive benefits per unit volume of depleted water.

Water is depleted by four generic processes (Keller *et al.*, 1995; Molden, 1997; Seckler, 1996):

- *Evapotranspiration*, where water is vaporized from surfaces or transpired by plants;
- *flows to sink*, when water flows into a sea, saline ground water, or other location where it cannot be economically recovered for further use;
- *pollution,* when water quality is degraded to an extent that it is not suitable for certain uses;
- *incorporation into product* by a process such as incorporation of irrigation water into plant tissues.

The depletion is *beneficial* if water is depleted in providing an input to produce a good such as agricultural output, or any other manner deemed beneficial such as supplying water for environmental uses. The beneficial depletion can further be classified into process and non-process. *Process depletion* is that amount of water which is depleted to produce a human-intended product like diverted water for crop production, water depleted by industries to produce intending goods etc. *Non-process depletion* occurs when water is depleted, but not by the process for which it was intended such as evapotranspiration by forest or natural vegetation. Non-process depletion can be either beneficial, or non-beneficial.

Committed outflow (CO) is that part of outflow from the water balance domain that is committed to other uses, such as downstream environmental requirements or downstream water rights.

Uncommitted outflow (UO) is water that is not depleted, nor committed and is, therefore, available for use within the domain, but flows out of the basin due to lack of storage or sufficient operational measures. Uncommitted outflow can be classified as *utilizable* or *non-utilizable*. Outflow is *utilizable* if by improved management of existing facilities it could be consumptively used. *Non-utilizable* uncommitted outflow exists when the facilities are not sufficient to capture the outflow otherwise utilizable outflow.

Available water (AW) is the net inflow minus both the amount of water set aside for committed uses and the non-utilizable uncommitted outflow. It represents the amount of water available for use at the basin, service, or use levels. Available water includes process and non-process depletion plus utilizable outflows.

A **closed basin** is one where all available water is depleted.
An **open basin** is one where there is still some uncommitted utilizable outflow.
In a **fully committed basin**, there are no uncommitted outflows. All inflowing water is committed to various uses.

Mathematical relationships for water accounting

The basic water balance equation is:

$$Q_{in} + P + S = Q_{out} + ET \quad (1.1)$$

Where:

Q_{in} = surface plus subsurface inflows
Q_{out} = surface plus subsurface outflows
P = precipitation
ET = evapotranspiration
S = change in storage within the domain consisting of changes in groundwater, surface water, or storage changes within the unsaturated zones. A positive sign indicates a removal from storage.

The water accounting terms of gross inflow and net inflow are defined in terms of the water balance as follows:

$$GI = Q_{in} + P \quad (1.2)$$

$$NI = GI + S \quad (1.3)$$

Where: GI = gross inflow
NI = net inflow

The water accounting outflow terms are:

$$NI = Q_{out} + ET = PD + NPD_b + NPD_{nb} + UO + NUO + CO \quad (1.4)$$

Where:

PD = process depletion = $ET_p + S_p$, where ET is evapotranspiration and S is flow to sinks (places where water is not readily recoverable, like flow to oceans, or deep percolation to groundwater that is very difficult to abstract). The subscript p indicates a process use.
NPD_b = non-process, beneficial depletion = $ET_{npb} + S_{npb}$, where the subscript npb indicates non-process but beneficial use.
NPD_{nb} = non-process and non-beneficial or low beneficial depletion, = $ET_{npnb} + S_{npnb}$
UO = utilizable, uncommitted liquid water outflows at the present state of infrastructure development
NUO = non-utilizable, uncommitted liquid outflows
CO = committed outflows.

Rearranging these terms so that all depletion terms are together, we obtain:

$$NI = TD + UO + NUO + CO \quad (1.5)$$

Where: TD = total depletion = PD + NPD

TD can be split between process and non-process, or beneficial and non-beneficial as shown below:

$$NI = D_b + D_{nb} + UO + NUO + CO \quad (1.6)$$

where

$$D_b = ET_p + S_p + ET_{npb} + S_{npb} \quad (1.7)$$

and

$$D_{nb} = ET_{npnb} + S_{npnb} \quad (1.8)$$

Available water (AW) at the present state of development is defined as:

$$AW = NI - C - NUO \quad (1.9)$$

1.3.2. Water accounting indicators

Once water is categorized following indicators can be computed.

Depleted Fraction (DF) is that part of the inflow that is depleted by both process and non-process uses. It reflects how much scope remains for water resources to be developed. It can be expressed in terms of gross inflow, net inflow and available water (e.g. **Table 1.1**).

Beneficial Utilization (BU) relates the amount of water depleted by all beneficial processes to the amount of water available for use. This indicator offers a more accurate view of basin efficiency than traditional indicators, because it takes into consideration water consumed by valuable natural ecosystems as well as the water consumed by human activities.

Table 1.1: Water accounting indicators

Indicator	Symbol	Definition
Depleted Fraction of Gross Inflow	DFGI	TD/GI
Depleted Fraction of Available Water	DFAW	TD/AW
Process Fraction of Available Water	PFAW	PD/AW
Process Fraction of Available Water for Agriculture	$PFAW_{ag}$	ET/AW_{ag}
Process Fraction of Depleted Water	PFTD	PD/TD
Beneficial Utilization of Available Water or Basin Efficiency	BU or BE	D_b /AW

Chapter 2. Study area description

2.1. Location

Nepal lies between 26°22'N and 30°27'N in latitude, and 80°04' E and 88°12'E Longitude. It is a land locked country being bordered by China on the North and by India on the remaining directions. The land is oblong extending about 885 km long in east-west direction and 193 km (at the centre) wide in north south direction. The territorial area is about 147,181 km^2.

Administratively, the county is divided in to 5 development regions and 75 districts. Village development committee (VDC) and Municipalities are the lower administrative units in each district. Currently there are 3,915 VDC's and 58 Municipalities. Ecologically, Nepal is subdivided in three regions, mountain region, hill region and the terai region.

The East Rapti River basin is located within the inner terai of Nepal. The basin extends from Latitude $27^0$21'23''N to $27^0$47'00''N and Longitude $84^0$08'43'' to $85^0$11'57''E. Administratively, the basin is located in two districts namely Chitwan and Makawanpur. About 56% of the basin area comes under Chitwan district and the remaining 44% comes under Makawanpur district. The Royal Chitwan National Park is the one of the major attraction in this basin. The location of the East Rapti river basin is shown in **Figure 2.1**.

2.2. Accessibility

The East Rapti river basin is easily accessible by land and air from the capital of the country and by land from the rest. The Mahendra Rajmarga (so called East West Highway) passes through the basin in east-west direction, and the Tribhuvan Highway (the oldest road which connect terai to capital) passes through north-south in the upper part of the basin. The link road from Bharatpur Municipality to Mugling Bazar of the Prithivi Rajmarga makes more easy access to capital from the basin. Road network in the Chitwan district within the basin is well developed, linking the national highway to all the village development committees except some northern hilly area. Whereas in the Makawanpur district, as being the mountainous landscape, the linking road network to National highway is not well developed. In addition to land transport, there are regular domestic flights that link Bharatpur Municipality (Chitwan District) to Kathmandu.

Figure 2.1: Physiographic division map of Nepal showing location of the East Rapti river basin.

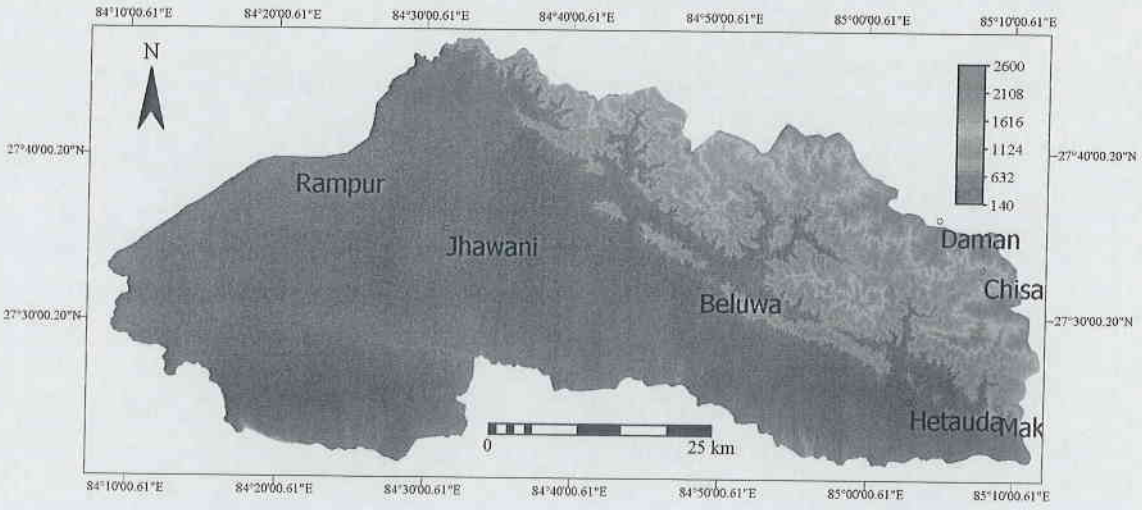

Figure 2.2: Digital Elevation Model (DEM) of East Rapti river basin created by ILWIS[1] from contour elevation data; and the rainfall stations within and around the East Rapti basin.

[1] Integrated Land and Water Information System

2.3. Topography

Nepal is divided in to five regions parallel to each east-west direction by its physiographical condition (**Figure 2.1**), which varies in the north-south direction related with the Himalayan orogenesis. The characteristics of each division are given in **Table 2.1**.

Table 2.1: Characteristics of physiographic division of Nepal (classification of regions)

Physiographic Division	Geographic division	Composition	Elevation [m amsl[2]]
1. High Himalayan Region	Tibetan tethys sediments	Precambrian schist, Phyllite, Quartzite	> 3,000
2. High Mountain Region	Himalayan gneiss	Precambrian gneiss	2,500 – 4,500
3. Mid mountain Region	Meta-sediments	Precambrian palaeozoichist, Limestone, Granite	500-2,500
4. Siwalik Region	Siwaliks	Semi-solid, Shale (Neogene-Quaternary) Sandstone conglomerate	200 – 900
5. Terai Region	Quaternary	Alluvium	200 – 600

Source: (NIPPON_Koei, 1989)

The East Rapti river basin lies in the mid mountain and Siwalik region according to the physiographic division. Northern part of the basin constitute mid mountain region with highest elevation goes upto 2600m. Southern parts constitute by Siwalik hills and the western part is the flat alluvium plane deposited by Narayani river and East Rapti river. The elevation at the confluence of East Rapti with Narayani river is about 140 m. The elevation map of the basin is presented as **Figure 2.2**.

2.4. Climate

The climate of Nepal is affected by the southeast monsoon during the wet season and the northwest monsoon during the dry season. These monsoons distinctly divide the climate into two pronounced seasons. The wet season generally lasts from June to September, while the dry season is from November to April. May and October are transition periods of these two seasons. In general, it is humid and hot in the wet season and dry and cold in dry season. This is due to the influence of the southeast and northwest monsoon.

From the climatological viewpoint, the climate in Nepal is divided into five climatic zones in terms of altitude, namely Arctic, Alpine, Cool Temperature, Warm Temperature and Sub-tropical. Sub-tropical zone is situated in low lands less than 1,000m amsl in elevation (Nippon Koie, 1989). The East Rapti river basin is characterized by humid sub-tropical under the influence of the prevailing monsoons.

[2] amsl – average mean sea level.

The temperature varies according to the elevation in the basin. The average temperature in the hottest month June, is about 30 °C in the Rampur station (181m amsl) situated in the flat valley whereas the average temperature for the same month is only about 18°C in Daman (2380 m amsl). January is the coldest month in the basin. Average temperature in this month is about 15 °C in Rampur and about 7°C in Daman.

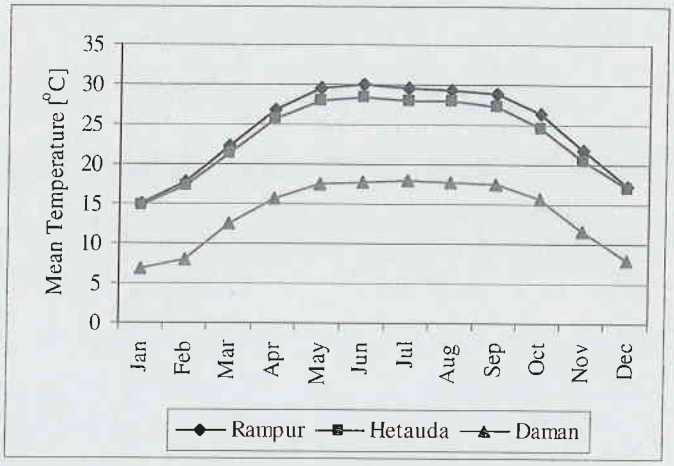

Figure 2.3: Mean monthly temperature [°C] at three stations in the East Rapti basin

There area seven rainfall stations in and around the East Rapti river basin, which are operated by Department of Hydrology and Meteorology (DHM). Out of seven, four stations Chisapani Gadhi, Daman, Hetauda, Makawanpur Gadhi are located in the upper part (hilly area) of the basin whereas three stations Beluwa, Jhawani and Rampur are located in the lower part (flat valley) of the basin.

Average annual rainfall in the basin is about 2008 mm. Rainfall is concentrated during six months of monsoon period from middle of May to end of October. More than 90% of total annual rainfall occurs during these months. July and August are the wettest months receiving nearly half the annual rainfall. The coefficient of variation among the stations is higher in dry months than the wet months.

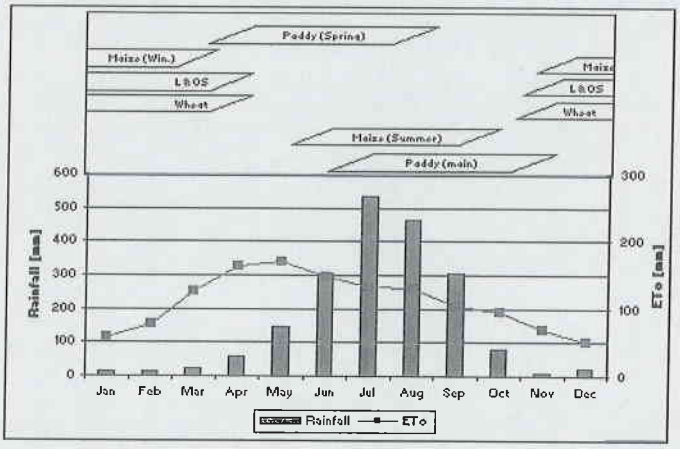

Figure 2.4: Long term mean monthly rainfall in the basin; Reference ET computed by the Penman-Monteith equation and cropping pattern for Jhawani station[3]

[3] L & OS – Lentil and Oilseeds

2.5. River system

The East Rapti river originates from the Mahabarat range of mountains, at about 25 km southwest of Kathmandu. From its origin, it flows southward and changes its flow direction to the west near Hetauda (the urban centre of Hetauda district) and then confluences with Narayani river, one of the major rivers in Nepal, at msl of about 140 m. The length of the main course of the river is about 122 km and its total catchment area is about 3109 km^2. The main tributaries of East Rapti River are *Samari, Bakaiya, Karra, Manahari, Lothar* in *Makawanpur district* and *Dhungre, Budhi Rapti, Pampa, Kair, Khageri* and *Riu Khola* in *Chitwan district.*

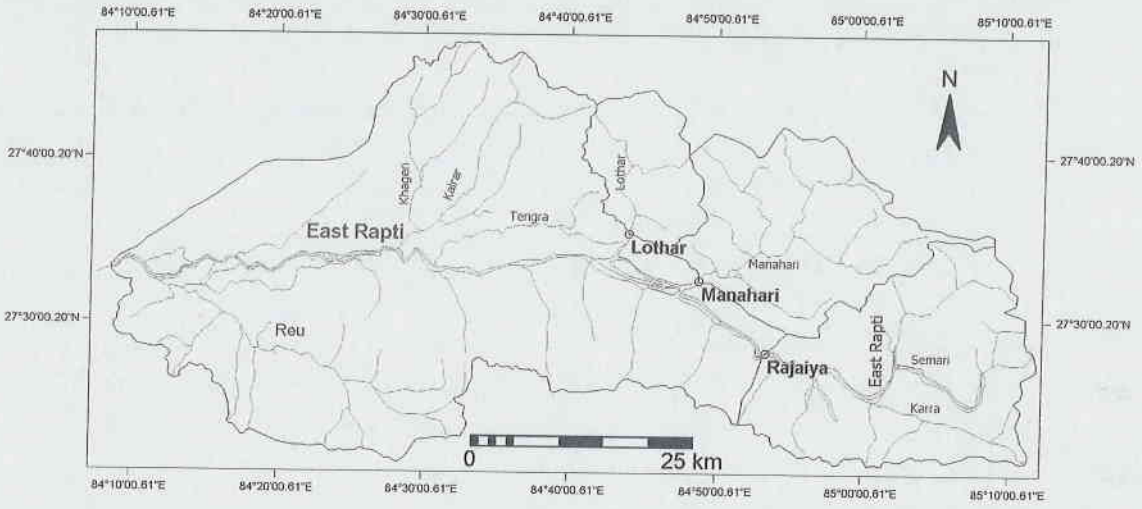

Figure 2.5: Map of the East Rapti river basin showing river network and the river stations

There are three gauging stations the Rajaiya, the Manahari and the Lothar, which records river flow within the East Rapti river system. All of them are located in the upper part of the basin (**Figure 2.5**).

The import of water from Bagmati basin to the East Rapti basin occurs through Kulekhani hydro-power reservoir which is operated throughout the year with a maximum monthly discharge of 4.8 $m^3 s^{-1}$ and a minimum of 1.0 $m^3 s^{-1}$ (IWMI-Nepal, 2000a). In addition to this, the Narayani lift irrigation system also imports water from Narayani basin to irrigate western part of Chitwan district (tail end of the basin) ~~of the basin.~~ The Narayani lift irrigation system operates for six months of a year from June to November with a total lift of about 53 million m^3 (IWMI-Nepal, 2000b).

2.6. Soil

According to the information provided in the land system map (1982) of the study area, prepared by the Topographical Survey Branch, Survey Department to the Ministry of Land Reform of HMG/N (published in 1984), the major soil types found in the flat valley of the study area are Ustorthents, Psamments, Ustifluvents, Fluvaquents, Ustochrepts, Haplaquepts, Haplustolls, Dystrochrepts and Rhodustalfs.

Ustorthents and Psamments extend over the active alluvial plains, especially river course of the East Rapti and their tributaries. Such soils have very coarse soil texture with cobbles. Ustifluvents and Fluvaquents occupy the low terrace land. The soils have deep effective soils with sandy soil textures. Ustochrepts and Haplaquepts occupy the recent flat alluvial land and non-dissected depositional land. These soils have deep effective soil depth with loamy soil texture in general. Haplustolls, Dystochrepts and Rhodustalfs extend over the very gently to undulating fan and old river terrace lands with gradient of less than 5°. These soils have deep effective soil depth with medium soil texture (loamy).

2.7. Agriculture

Agriculture is major occupation of Nepal where nearly 81 percent of economically active population is engaged in producing roughly only 41 percent of the total gross domestic product (GDP). Similar is the case with both the districts in the basin. Of the total economically active population of *Makawanpur district*, 82.7 percent, i.e. slightly more than national figure are still involved in agriculture and live in rural areas whereas considerably lower population, i.e. only about 75 percent are engaged in agriculture in *Chitwan district*.

The farming system in the basin is mainly subsistent farming instead of commercial farming. The river valleys and inner terai part of the Basin is most important from agricultural development point of view. The cropping intensity in the basin is very much depending on irrigation facility availability. The cropping intensity in the area having year round irrigation facility is between 200-300 percent. The cropping pattern in this area having year-round-irrigation facility is: Paddy-Fallow-Paddy; Paddy-Wheat-Paddy; Paddy-Wheat-Fallow; Paddy-Lentil-Paddy; Paddy-Lentil-Fallow. But the cropping intensity in the area with seasonal irrigation facility remains below 200 percent. The cropping pattern in such areas is: Paddy-Wheat; Paddy-Lentil; Paddy-Maize; Maize-Oilseeds; Maize-Maize; Paddy-Vegetables; Maize-Vegetables etc. In *Bari Land* (rainfed areas) of hilly areas of the basin of both the districts; maize, potato and millets as single crops as well as in mixture are grown. The dominant cropping pattern in these hilly areas is: Maize-Millet; Potato-Millet; Maize-Potato-Fallow; Maize-Fallow etc. In the *Khet Land* (irrigated river valleys and terraces) the dominant cropping pattern is: Paddy-Wheat; Paddy-Vegetables; Paddy-Oilseeds; Paddy-Lentil; Paddy-Fallow etc.

Chapter 3. Materials and methods

3.1. Materials

3.1.1. Satellite imagery

East Rapti river basin lies in row 41 of two Landsat paths, 141 and 142. Path 141 covers about 85% of the Basin area. Three Landsat 7 ETM+[4] images for path/row 141/41 with limited cloud cover were purchased from National Aerospace Laboratory (NLR), the Netherlands (the local distributor of Landsat ETM+ in the Netherlands) for the investigation. The number of images was limited to three due to limitation on resources. The acquisition dates of images chosen to avoid cloud contamination were 24 October 2001, 27 December 2001 and 1 March 2002 and the overpass times were 10.36, 10.367 and 10.37 hours local time respectively. Landsat 7 ETM+ has 8 bands in the electromagnetic spectrum. Bands 1-3 lies in the visible part of the spectrum (0.45-0.69 μm), band 4 in the near-infrared range (0.76-0.90 μm), band 5 and 7 in the middle-infrared range (1.55-2.35 μm), band 6 in the thermal infrared range (10.4-12.5 μm) and band 8 is the panchromatic (0.5–0.9 μm). The spatial resolution of ETM+ imagery is 15x15m at the panchromatic band, 30x30m at the visible and near infrared bands and 60x60m at thermal infrared band. The spectral radiance reflected and emitted in each band varies with land characteristics (land use, fractional vegetation cover, soil type, soil moisture etc.).

The investigated images are provided in FAST-L7A format, which are radiometrically and geometrically corrected (level-1G) products. Images are geo-referenced to the coordinate system of the referenced topographic maps (1:25000) published by the Survey Department of His Majesty's Government of Nepal (HMG/N), 1994. The description of the coordinate system used in all maps and images (unless stated) in this study are as follows:

Spheroid: Everest 1830
Projection: Modified Universal Transverse Mercator
Origin: Longitude 84° East, Latitude 0° North
False co-ordinates of origin: 500,000 m Easting, and 0 m Northing
Scale factor at Central Meridian: 0.9999

3.1.2. Digital elevation model

The digital contour elevation data of the basin was purchased from the Department of Survey, Nepal. The contour data are of 20m intervals in hilly area and 10 m intervals in flat area. There were some irregularities found in the contour data, which have been corrected according to the neighbouring contours. Using the contour interpolation facility in ILWIS, a Digital Elevation Model (DEM) with 30 m pixel resolution was created.

[4] Enhanced Thematic Mapper Plus Instrument

3.1.3. IWMI Water and Climate Atlas

Recently the International Water Management Institute (IWMI) published global Water and Climate Atlas (IWMI, 2000). The Atlas includes monthly and annual summaries for precipitation, temperature, humidity, hours of sunshine, evaporation estimates, wind speed, total number of days with and without rainfall, days without frost and the Penman-Monteith reference evapotranspiration rates. Out of 11 major agro-climate variables available in the atlas the hours of sunshine and mean wind speed is being used in this analysis. The IWMI database is available in 15 km grids at the equator, and can be downloaded from http://www.cgiar.org/iwmi/WAtlas/atlas.htm.

3.2. Methods

3.2.1. Surface energy balance algorithm for land (SEBAL)

As stated above, estimation of evapotranspiration is one of the critical parts in water accounting, and main aim of this study is to estimate evaporative depletion of water in the basin. The application of remote sensing technique in estimation of actual evapotranspiration in mountainous terrain will be elaborated herein. The Surface Energy Balance Algorithm for Land (SEBAL) has been applied in this study for the investigation of actual evapotranspiration.

SEBAL is a satellite image-processing model to compute evapotranspiration and other energy exchanges at the earth's surface. SEBAL uses digital image data measuring thermal infrared radiation in addition to visible and near-infrared bands. SEBAL is based on raster maps of surface albedo, vegetation index and surface temperature and solves the surface energy balance explicitly (Bastiaanssen *et al.*, 1998). SEBAL was originally developed in the Netherlands by Bastiaanssen and was modified some of the sub-models by (Allen & Tasumi *et al.*, 2000; Morse *et al.*, 2001; Tasumi *et al.*, 2000) in an application to Bear river basin of southern Idaho, USA. A detail description of the model is provided in (Allen & Tasumi *et al.*, 2000; Bastiaanssen, 2000; Bastiaanssen *et al.*, 1998; Tasumi *et al.*, 2000) and step by step procedure is included as Appendix 1. Some main improvements in relation to SEBAL application in mountainous terrain are outlined below.

3.2.1.1 Solar radiation

The clear sky shortwave solar radiation is varies according to the surface latitude, longitude, surface gradient (slope) and surface orientation (aspect). The estimation of solar radiation in the flat surface is straightforward. Traditionally, solar radiation is estimated or measured for representative climate station and extrapolated for large area. As, the solar radiation varies significantly according to the surface slope and aspect, the extrapolated solar radiation from point measurement; especially in the hilly terrain mislead whole computation process. The estimated radiation should be corrected for the mountain effect. Which can be performed in Geographic Information System (GIS) environment.

The process to estimate solar radiation in mountainous area as explained in Allen & Tasumi (2000) and Tasumi *et al.* (2000) has been applied in this study. The process is briefly outlined below.

Surface steepness (slope): Slope indicates the land surface steepness in degree. Its value ranges from 0° to 90°. 0° means that there is no slope (i.e. flat) and 90° means that the land surface profile is vertical.

Surface orientation (aspect): The orientation of the land surface is express as aspect in degrees. In general, in an aspect map 0° represents directed towards north, and with values increasing positively in a clockwise direction. There is no sense of aspect for the flat area, so that it is corrected by 361°. But, for the application of aspect on solar radiation correction, the aspect has been corrected so that 0° indicates South and the value increasing negatively towards East and positively towards West. The

value in aspect map for this application ranges from –180 ° to 181 ° indicating ± 180° North, -90° East, 0° South, 90° West and 181 ° flat area. All the term containing aspect 181 ° will be vanishes while calculating cosine of solar incident angle, as sin0 ° is equal to zero (equation 3.1).

The solar incident angle θ is the angle between the solar beam and a vertical line perpendicular to the land surface. If the land surface is flat then the computation of solar incident angle is straight forward as, θ = 90° - (Sun elevation above the horizon). If there is any slope in the land surface, θ changes depending on the slope and aspect of the land surface and the Sun position.

The cosine of solar incident angle has been computed by the following equation (Tasumi *et al.*, 2000):

$$\cos\theta = \sin(\delta)\sin(\phi)\sin(s) - \sin(\delta)\cos(\phi)\sin(s)\cos(\gamma) + \cos(\delta)\cos(\phi)\cos(s)\cos(\omega) + \cos(\delta)\sin(\phi)\sin(s)\cos(\gamma)\cos(\omega) + \cos(\delta)\sin(\phi)\sin(s)\sin(\omega) \quad [-] \quad (3.1)$$

Where,

δ declination of the earth (positive in summer in northern hemisphere)

ϕ latitude in radian of the pixel (positive for northern hemisphere)

s slope in radians, where s = 0 is horizontal and s = π/2 is vertical downward (s is always positive and represents a downward slope in any direction).

γ the deviation of the normal to the surface from the local meridian, where γ = 0 for aspect that is due south, γ = - for east and γ = + for western aspect. γ = -π/2 represents an east facing slope and γ = +π/2 represents a west-facing slope. γ = -π and γ = +π represents a north-facing slope.

ω hour angle. ω = 0 at solar noon, ω is negative in morning and ω is positive in afternoon.

Total instantaneous incoming solar radiation, $K_a^{\downarrow}$ has been computed as (Tasumi *et al.*, 2000):

$$K_a^{\downarrow} = G_{sc} \times dr \times \cos\theta \qquad [\mathrm{Wm^{-2}}] \quad (3.2)$$

Where, G_{sc} is the solar constant [1367 $\mathrm{Wm^{-2}}$], dr is inverse square relative distance Earth-Sun in Astronomical unit [AU], its value ranges from 0.97 to 1.03.

The inverse squared relative distance Earth-Sun dr was computed as (Tasumi *et al.*, 2000):

$$dr = 1 + 0.033 \cdot \cos\left[\frac{J \times 2\pi}{365}\right] \qquad [\mathrm{AU}] \quad (3.3)$$

Where, J is the Julian date (i.e. day number starting from January 1st to December 31st).

The twenty-four hour extraterrestrial radiation $K_{a24}^{\downarrow}$ is the daily incoming solar radiation unadjusted for atmospheric transmittance. It can be derived by the equation (Tasumi *et al.*, 2000):

$$K_{a24}^{\downarrow} = G_{sc} \cdot dr \cdot \int_{\omega 1}^{\omega 2} \cos\theta \cdot d\omega \qquad [\mathrm{Wm^{-2}}] \qquad (3.4)$$

Where, G_{sc} is the solar constant [1367 Wm^{-2}], dr is inverse relative distance Earth-Sun. ω_1 and ω_2 are the beginning and ending sun hour angles where the sun's beam first strikes the surface.

For a horizontal surface, ω_1 and ω_2 are equal to $-\omega_s$ and ω_s, where ω_s is the sunset hour angle.

The analytical solution of equation (3.4) is more complex and difficult to perform the integration operation in most of the image processing softwares like ILWIS. Allen & Tasumi (2000) proposed a numerical solution for the equation (3.4), which compute 24-hour total extraterrestrial radiation by solving equation (3.4) a large number of times during the day and then integrating numerically. An ILWIS script (Appendix 2) was prepared to perform the numerical solution. Allen & Tasumi (2000) mentioned that this procedure also calculates accurately under all conditions, including those where a north-facing slope may shadow itself during midday, but receive beam radiation during early and late day.

The numerical solution has been applied in ILWIS by making 48 time steps each of 0.5 hours for a day from midnight to midnight (i.e. $-\pi \leq \omega \geq \pi$). Equation (3.4) has been solved for each 0.5 hours time step during the day. Here the value of ω varied from $-\pi$ to π by increments of $0.5\pi/12$.

To account for diffuse radiation during the daytime and to correct for night time, two conditions were applied.

1. $\cos\theta_\omega$ is limited to a non-negative number: if $\cos\theta_\omega < 0.1$ then $\cos\theta_\omega = 0.1$, to account for diffuse radiation during day time.
2. Correction for night time: if $\omega < -\omega_s$ then $\cos\theta_\omega = 0$, i.e. before sunrise and if $\omega > \omega_s$ then $\cos\theta_\omega = 0$, i.e. after sunset

3.2.1.2 DEM corrected apparent surface temperature

Generally, air temperature decreases 6.5°C when elevation increases by 1 km under neutral stability conditions. Since surface temperatures are in strong equilibrium with air temperature, one can usually observe similar decreases in surface temperature (Tasumi *et al.*, 2000).

During the estimation of sensible heat flux in SEBAL, an estimation of the surface to air temperature difference (dT_a) is needed. In SEBAL dT_a is estimated as a linear function of surface temperature. However the surface temperature estimated from satellite image, needs to be uniformly adjusted to a common reference elevation for accurate prediction of dT_a in mountainous area. Otherwise, high elevations that appear to be "cool" may be interpreted as having high evapotranspiration. Therefore a "lapsed" (an artificial) surface temperature map was made for purpose of computing surface-to-air temperature differences by assuming the rate of decrease in surface temperature by the orographic effect is the same as that for a typical air profile using the equation (Tasumi *et al.*, 2000):

$$T_{o\_dem} = T_o + 0.0065 \cdot \Delta z \qquad [K] \qquad (3.5)$$

Where, T_o is the surface temperature [K], Δz is the difference of a pixel's elevation from the datum [m]. The datum was selected from the flat valley near Jhawani station, which has an elevation of 181 m.

The temperature difference dT_a required to predict H was estimated assuming that dT_a has a linear relation to T_{o_dem}.

$$dT_a = a + b \cdot T_{o\_dem} \qquad [K] \qquad (3.6)$$

Where, a and b are constants.

The estimation of constants a and b follows some iteration process. First, two extreme evaporating pixels (wet and dry pixel) were selected. This was done by assessing T_{o_dem} with the help of scatter plots of Normalized Difference Vegetation Index (NDVI) vs T_{o_dem} and r_o verses T_{o_dem}. In general the wettest pixel has high NDVI and low surface temperature indicating high evapotranspiration and dry pixel has medium albedo and high surface temperature indicating no evapotranspiration. The DEM corrected surface temperature corresponds to selected wet pixel and dry pixel have been noted as T_{o_wet} and T_{o_dry} respectively. Other parameters required to solve general equation for sensible heat flux were noted for the dry pixel from the corresponding maps. In the wet pixel SEBAL assumes sensible heat flux zero. Sensible heat flux for dry pixel was estimated by solving general equation for sensible heat flux in inverse mode. Using these two extreme sensible heat fluxes, the linear constants a and b were predicted. The iterative steps for buoyancy correction on sensible heat flux at dry pixel were carried out in Excel spreadsheet and attached in the Appendix 1.

Both the dry and wet pixels were selected from the flat valley area to avoid uncertainty due to mountain effect. The wet pixel is selected from the swampy forest area with high NDVI and low temperature among the surrounding pixels. And the dry pixel selected from the dry sandy riverbed with high T_{o_dem} within the area, medium albedo and less (but positive) NDVI.

3.2.1.3 Surface energy balance and evapotranspiration

Evapotranspiration is related to the surface energy balance, which is expressed as:

$$R_n = G_o + H + \lambda E \qquad [Wm^{-2}] \qquad (3.7)$$

Where, R_n is the net radiation flux [Wm^{-2}], G_o is the soil heat flux [Wm^{-2}], H is the sensible heat flux [Wm^{-2}] and λE is the latent heat flux [Wm^{-2}].

Computation procedure for Net radiation, Soil heat flux and Sensible heat fluxes are explained in Appendix 1.

Equation (3.7) can be re-written and expressed as latent heat flux by considering evaporative fraction Λ [-] and net available energy (R_n-G_o):

$$\lambda E = \Lambda(R_n - G_o) \qquad [\mathrm{Wm^{-2}}] \qquad (3.8)$$

Where, Λ is the evaporative fraction [-].

The evaporative fraction was computed using instantaneous surface energy fluxes as:

$$\Lambda = \frac{\lambda E}{R_n - G_o} = \frac{R_n - G_o - H}{R_n - G_o} \qquad [-] \qquad (3.9)$$

Following Shuttleworth et al.(1989), the instantaneous evaporative fraction was considered similar to its 24 h counterpart (Brutsaert *et al.*, 1992), which was used to compute the actual 24 h evapotranspiration from instantaneous latent heat fluxes (Bastiaanssen, 2000):

$$ET_{24} = \Lambda R_{n24} \qquad [\mathrm{Wm^{-2}}] \qquad (3.10)$$

Where, ET_{24} is the 24 hours actual evaporation, R_{n24} is the 24 hours net radiation.

The 24 hours net radiation can be computed according to de Bruin (1987) where surface albedo is assumed to be similar to the surface albedo during the satellite overpass:

$$R_{n24} = (1 - r_o) \cdot \tau_{sw24} \cdot K_{a24}^{\downarrow} - 110\tau_{sw24} \qquad [\mathrm{Wm^{-2}}] \qquad (3.11)$$

Where, r_o is the surface albedo, $K_{a24}^{\downarrow}$ is the 24 hours incoming extraterrestrial solar radiation and τ_{sw24} is the daily atmospheric transmittance.

3.2.1.4 Extrapolation of daily ET to monthly ET

The Penman-Monteith equation for actual evaporation is the most widely accepted framework for computing land surface evapotranspiration, the equation is as follows (Allen *et al.*, 1998):

$$\lambda E = \frac{\Delta(R_n - G_o) + \rho_a c_p \dfrac{(e_s - e_a)}{r_a}}{\Delta + \gamma\left(1 + \dfrac{r_s}{r_a}\right)} \qquad [\mathrm{W\ m^{-2}}] \qquad (3.12)$$

Where, R_n is the net radiation [W m^{-2}], G_o is the soil heat flux [Wm^{-2}], (e_s-e_a) is the vapour pressure deficit of the air [kPa], ρ_a is the mean air density at constant pressure [kg m^{-3}], c_p is the air specific heat [J kg^{-1} $^{\circ}C^{-1}$], Δ is the slope of the saturation vapour pressure temperature relationship [kPa $^{\circ}C^{-1}$], γ is the psychrometric constant [kPa $^{\circ}C^{-1}$], and r_s and r_a are the surface and aerodynamic resistances [s m^{-1}].

For the monthly time step, G_o in above equation can be approximated to zero and the net radiation was computed by equation (3.11) by replacing the monthly values for surface albedo and atmospheric transmissivity. The monthly transmissivity was computed from the sunshine duration data provided in IWMI Water and Climate Atlas. The albedo at the satellite overpass day has been considered average monthly albedo for the corresponding months of the images. From these three albedo values, average monthly albedo for other months were approximated by linear extrapolation.

The slope of saturation vapour pressure curve was computed as function of mean monthly temperature by following equation (Allen *et al.*, 1998):

$$\Delta = \frac{4098\left[0.6108\exp\left(\frac{17.27T_{avg}}{T_{avg}+237.3}\right)\right]}{\left(T_{avg}+237.3\right)^2} \qquad [\text{kPa C}^{-1}] \qquad (3.13)$$

Where, T_{avg} is the average air temperature [°C].

The air density map has been created as a function of atmospheric pressure and average temperature by following relation (Allen *et al.*, 1998):

$$\rho_a = \frac{P}{T_{kv} \cdot R} \qquad [\text{kg m}^{-3}] \qquad (3.14)$$

Where, P is atmospheric pressure in [kPa], R specific gas constant [0.287 kJ $kg^{-1}K^{-1}$] and T_{kv} is the virtual temperature [K].

The atmospheric pressure was compute as the function of elevation by the equation (Allen *et al.*, 1998):

$$P = 101.3\left(\frac{293-0.0065z}{293}\right)^{5.26} \qquad [\text{kPa}] \qquad (3.15)$$

Where, z is the elevation in m.

And the virtual temperature T_{kv} is computed as (Allen *et al.*, 1998):

$$T_{kv} = 1.01(T+273) \qquad [\text{K}] \qquad (3.16)$$

Where, T is mean air temperature in [°C].

The psychrometric constant has been estimated from atmospheric pressure (Allen et al., 1998).

$$\gamma = \frac{c_p \cdot P}{\varepsilon \cdot \lambda} = 0.665x10^{-3} P \qquad [\text{kPa } ^{\circ}\text{C}^{-1}] \tag{3.17}$$

Where, ε is ratio molecular weight of water vapour/dry air (=0.622), λ is latent heat of vaporization (2.45 MJ kg^{-1}) and P is atmospheric pressure.

The saturated vapour pressure (e_s) has been computed from mean monthly temperatures. The actual vapour pressure (e_a) has been computed from mean monthly minimum temperature making an assumption that mean monthly minimum temperature can be approximated to mean monthly dew point temperature (Allen *et al.*, 1998).

The monthly aerodynamic resistances have been computed from the surface roughness for momentum transfer (z_{om}) and wind speed using following relation;

$$r_a = \frac{\ln\left(\frac{z_{ref}}{z_{om\_avg}}\right) \cdot \ln\left(\frac{z_{ref}}{0.1 z_{om\_avg}}\right)}{k^2 \cdot u_z} \qquad [\text{s m}^{-1}] \tag{3.18}$$

Where, z_{om_avg} is the arithmetic average of z_{om} values computed from the images. The mean monthly wind speed (u_z) maps were derived from IWMI water and climate atlas.

The Penman-Monteith equation has been applied in inverse mode to estimate the surface resistance to evaporation (r_s) using SEBAL derived laten heat flux as input. The r_s values for the image dates were considered representative monthly surface resistance for the corresponding months. These three estimated values were used to compute mean monthly r_s values by linear interpolation technique. The value for r_s was restricted to 80 sm^{-1} for the wet months having monthly rainfall greater than 200 mm.

Finally, by solving equation 3.12 for monthly time step, the monthly actual evaporation has been estimated.

3.2.2. Rainfall

Rainfall is the main inflow in the basin. A high spatial variation in rainfall is found in the basin. So, the estimation of catchment rainfall by dividing the catchment into area-governed polygons around each of the rainfall station will not be a good estimate in the mountainous area. To get aerial estimation of the rainfall, two approaches were analysed. First, a multiple regression analysis was carried out for monthly rainfall with elevation, latitude and longitude. Next, second degree polynomials were fitted for the monthly rainfall against elevation alone. Multiple regression shows better statistical relation than that of elevation alone by means of a second degree polynomials. Thus, the long term mean monthly rainfall maps were prepared as function of elevation, latitude and longitude by following equation:

$$P = A \cdot z + B \cdot \phi + C \cdot \lambda + D \quad [\text{mm}] \tag{3.19}$$

Where, P is monthly rainfall, z is elevation in [m], ϕ is latitude [dd], and λ is longitude [dd] and A, B, C and D are monthly constants, which are given in Appendix 3.

3.2.3. Mean monthly air temperature

It has been argue that the temperature is the single most important component of mountain climate e.g. Barry, 1992 cited in (Lookingbill ~~et al.~~, 2003). Among the long list of ecological processes influenced by temperature, evapotranspiration is the one. Since temperature is such an important component of mountain climate, developing a simple geographic model of temperature differences should be an important first-step in many landscape scale ecological studies (Lookingbill ~~et al.~~, 2003).

A study carried out by Tahal Engineering (a consulting company) for Department of Hydrology and Meteorology in western Nepal concluded that the mean monthly maximum temperature (T_{max}) and minimum temperature (T_{min}) for the area can be estimated by the equation (TAHAL-Consulting, 2002):

$$T = A + B \cdot \phi + C \cdot \lambda + D \cdot z \quad [^{\circ}\text{C}] \tag{3.20}$$

Where, T is mean monthly maximum or mean monthly minimum temperature [°C], ϕ is latitude [dd], λ is longitude [dd], z is elevation [m], and A, B, C and D are monthly constants (Appendix 3).

Equation 3.20 has been applied to create the temperature maps.

3.2.4. Reference evapotranspiration

Evapotranspiration rates are related to the evapotranspiration rate from the reference surface (ETo) by means of relative coefficient (ETa/ETo), same as crop coefficient (k_c) for crops. Among the several existing ETo equation, the FAO-56 application of the Penman-Monteith equation is currently commonly used method to estimate ETo. The Penman_Monteith equation to estimate ETo is as follows (Allen et al., 1998).

$$ETo = \frac{0.408\Delta(R_n - G) + \gamma \dfrac{900}{T + 273} u_2 (e_s - e_a)}{\Delta + \gamma(1 + 0.34u_2)} \quad [\text{mm d}^{-1}] \tag{3.21}$$

Where, ETo reference evapotranspiration [mm day^{-1}], R_n net radiation at the crop surface [MJ m^{-2} d^{-1}], G soil heat flux density [MJ m^{-2} d^{-1}], T mean daily air temperature at 2 m height [°C], u_2 wind speed at 2 m height [m s^{-1}], e_s saturation vapour pressure [kPa], e_a actual vapour pressure

[kPa], e_s-e_a saturation vapour pressure deficit [kPa], Δ slope vapour pressure curve [kPa $^oC^{-1}$], γ psychrometric constant [kPa $^oC^{-1}$].

The Penman-Monteith equation needs standard climatological records of solar radiation (sunshine), air temperature, humidity and wind speed. However, Allen *et al.* (1998) proposed several alternative ways to estimate ETo in data scarce condition. The alternative method, which uses temperature and windspeed was used to estimate monthly ETo.

3.2.5. Land cover

Land cover and land use classification is the one of the commonly used application of satellite remote sensing. There are several methods exit for land cover and land use classification from the satellite images. Bastiaanssen (1998) mentioned that, a uniform classification procedure does not exist, and the probability of discerning thematic land classes and determining their accuracy depends on the type of object, image material, and the availability of ancillary data.

Land cover has been derived from a combination of supervised classification and band ratio method. The images were divided in to two sub-regions hills and flat valleys. In flat valley region supervised classification with maximum likelihood estimator were applied using 192 sample points gathered during the field survey from East Chitwan area of the basin. Supervised classification approach is the most commonly used methodology of forming classes that are similar in spectral reflectance e.g. Settle and Briggs 1987 cited in (Bastiaanssen *et al.*, 2001). In this approach, pixels are assigned to one of the training classes obtained from the field survey. The maximum likelihood classifier has been applied, which is a criterion that decides the grouping of a pixel to a training class. This is based on a Gaussian probability distribution, taking the mean and standard deviation in every bands into consideration.

Due to shadow effect on mountainous terrain, accurate classification of land cover may not be possible. Meijerink *et al.* (1994) concluded that the simplest classification method using the band ratio of red band (band 3) and near infrared band (band 4) gives more satisfactory result on land cover classification in mountainous area. The band ratio of band 3 and band 4 was applied for the land classification in the mountainous area following the procedure explained in Meijerink *et al.* (1994). Four land cover classes were identified according to the topographic map of the basin. A feature space of band 3 and band 4 was created to identify the threshold values representing the identified land cover classes. Then the image of band ratio (band3 and band4) was classified using slicing operation in ILWIS. The band ratio were applied for October and March images and the output images were overlaid to get a single land cover map for the hilly area using a value judgement for the conflicting classes in two images.

The independently classified images for the flat valley and hilly area are joined together to produce a land cover map of the basin.

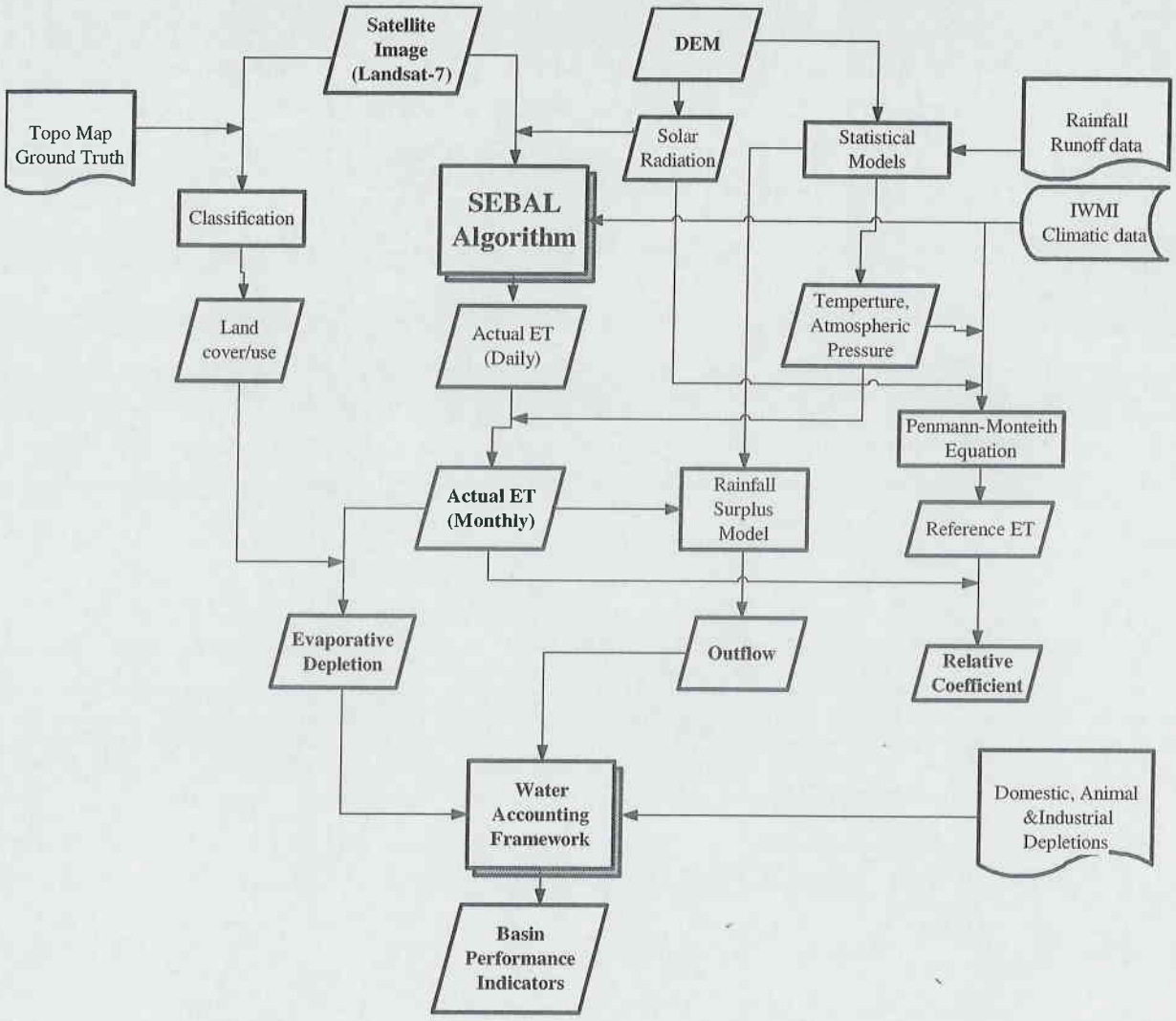

Figure 3.1: Process Model

Chapter 4. Results

4.1. Rainfall

The rainfall data was collected from the Department of Hydrology and Meteorology during the field visit. To assess the consistency in the recorded data, a double mass curve analysis was carried out for each station. Out of seven stations four stations, Daman, Chisapani Gadhi, Makawanpur Gadhi and Hetauda are located in the upper part (mountainous area) of the basin. The other three stations, Beluwa, Jhawani and Rampur, are located in the lower part (flat valley) of the basin (**Figure 2.2**). The double mass curve analysis was carried out separately for these two groups of stations. The stations cumulative annual rainfall was plotted against the cumulative of the average annual rainfall of the other stations within the group. The result shows that all rainfall records are consistent. The long term mean monthly rainfalls are summarized below.

Table 4.1: Observed mean monthly rainfall (long term average 1976 to 2001) within and around the basin.

Station	Elevation	Lati	Long	Mean monthly and annual rainfall [mm]												
Name	[m]	[dd]	[dd]	Jan	Feb	Mar	Apr	May	Jun	Jul	Aug	Sep	Oct	Nov	Dec	Annual
Rampur	181	27.65	84.35	15	13	20	49	159	328	557	435	272	77	7	21	1953
Jhawani	187	27.53	84.78	14	15	24	55	137	296	518	447	290	78	8	23	1905
Beluwa	294	27.53	84.81	16	15	20	52	131	269	520	484	326	83	9	15	1940
Hetauda	443	27.42	85.05	15	18	22	61	186	366	601	546	389	99	17	18	2339
Makawanpur	960	27.41	85.15	16	11	22	54	162	345	584	534	344	82	15	20	2188
Chisapani	1280	27.55	85.13	17	18	44	76	170	331	559	476	302	66	9	26	2094
Daman	2380	27.60	85.08	14	24	31	80	162	289	461	374	215	61	9	20	1739
Average				15	16	26	61	158	318	543	471	306	78	11	20	2023
St dev				1.13	4.30	8.73	12.09	18.81	34.30	47.26	59.29	55.55	12.38	3.85	3.44	199.49
Coeff. Vari.				0.07	0.26	0.33	0.20	0.12	0.11	0.09	0.13	0.18	0.16	0.36	0.17	0.10

The orographic effect on rainfall distribution has been analysed using the scatter plots of elevation with monthly rainfall recorded at the rainfall stations.

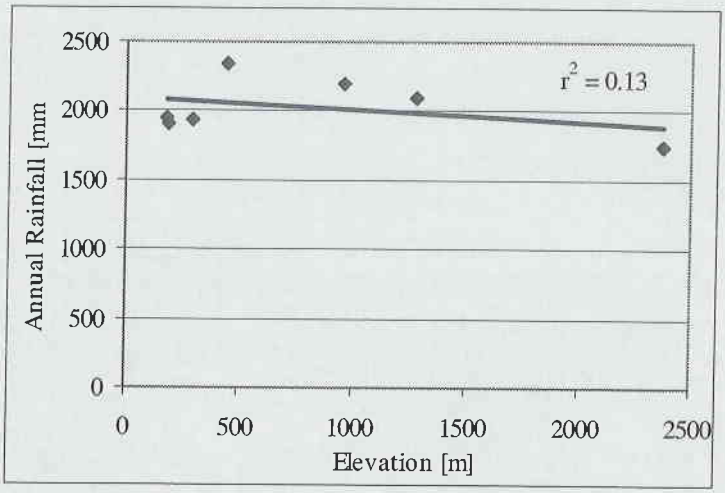

Figure 4.1: Scatter plot of annual rainfall and elevation

It can be noticed from the **Figure 4.1** that there is no relationship between elevation and rainfall. The Daman station (2380 m) recorded least rainfall whereas the Hetauda station (443 m), situated in the foothill near to Hetauda town recorded highest rainfall (**Table 4.1**). This may be due to the effect of monsoon direction in the area. The rainfall in the rainy season in Nepal is due to heavily humid south wind, which blows from strong high pressure in the Indian Ocean (Bengal Bay) and bumps against the Himalayan range causing rainfall on the south side of the range. Accordingly, it rains much on the south sides of Mahabharat range and the Siwalik range. The further analysis on this rainfall pattern is beyond the scope of this study.

To get areal estimation of the rainfall, two approaches were analysed. First, a multiple regression analysis was carried out for monthly rainfall against elevation, latitude and longitude. Next, second degree polynomials were fitted for the monthly rainfall against elevation. The regression coefficients for both methods are listed in **Table 4.2**:

Table 4.2: Regression coefficients (r^2) for rainfall analysis

Method	Jan	Feb	Mar	Apr	May	Jun	Jul	Aug	Sep	Oct	Nov	Dec
Second degree polynomial	0.55	0.69	0.52	0.78	0.26	0.34	0.74	0.74	0.65	0.5	0.23	0.16
Multiple regression	0.26	0.62	0.83	0.89	0.26	0.32	0.56	0.87	0.89	0.86	0.92	0.27

The r^2 values shown in **Table 4.2** reflects that the multiple regression equations can be considered as better estimator of monthly rainfall than that of elevation alone by means of a second degree polynomial. So, the monthly rainfall maps were prepared by multiple regression equation. The longer term average monthly average rainfall is summarized in **Table 4.3** and the annual rainfall is presented as Figure 4.2.

Table 4.3: Estimated average monthly rainfall (mm) in the East Rapti river basin.

Jan	Feb	Mar	Apr	May	Jun	Jul	Aug	Sep	Oct	Nov	Dec	Annual
11	15	27	55	158	322	545	463	300	81	12	19	2008

Rainfall is concentrated during six months of monsoon period from middle of May to end of October. About 93% of total annual rainfall occurs during these months. July and August are the rainiest months receiving nearly half the annual rainfall.

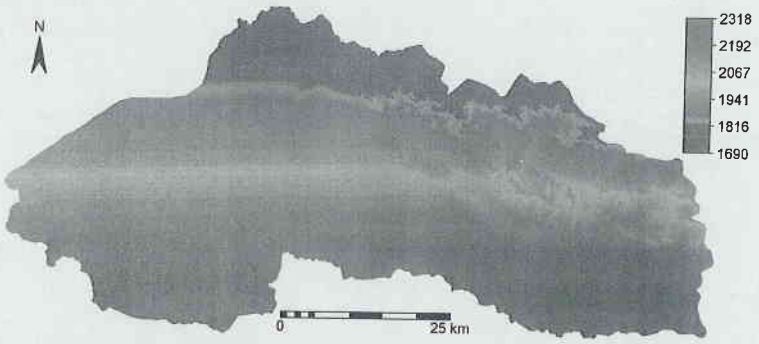

Figure 4.2:Spatial pattern of annual rainfall distribution in the East Rapti basin [mm]

4.2. Mean monthly temperature

The estimated temperatures were noted from the pixels corresponding to the climate stations within the basin, which records temperature and compared with the recorded average values from 1995 to 2000 (Figure 4.3).

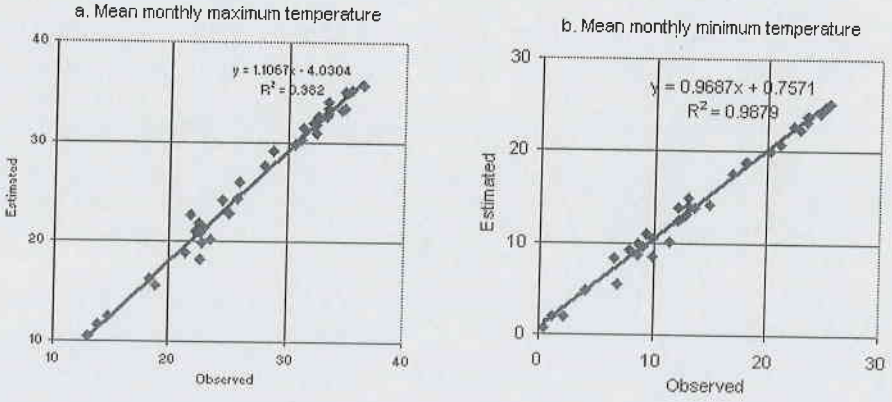

Figure 4.3: Scatter plot of estimated and observed mean monthly temperatures for the selected pixels corresponds to Rampur, Hetauda and Daman stations

The scatter plot of maximum temperature shows that the model slightly under estimated the mean monthly maximum temperature in the lower temperature region i.e. higher elevation area. The slope of the trend line is 1.1 with 0.98 of R^2, indicating the overall deviation is very low. This slight deviation in estimated mean monthly temperature can be neglected as it gives very less error on ET calculation on monthly basis. Whereas the model works well on estimating mean monthly minimum temperatures.

4.3. Reference evapotranspiration

In general, reference evapotranspiration (ETo) is the first entry point for water resources analysis. It is used for the planning process in water resource development specially in designing irrigation schemes. In this study the estimated ETo were used to compute relative coefficients (ETa/ETo), which is same as the crop coefficient (k_c) for crops. This relative coefficients helps to get first idea about the accuracy of the SEBAL derived ETa.

Among the several existing ETo equation, the FAO-56 application of the Penman-Monteith (PM) equation is currently commonly used and can be considered as a sort of standard method for estimation of ETo (Walter et al., 2000). The PM method needs standard climatological records of solar radiation (sunshine), air temperature, humidity and wind speed. There is not a single climatological station within and around the East Rapti basin, where all of above climatological data are measured. To overcome the problem with the scarce meteorological data, the Hargreaves (1985) method was also fitted. This method uses only temperature as input from the meteorological data. This method is much simpler and less data demanding than the PM equation but a major drawback of this method is that it overestimates ETo in humid area (Droogers *et al.*, 2002).

& Allen

To overcome this problem, recently, Droogers & Allen (2002) revised the Hargreaves (1985) equation using a global climate dataset published by International Water Management Institute (IWMI). They introduced an additional term of monthly precipitation in the original Hargreaves (1985) equation. Both the Hargreaves, 1985 and the Modified Hargreaves, 2002 (MH) equations are given in Appendix 4.

To select an appropriate method ~~for~~ to compute ETo maps of the basin, all three equations mentioned above were fitted for the Rampur station. The result is summarized in the following figure.

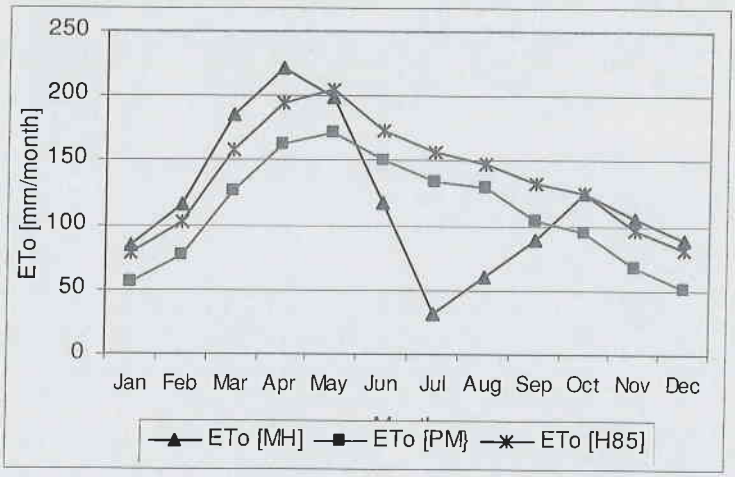

Figure 4.4: Comparison of estimated ETo for Rampur Station by Penmann-Monteith (PM), Hargreaves, 1985 and Modified Hargreaves, 2002 (MH) methods.

From **Figure 4.4**, it could be noted that the original Hargreaves (1985) method overestimates the PM method in all months, whereas the MH method estimates less in wet months and is almost the same as H85 in other months. Due to the uncertainty observed in Hargreaves method, the PM method was selected for the computation of ETo maps for the basin. The estimated annual ETo map is presented as Figure 4.5.

Figure 4.5: Spatial pattern of annual reference evapotranspiration (ETo) in East Rapti river basin computed by the Penmann-Monteith equation being complemented with a mountain radiation model.

Figure 4.5 shows that the annual ETo varies according to the elevation, surface steepness (slope) and surface orientation (aspect). The flat valley and the steep surface oriented towards sun direction have higher ETo whereas the steep slopes oriented opposite to sun direction have very low ETo. The highest annual ETo is 1492 mm y^{-1}, whereas lowest goes as low as 262 mm y^{-1}. According to (TAHAL-Consulting, 2002), the estimated annual ETo for the climate station within the East Rapti basin ranges from 1168 mm y-1 at Daman to 1304 mm y^{-1} at Rampur. A similar range can observed by solving the PM equation without correction of the solar radiation for surface slope and aspect. This implies that the ETo varies significantly by surface steepness and orientation. The higher variation in ETo in the mountain environment is mainly due to higher variation in solar radiation resulting from surface steepness and orientation. This implies that a mountain radiation model is deemed necessary for accurate estimation of the evapotranspiration in the sloping terrain.

4.4. SEBAL Results

The October image is chosen for the interpretation of the major results of SEBAL procedure because of high vegetation cover, as the main objective is to compute ET from vegetation. A summary of the major instantaneous parameters observed on two extreme evaporating pixels (i.e. dry and wet pixels) for all three images are shown in Table 4.4. Other parameter values reported in the paragraphs are just to give rough idea about the range, which were noted from some known area using pixel information window in ILWIS.

4.4.1. Albedo, NDVI and surface temperature

Surface Albedo

Figure 4.6 shows the spatial pattern of broadband surface albedo. The image is stretched from 0.01 to 0.4, the actual values ranges from 0.01 to 0.99. The highest albedo values were noted for clouds. Besides clouds, some of the dry pixels (may be rock outcrop) in the mountains also have very high albedo. The least albedo, around 0.06 can be observed in water body and shadow part of the mountains. The surface albedo in forest is about 0.11 and in agricultural areas slightly higher than forest (around 0.14). Among the bare soils, the recently harvested paddy fields have lower surface albedo (0.18) than others (0.23). The sand and gravel riverbeds are characterised by high albedo (0.35). The observed values for surface albedo show very good agreement with the approximate mean albedo values for various natural surfaces by Brutsaert (1982) reported in (ASCE-Manuals, 1996)[5] for the corresponding land covers.

[5] ASCE (1996), Table 4.4 in page 133.

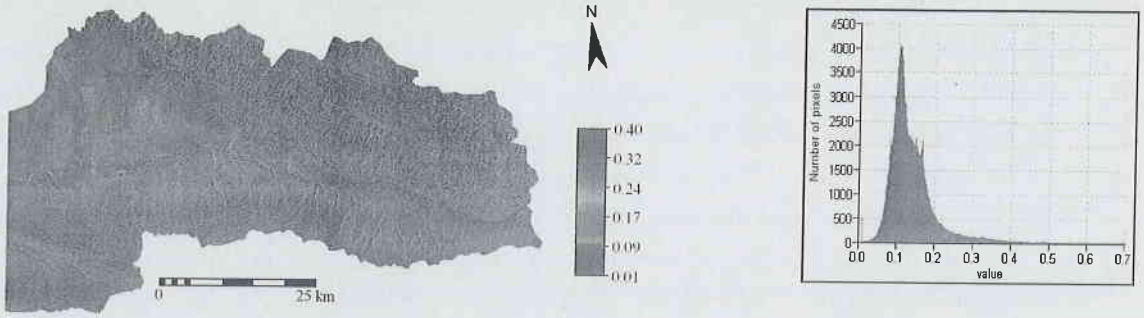

Figure 4.6: Spatial patterns of surface albedo and corresponding histogram – 24 October 2001

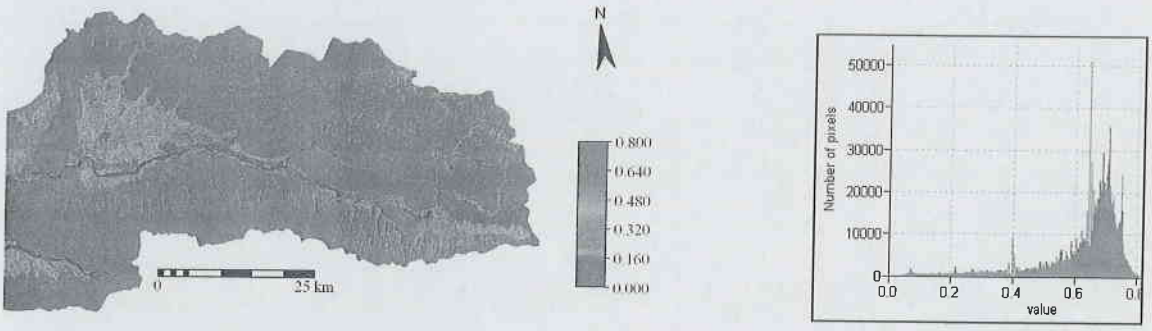

Figure 4.7: Spatial patterns of NDVI and corresponding histogram – 24 October 2001

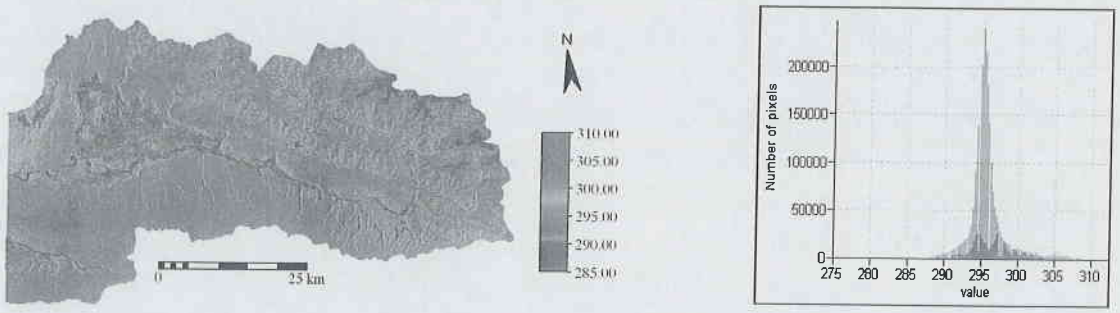

Figure 4.8: Spatial patterns of surface temperature [K] and corresponding histogram - 24 October 2001

NDVI

Spatial patterns of NDVI and corresponding histogram for 24 October 2001 is presented as **Figure 4.7**. The image is stretched from 0.0to 0.8. The actual minimum value was –0.476 indicating a water body. From the image, it could be noted that the NDVI is higher in forest (around 0.7) and even greater for the forest located in sun lit slopes of the lower hills. The Paddy area (mid- western part) has a NDVI around 0.55. This lower value of NDVI in the Paddy than the forest is reasonable as the Paddy, during the image date was in mature stage. The cropped land in the mountain area mainly covered by Maize, characterized by NDVI value around 0.65. This is reasonable for mid stage Maize. Bare soils have a NDVI around 0.17 whereas the clear paddy fields have only 0.06, this may be due to difference in soil moisture content. Similar values were observed for the wet riverbeds also. Sand and gravel riverbed were characterized by the NDVI value around 0.09.

Surface Temperature

The spatial pattern of surface temperature is presented as **Figure 4.8**. From **Figure 2.3** it could be noted that the typical air temperature on 2nd part of October ranges from 14°C to 25°C (i.e. 287-298 K). The image is stretched form 285 - 310K to avoid the effect of cloud. The temperature values in the image are lesser than 285K for the pixels corresponding to clouds. The sand and gravel riverbeds, bare soils (dry) were characterized by high surface temperatures (around 309 K). The vegetation shows a medium surface temperature. The water body (river) in the valley has lower temperature than the adjacent vegetated area. The temperature difference between water bodies and vegetation is only a couple of degrees. This is due to the fact that the water depth in the river is shallow. The distinct pattern of the elevation effect on surface temperature can also be seen in the image. Higher elevated areas have a low surface temperature. The dark blue tone in North-eastern corner corresponds to the high elevation area in the basin. The cold pixels have surface temperatures around 285 K in this area. The surface temperature is even lower in some pixels. These correspond to clouds.

4.4.2. Energy balance

The minimum and maximum values for DEM adjusted surface temperature were found in well-vegetated area and sandy riverbed respectively for all three images. These were considered extreme evaporating surfaces. More specifications of these two extreme evaporating pixels, selected as dry and wet pixels are provided in **Table 4.4**.

Table 4.4: Major instantaneous parameters and fluxes during the Landsat overpass at the wet and dry pixels

		24 Oct. 2001		27 Dec. 2001		1 Mar. 2002	
Parameter	Unit	Dry pixel	Wet pixel	Dry pixel	Wet pixel	Dry pixel	Wet pixel
Coordinates:							
x	m	551628	547378	552183	547418	551537	546318
y	m	3047811	3051878	3048513	3052113	3047847	3052858
NDVI	-	0.075	0.771	0.164	0.681	0.102	0.506
SAVI	-	0.055	0.476	0.092	0.390	0.070	0.262
Surface albedo	-	0.329	0.137	0.175	0.126	0.274	0.126
Surface emissivity	-	0.920	1.000	0.924	0.991	0.920	0.977
Surface temperature	K	312.1	294.8	302.7	287.8	304.7	291.8
DEM corrected surface temperature	K	312.2	294.8	302.7	287.8	304.8	291.8
Incoming short-wave radiation	Wm^{-2}	742.5	741.8	581.1	580.2	737.3	734.5
Incoming long-wave radiation	Wm^{-2}	336.5	336.5	308.6	308.7	317.1	317.1
Outgoing long-wave radiation	Wm^{-2}	494.6	428.0	440.1	385.7	450.0	402.1
Net radiation	Wm^{-2}	312.9	548.0	324.5	427.3	377.0	549.7
Soil heat flux	Wm^{-2}	73.1	35.5	46.6	22.33	66.7	42.9
Roughness momentum	m	0.0041	0.0435	0.005	0.026	0.004	0.013
Roughness heat	m	0.0004	0.0044	0.0005	0.0027	0.0005	0.0013
Friction velocity	$m\ s^{-1}$	0.1466	0.1244	0.103	0.067	0.1652	0.1103
Monin Obukhov length	m	-1.197	-197.741	-0.348	-105.791	-1.250	-1613.474
Temperature difference (dTa)	K	21.33	0.0	27.8	0.0	24.7	0.0
Sensible heat flux	Wm^{-2}	234.34	0.82	279.4	0.26	316.4	0.07
Latent heat flux	Wm^{-2}	5.4	511.7	0.01	404.7	0.01	506.7
Evaporative fraction	-	0.023	0.998	0.00	0.999	0.00	1.00

The energy partitioning can be expressed as the evaporative fraction (Λ). The forest converts a large portion of the available energy into evaporation ($\Lambda > 0.95$). Agricultural area also converts a large portion of the available energy into evaporation but slightly lesser than that of forest. Average evaporative fraction for paddy is around 0.92. Maize converts slightly less than paddy, the average Λ in this case was around 0.88. Average Λ in clear paddy field were found around 0.5 whereas it is slightly less in bare soils (about 0.4). Minimum evaporative fraction was found in sand and gravel riverbed.

4.4.3. Actual ET

As stated above, the ultimate goal of whole SEBAL process is to compute actual evapotranspiration (ETa) maps. Three daily ETa maps, twelve monthly ETa maps and one annual ETa map were prepared. The cloud-contaminated pixels were masked out using a cloud map, which is prepared by analysing histograms of the visible and thermal bands. The procedure of cloud detection is summarized in appendix 5. Estimated daily and annual evapotranspiration maps are presented as **Figure 4.10** and in **Figure 4.11** respectively. The frequency distribution of the estimated daily ETa is presented in **Figure 4.9**.

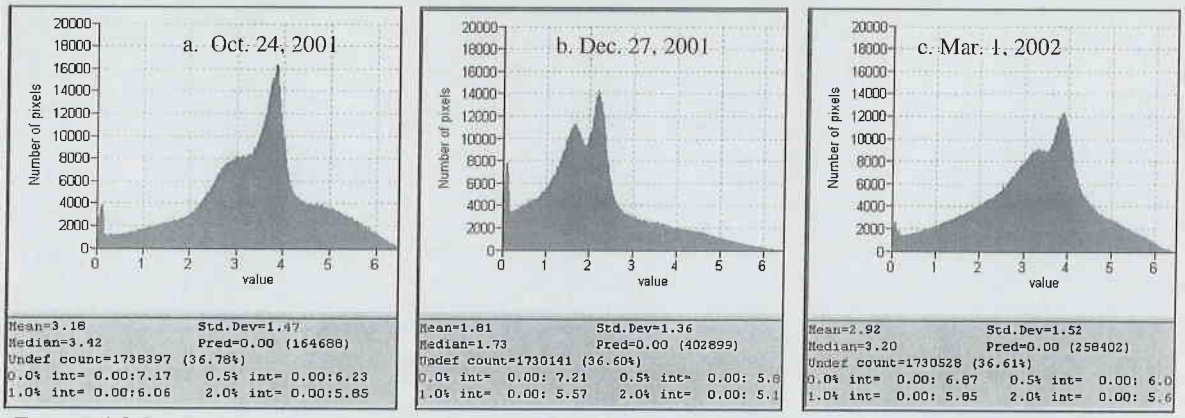

Figure 4.9: Histograms of daily ETa for three Landsat overpass days in East Rapti river basin (value is expressed in mm d^{-1})

The mean daily ETa for three Landsat overpass days is found to be 3.2, 1.8 and 2.92 for October 24th, December 27 th and March 1st images respectively. Out of three, the highest average ETa was observed on October 24th image. This is reasonable as the image date was just after the rainy season, the vegetation is healthy and abundant soil moisture availability explains why ET is higher in October 24th than others. Due to low Sun elevation in December 27th, available energy for evaporation is also lower compared to the other two images; which is reflected as low ET. Besides, winter crops were in developing stage in December 27th whereas it was on mid and mature stage on March 1st. This also explains higher mean ETa on March rather than December 27th.

The surface resistance (r_s) was estimated by solving the Penman-Monteith equation (equation 3.12) in inverse mode using the evapotranspiration in the form of λE from SEBAL as input. This implies that the accuracy of r_s values reflects the accuracy of extrapolated monthly and yearly ET to some extent. The estimated value of r_s from the paddy and forest were assessed using the pixel information window. For paddy, r_s is found around 77 s m^{-1} and for forest is about 56 s m^{-1}. Harazono *et al.*(1998) reported the daytime rice resistance values that ranged between 78 and 111 s m^{-1} in Okayama (Japan). Kelliher *et al.* (1995) reported a value of 59 sm^{-1} for surface resistance of eucalyptus forest and 77 s m^{-1} for tropical rain forest. Bastiaanssen & Bandara (2001) concluded that the surface resistance values obtained from SEBAL in Kirindi Oya basin of Sri Lanka; 63 s m^{-1} for mountain forest and 66 sm^{-1} for homesteads are good agreement with the experimental evidence from the other humid forests. The estimated average values for paddy and forest were very much close to above literature values. This shows the estimated values are in good agreement with the literature values.

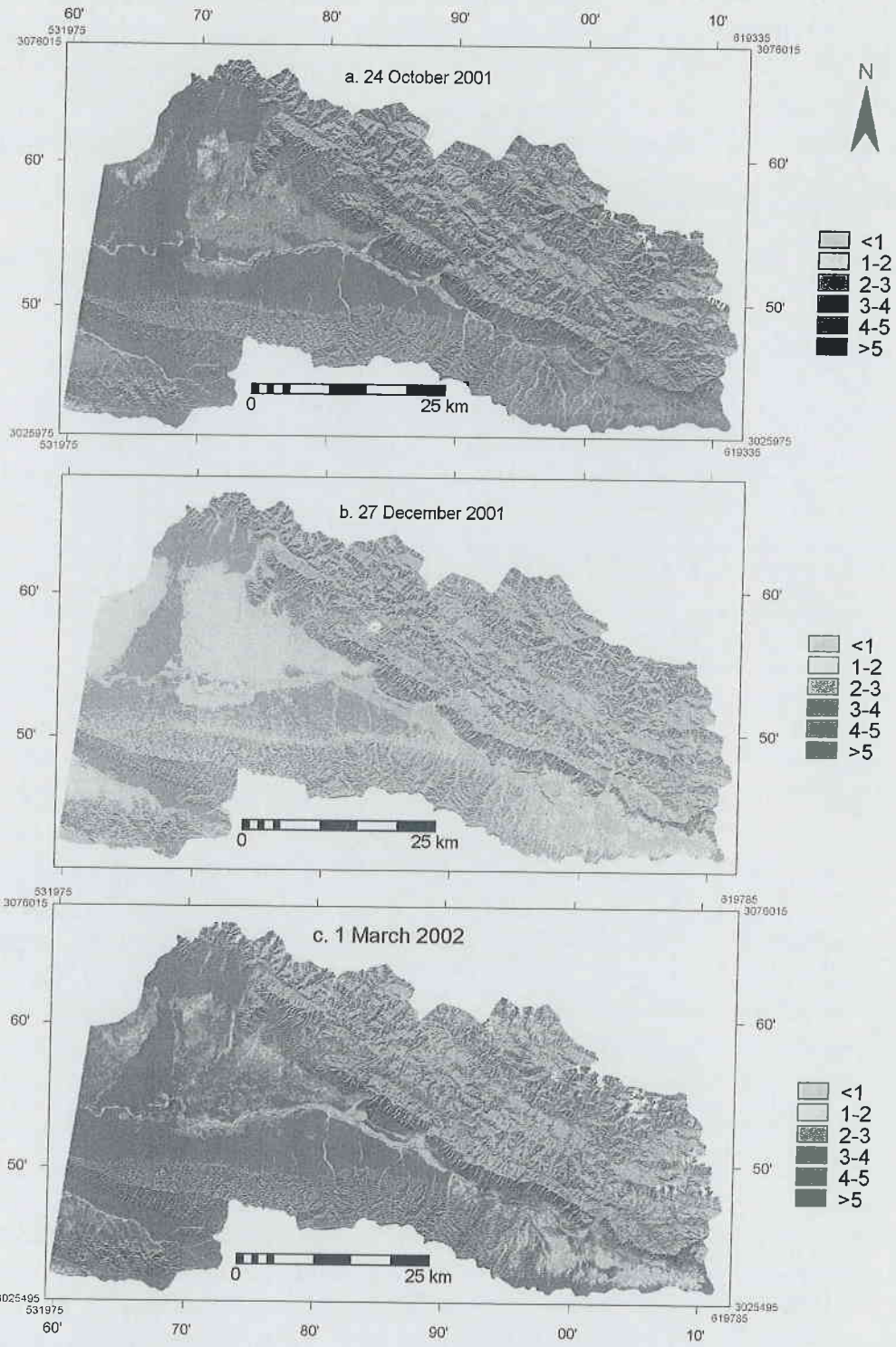

Note: White area within the basin were covered by clouds

Figure 4.10: Spatial patterns of daily evapotranspiration for three Landsat overpass days in the East Rapti river basin [mm d^{-1}]

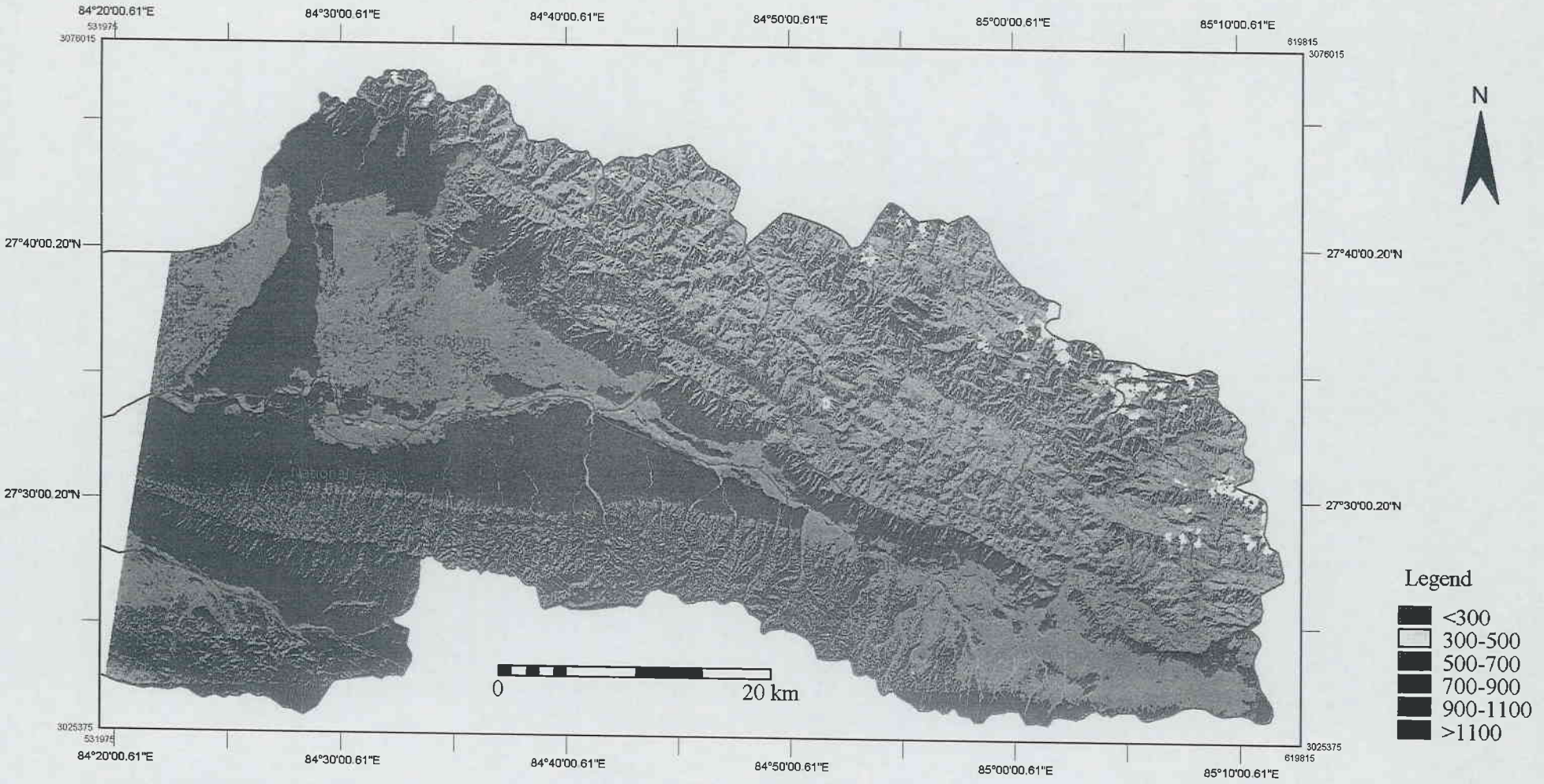

Coordinate System Information:
Spheroid: Everest 1830
Projection: Modified Universal Transverse Mercator
Origin: Longitude 84o East, Latitude 0o North
False co-ordinates of origin: 500,000 m Easting, and 0 m Northing
Scale factor at Central Meridian: 0.9999

Note: White area within the basin - Cloud

Figure 4.11: Spatial patterns of actual evapotranspiration in the East Rapti basin [mm y^{-1}] – 2001/02

The monthly variation of average ETa along with monthly average ETo and relative coefficients (ETa/ETo) are shown in **Figure 4.12**. The average monthly ETa close to ETo reveals high vegetation cover in the basin. The relative coefficients are lower in dry months and gradually increased from May till September and decreases again. The monsoon starts from mid may and cultivation of summer paddy starts from June. This explains the effect of monsoon period and crop growing stage of summer crop on evapotranspiration in the basin.

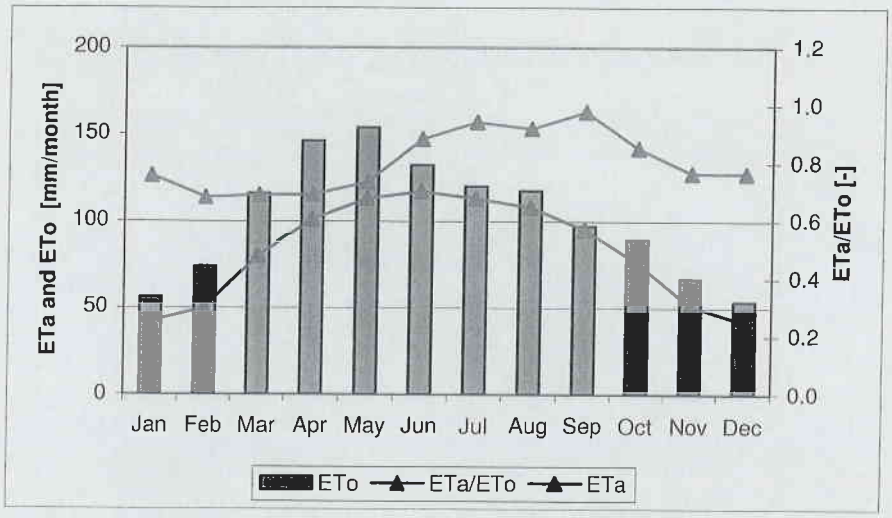

Figure 4.12: Average monthly ETa, ETo and the relative coefficient (ETa/ETo) in the East Rapti basin

The spatial patterns of annual ETa shows that ETa is lower in mountainous catchments and highest in the National Park area (**Figure 4.13**). The Lothar and the Manahari catchments consist of mainly hilly area, whereas the Rajaiya catchment consists of mountains as well as small valley (south-eastern part of the basin). The Rajaiya has slightly higher ETa than in Lothar and Manahari catchments. The Chitwan valley has comprises of intensive farming area and protected forest in between East and West Chitwan. It has higher annual ETa than the Rajaiya, Manahari and Lothar and slightly lower annual ETa than the National Park.

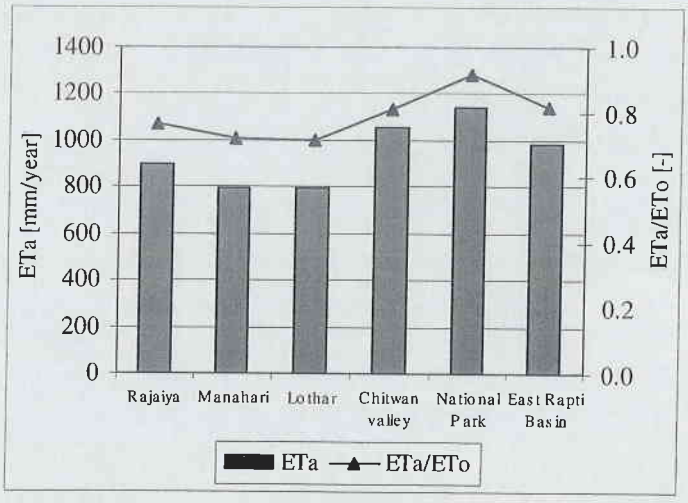

Figure 4.13: Average annual ETa and ETa/ETo by catchments

The highest annual ETa is found in the forests located in foothills oriented towards the sun. The sunlit slopes receive higher solar radiation per unit area than others and soil moisture is abundant in foot hills due to subsurface flow. This explains high ETa from the region. Maximum annual ETa is found 1478 mm whereas maximum annual ETo is 1411 mm. This gives a relative coefficient of 1.05, which is quite reasonable. Among the Land cover classes, water exhibited higher average annual ETa (1217 mm y^{-1}) with the average annual relative coefficient close to one (**Table 4.6**). It is slightly lower than normally expected value (i.e. greater than one). This may be due to the fact that, there are very low pure water pixels in the study area as there are no storage reservoir exit within the basin, perhaps also turbid water due to sediments and erosion. Among the vegetated area, average ETa is higher in bush, this may be due to error in land cover classification or effect of extreme value on arithmetic mean. While preparing the land cover map, all the pixels, which were classified as cultivated land within the National Park were assigned bush. The bush area is very small compared to forest and cultivated classes. And most of them are appeared in flat valleys along the river course, where ETa is higher in general. Few high values would have higher effect on overall mean from a lower numbers of pixels. The agricultural area shows average annual ETa of 960 mm y^{-1} with relative coefficient of 0.75.

Table 4.5: Average monthly and annual ETa by land cover type [mm]

Land cover	Jan	Feb	Mar	Apr	May	Jun	Jul	Aug	Sep	Oct	Nov	Dec	Annual
Forest	47	55	86	106	116	116	113	108	96	82	56	47	1029
Cultivated[6] land	34	42	72	96	114	125	121	114	97	69	43	33	960
Grass/grazing	32	42	74	100	118	124	120	113	96	57	38	30	944
Bush	42	52	85	112	128	130	125	118	101	80	52	41	1065
Sand/Gravel	18	26	53	75	96	114	108	102	85	36	23	16	753
Bare	14	18	35	50	66	83	79	71	57	26	17	14	528
Built-up area	31	39	69	95	117	129	124	117	99	57	39	30	946
Water body	50	62	101	131	147	144	139	131	112	92	60	47	1217
Unclassified	1	2	3	6	11	16	15	11	7	4	2	2	80

Table 4.6: Average monthly and annual relative coefficient (ETa/ETo) by land cover type [-]

Land cover	Jan	Feb	Mar	Apr	May	Jun	Jul	Aug	Sep	Oct	Nov	Dec	Annual
Forest	0.83	0.75	0.76	0.76	0.79	0.92	0.98	0.95	1.01	0.92	0.80	0.84	0.86
Cultivated land	0.62	0.57	0.60	0.63	0.71	0.90	0.95	0.93	0.97	0.76	0.63	0.63	0.76
Grass/grazing	0.56	0.54	0.58	0.61	0.69	0.83	0.90	0.87	0.91	0.60	0.54	0.57	0.71
Bush	0.75	0.69	0.69	0.71	0.77	0.90	0.97	0.94	0.99	0.86	0.75	0.77	0.82
Sand/Gravel	0.33	0.34	0.43	0.47	0.58	0.79	0.83	0.80	0.82	0.39	0.33	0.32	0.58
Bare	0.34	0.31	0.36	0.38	0.46	0.65	0.68	0.65	0.67	0.36	0.32	0.34	0.49
Built-up area	0.55	0.51	0.55	0.59	0.70	0.89	0.95	0.92	0.96	0.61	0.56	0.56	0.72
Water body	0.87	0.81	0.80	0.81	0.86	0.98	1.05	1.02	1.07	0.97	0.85	0.88	0.92
Unclassified	0.06	0.04	0.05	0.06	0.09	0.15	0.16	0.13	0.12	0.09	0.06	0.07	0.10

According to previous estimate (IWMI-Nepal, 2000b)[7] the average annual ETa in the East Rapti basin for average year was 390 mm in agricultural land, 718 mm in dense forest, 629 mm in grass. These figures are significantly lower than current estimate (**Table 4.5**). This low figure is due to the way in

[6] The term cultivated land represents agricultural land only in this document.
[7] Derived from Table 4 in Page 10 and Appendix 4.5 in Page 27 of (IWMI-Nepal, 2001a.)

which ET was calculated. In the previous estimate effective rainfall and potential ET was computed for every 10 days of the crop-growing season. If effective rainfall is less than potential ET, then actual ET is taken to be equal to effective rainfall except for the irrigated crops. The main error in this kind of computation is that it does not accounted the evaporative depletion of soil moisture from root zone depth. The rainfall pattern showed that about 93% rainfall occurs from June to October. Very nominal rainfall receives in the remaining months. During these months, the evapotranspiration is contributed from the soil moisture from root zone depth, which was not accounted in previous estimation. This explains the very low ET observed in previous estimation.

According to Jhorar (2002), the cumulative (for 270 days) ETa estimated from remote sensing in the Sirsa Irrigation Circle in India was ranges from about 460 to 700 mm. At an annual basis this will be around 650 to 950 mm. Bastiaanssen & Bandara (2001) reported that the SEBAL derived average annual ETa from an irrigated watershed (Kirindi Oya) in Sri Lanka was 1356 mm/year. The country average for Sri Lanka is 1279 mm y^{-1} (Bastiaanssen *et al.*, 2003). Bastiaanssen *et al.* (2002) found that the mean seasonal ETa from rice, wheat and sugarcane in Indus Basin is 410, 360 and 970 mm respectively and the annual ETa ranges from 500 mm y^{-1} to 1275 mm y^{-1}. The results of present study supports these published figures of annual ETa (**Figure 4.13** and **Table 4.5**).

4.5. Water balance

As the images do not cover entire basin, the hydrological boundary from the confluence of Khageri and East Rapti rivers (**Figure 4.14**) is considered for water balance computation. This boundary is termed as Rapti sub-basin (or simply sub-basin) hereafter and the basin indicates the entire area covered by the images. The confluence point is located about 34.5 km up-stream from the basin outlet and its catchment area is about 2217 km^2.

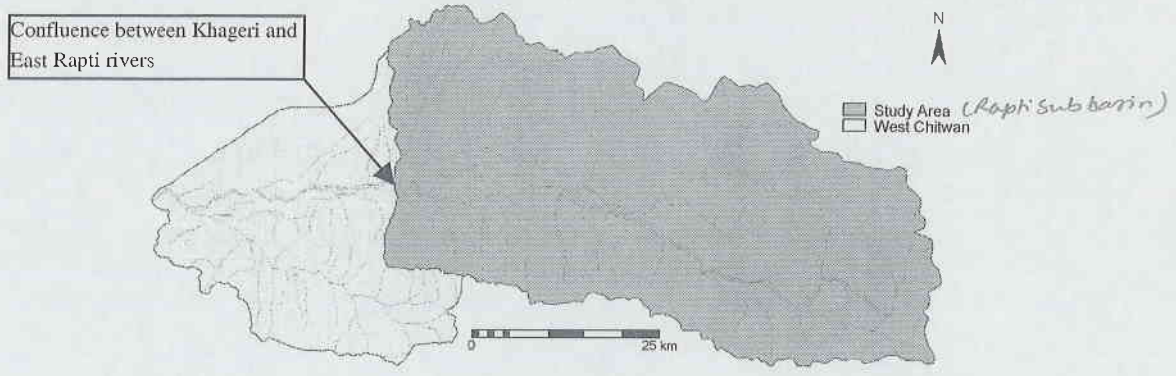

Figure 4.14: Hydrological boundary of the Rapti sub-basin.

The water balance is a simple accounting procedure that is based on the conservation of mass principle. The central idea applied in any hydrological system is simply that the algebraic sum of all flow elements can be equated to zero when additions and losses are given with an opposite sign.

This section mainly focuses on the runoff estimation from the sub-basin and the selected catchments. The longterm average data were used to compute the water balance components for the case of an av-

erage year. Rainfall and inflow from Kulekhani reservoir were the components of the inflow to the sub-basin. Outflow constitutes evaporative depletions and river runoff. The domestic and industrial depletion terms were very low i.e. about 4.5 million m^3 (Mm^3) per year, which could be neglected in monthly water balance analysis. Monthly average evaporative depletion was taken from SEBAL results. For the long term analysis annual change in storage was considered zero, assuming that the basin storage is steady and only subject to random seasonal fluctuation.

River runoff measurement is an important aspect of water resources management in a river basin. Traditionally, river runoff is estimated from rainfall events, soil properties, antecedent moisture and vegetation cover using empirical relationships such as the Soil Conservation Service Curve Number method (Schaake *et al.*, 1996). Bastiaanssen & Chandrapala (2003) suggested a simple and novel approach to estimate the river run-off, which incorporates ETa directly into the water balance and compute river runoff as the rainfall surplus (Sp). Similar method is applied in this study with slight modification according to data availability.

There are three gauging stations that measure river flow in the East Rapti river basin. All of them are located in the upper part of the basin. Out of these three, the Rajaiya station is considered to be more reliable in terms of data availability. Also, according to topographic setting, the catchment of Rajaiya is more representative to the basin than the other two stations. So, run-off records of Rajaiya station have been used to estimate the catchment run-off in this analysis.

The monthly rainfall surplus (Sp) for every pixel is taken as the difference between monthly rainfall (P) and ETa as follows:

$$Sp = P - ETa \qquad [mm] \qquad (4.1)$$

To take into account the delayed response in the catchment due to storage mechanisms and subsequent releases, Sp is adjusted by taking moving average of two months.

$$Sp_{mavg} = (Sp\_pre + Sp)/2 \qquad [mm] \qquad (4.2)$$

Where, Sp_pre is the rainfall surplus for previous month and Sp is rainfall surplus for current month.

This adjusted surplus rainfall was plotted against the observed run-off depth for the Rajaiya catchment.

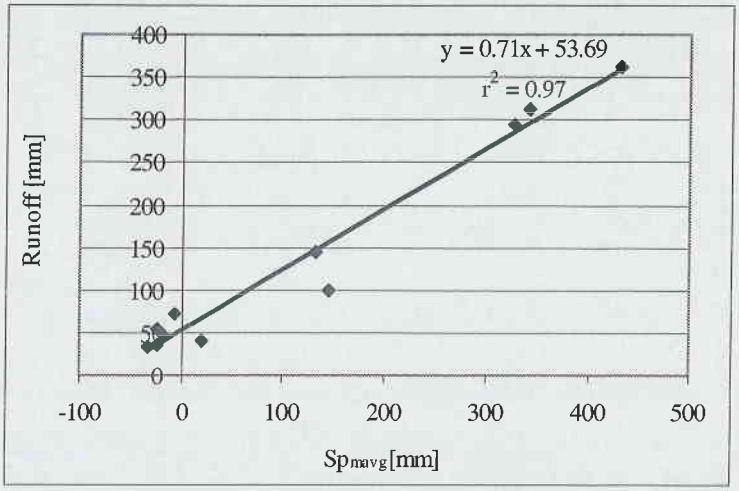

Figure 4.15: Scatter plot of rainfall surplus and run-off depth for the Rajaiya catchment

The scatter plot shows that there is high statistical relation (r^2=0.97) between rainfall surplus and the run-off depth. Using the linear constants for the Rajaiya catchment, the monthly catchment run-off depth (R in mm) was estimated by the relation:

$$R = 0.71\ Sp_{mavg} + 53.69 \qquad [mm] \qquad (4.3)$$

Which basically expresses that there is a permanent base flow.

The monthly water balance components for Rajaiya catchment are summarized in Table 4.7.

Table 4.7: Monthly water balance components for the Rajaiya catchment

Catchment: Rajaiya — Catchment Area: 570 km^2

Parameter	Unit	Jan	Feb	Mar	Apr	May	Jun	Jul	Aug	Sep	Oct	Nov	Dec	Annual
Rainfall (long term)	mm	14	16	25	59	166	337	565	508	339	86	15	19	2149
ETa (2001/02)	mm	35	41	67	85	99	111	108	104	92	70	45	36	893
Surplus rainfall		-21	-25	-42	-26	67	226	457	404	247	16	-30	-17	1256
Sp_{mavg}		-19	-23	-34	-34	20	146	341	431	326	132	-7	-24	1256
Observed discharge (long term)	m^3s^{-1}	10.2	8.8	7.4	7.3	8.5	22.0	66.4	77.1	64.4	30.7	16.0	11.7	27.5
Observed runoff depth (long term)	mm	48	37	35	33	40	100	312	362	293	144	73	55	1532
Estimated Runoff (long term)	mm	40	37	30	30	68	157	295	358	284	147	49	37	1532
Estimated discharge (long term)	m^3s^{-1}	8.6	8.8	6.4	6.5	14.5	34.5	62.8	76.2	62.4	31.2	10.7	7.9	27.6
Rest term	mm	-69.0	-62	-76	-59	26	126	144	42	-45	-128	-103	-71	-277

From **Table 4.7** it could be noted that the water balance rest term is –277 mm y^{-1}. This indicates there is abstraction from the storage when the rest term is negative and there is addition to storage when the rest term is positive.

From water balance analysis of Rajaiya catchment it could be noted that the annual value for rest term possibly due to error in rainfall or ETa estimation. As described in previous section, the estimated average range of ETa is quite reasonable whereas uncertainty was observed in rainfall patterns. So, the rest term has been considered as an error due to rainfall patterns and included in gross inflow for convergence of the water balance during water accounting analysis. The rest term is 12% of the rainfall, which is acceptable.

A comparison of observed vs estimated longterm river runoff according to the calibration procedure in **Figure 4.15** and equation 4.3 at the Rajaiya and the observed vs estimated longterm runoff using coefficient of equation 4.3 at the Manahari catchments are presented as **Figure 4.16**.

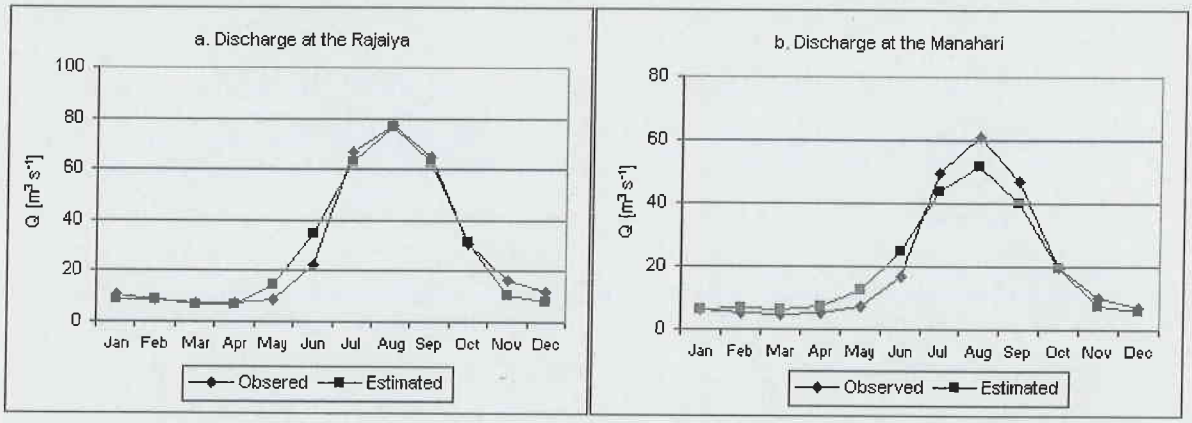

Figure 4.16: a) Observed vs estimated longterm river flows according to the calibration procedure in Figure 4.15 and Equation 4.3; b) Observed vs estimated longterm runoff using the coefficient of equation 4.3 at the Manahari.

In the Manahari catchment, the model underestimates in wet months. This indicates the runoff coefficient (runoff/rainfall) is higher in Manahari than that of Rajaiya. But, the model performed well in dry months. In annual scale the observed runoff is higher than estimated run-off by only 45 mm. The Manahari catchment receives about 84 Mm^3 inflows from the Kulekhani hydropower per year. This is equivalent to 195 mm per year for the Manahari catchment. If we consider this flow in the observed flow, the estimated flow is slightly higher. The water balance components are given in Appendix 6.

The monthly water balance components for the sub-basin are summarized in **Table 4.8.**

Table 4.8: The estimated monthly water balance components for the Rapti sub-basin.

Catchment area: 2217 km^2

Parameter	Unit	Jan	Feb	Mar	Apr	May	Jun	Jul	Aug	Sep	Oct	Nov	Dec	Year
Rainfall (long term)	mm	14	16	28	59	158	322	545	463	298	76	12	20	2011
Inflow from Kulekhani	mm	4	4	5	6	5	1	1	2	2	3	2	2	38
ETa (2001/02)	mm	40	47	75	96	108	114	110	106	93	73	49	40	951
Estimated runoff (long term)	mm	37	34	26	24	58	145	281	334	252	127	42	34	1394
Rest term	mm	-59	-61	-68	-55	-3	64	155	25	-45	-121	-77	-52	-296

4.6. Land cover

The area is segmented in two parts, flat valley and hilly area. The Land cover map were created separately and joined together to get land cover map for the basin.

4.6.1. Supervised classification in the flat valley area

The available images were corresponds to two crop seasons in the flat valleys of the basin. The October image corresponds to the *Kharif* (summer) season. Paddy is the main crop during the season. Some of the farmers already harvested the paddy during the image date. Many clear paddy fields can be seen in the image. The sample points from the standing paddy field were also collected from the west Chitwan (mid western part of the image), where the paddy was in mature stage during the image date. The other main crop was maize, which was in growing stage during the satellite overpass day. Next two images correspond to *Rabi* (winter) season. Wheat, lentil, oilseed were the main crops during this season. December image correspond to early stage of winter crop whereas March image correspond to mature stage of winter crop.

The image acquired on 24 October 2001 was classified (supervised) into 12 different land cover classes identified during the fieldwork (forest sparse, forest dense, paddy, maize, clear paddy field, grass, bush/shrubs, sand and gravel, bare, water, built-up and wet river bed). Out of 192 sample points colleted during the field survey (September and October, 2002), 109 were used as training samples and the remaining were used for accuracy assessment. Additional samples points were created from the identified plots on the hard copy of the image. The maximum likelihood estimator was applied for the classification. An accuracy matrix was created for the independent assessment of the accuracy of the classification (Appendix 7). The accuracy matrix shows overall classification accuracy of 77%. Which is satisfactory for the detailed land cover classification.

The field work was carried out only in the East Chitwan valley, no cover details was collected from the mountainous area. The classified land cover classes were grouped in general land cover classes. All land covered by crops and the clear paddy field were grouped as cultivated, the sparse and dense forest were grouped into single class forest. The wet riverbed was included into sand and gravel. Finally the classified image for October 2001 was made for flat valley with eight land cover classes i.e. forest, cultivated (agricultural land), grass/grazing, bush, sand and gravel riverbed, bare, builtup area and water body.

Similarly, the image acquired on 01 March 2002 was also classified into 11 cover classes. The cultivated land constitutes 3 major crops wheat, lentil and oilseed in this case. The lentil and oilseed are grown as mixed crop in most of the cases. Other land cover classes are same as above. Again, the classified cover classes were groped into general land cover classes. The accuracy matrix was prepared with general land cover classes. The overall accuracy was 84.5%. The accuracy is higher due to grouping of more detail cover classes in to a single class.

The independently classified land cover maps were overlaid into one map to get the final land cover map for flat valley area.

4.6.2. Band ratio method in the mountainous area

Due to shadow effect on mountain environment, accurate classification of land cover may not be possible. Meijerink *et al.* (1994) concluded that the simplest classification method using the band ratio of red band (band 3) and near infrared band (band 4) gives more satisfactory result on land cover classification in mountainous area.

As there is not ground truth points available form the hilly part of the basin, the topographic maps were used to create training samples. Four general land cover classes forest, cultivated, bush and bare were noted according to the topographic maps. Forest was characterized by all natural and planted forest area. Cultivated land represents all the agricultural land. Bush includes grass and bamboo also. Bare class represents all bare land, rock out crops, sand and gravel riverbed. The topographic map of Hetauda (sheet no. 2785 09A) area was used as ground truth. The northern part of Hetauda sheet is characterised by mountains, the middle part is small valley where Hetauda town located and the southern part is the Siwalik hills. The Hetauda sheet was selected simply because of the availability of digitised land cover map of some part of the sheet at the ITC (Joshi, 2001).

Feature space of band 3 and band 4 was created to identify the threshold values on the band ratios for separating the identified classes. From the feature space, the threshold values for each identified cover classes were computed. The feature spaces of two Landsat dates were presented as **Figure 4.17** and the computation of threshold values is summarized in **Table 4.9** and **Table 4.10**.

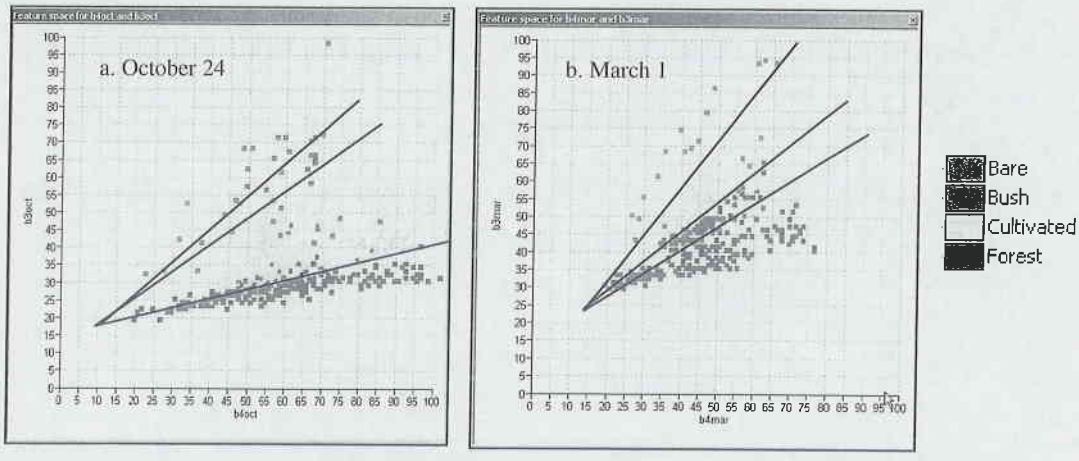

Figure 4.17: Feature spaces for hilly area

Table 4.9: Band ratio range for the land cover class – 24 October 2001

Origin shift:	Band 3 = 17		Band 4 = 10		
Land cover	DN Values				Band ratio
Class	B3	B4	B3_new	B4_new	B3_new/B4_new
Bare	-	-	-	-	>0.97
Bush	75	70	58	60	0.78 - 0.97
Cultivated	64	70	47	60	0.22 - 0.78
Forest	30	70	13	60	< 0.22

Table 4.10: Band ratio range for the land cover class – 1 March 2001

Origin shift:	Band 3 = 25		Band 4 = 15		
Land cover	DN Values				Band ratio
Class	B3	B4	B3_new	B4_new	B3_new/B4_new
Bare	-	-	-	-	> 1.44
Cultivated	97	65	72	50	0.86 - 1.44
Bush	68	65	43	50	0.80 - 0.86
Forest	65	65	40	50	< 0.80

The values identified as origin shifts from the feature spaces were subtracted from the original images to create new image (B3_new and B4_new). The negative values were forced to 1. Then the new band ratio image (B3_new/B4_new) was classified according to the computed threshold values using slicing operation in ILWIS. In the histogram of extraterrestrial radiation map, the peak relating to the lowest extraterrestrial radiation was considered the deep shadows. Corresponding pixels were assigned unclassified class. The band ratio method was applied in October and March images. As explain above October image represents *Kharif* season and the March image represents *Rabi* season. These two maps were overlaid to get the land cover map for hilly area using decision criteria according to **Table 4.11**.

Table 4.11: Decision matrix for merging two conflicting classes in two seasons:

March / October	Cultivated	Forest	Bush	Bare
Cultivated	Cultivated	Forest	Bush	Cultivated
Forest	Cultivated	Forest	Cultivated	Cultivated
Bush	Cultivated	Forest	Bush	Bush
Bare	Cultivated	Cultivated	Cultivated	Bare

4.6.3. Final land cover map of the basin

Finally, the classified maps for valley area and hilly area were joined together to prepare a final land cover map, which is presented as **Figure 4.19**.

Table 4.12: Percentage distribution of land cover/use in East Rapti river basin –present classification

Landuse Type	Area [km^2]	%
Forest	1734.15	65.4
Cultivated (Agricultural) land	739.15	27.9
Grass/grazing	9.08	0.3
Bush	66.90	2.5
Sand/Gravel	51.55	1.9
Bare	44.71	1.7
Built-up area	1.94	0.1
Water	2.50	0.1
Total	2649.99	100

To get the general idea about the overall accuracy of the classification, the land cover/use distribution was compared with the land use distribution reported by IWMI 2000.

Figure 4.18: Comparison of percentage distribution of land cover/ use in East Rapti basin: Present estimate and (IWMI-Nepal, 2000a)

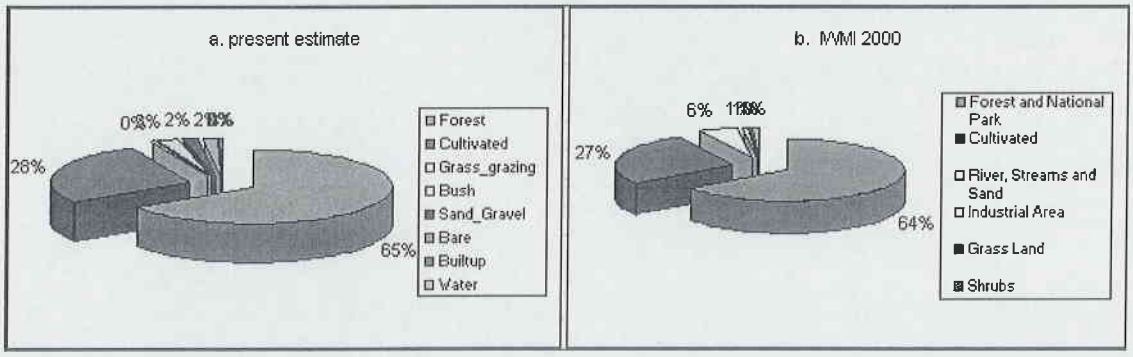

From **Figure 4.18**, it could be noted that the percentage distribution of major land cover/use classes forest and cultivated are very much close to each other. Deviation is only 1% in both classes. Very nominal differences could be noted in other classes.

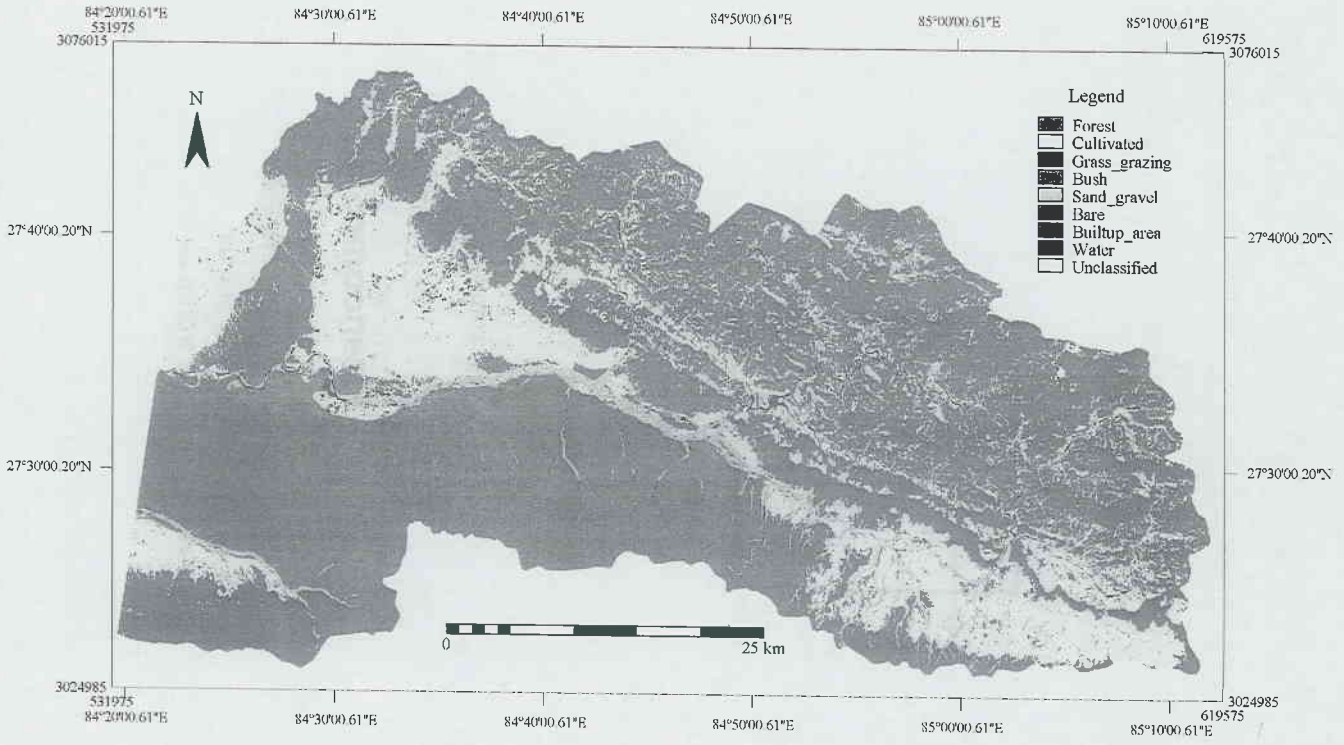

Figure 4.19: Land cover map of the East Rapti river basin (2001/02)

Note: The sand and gravel riverbed in the hilly area is included in the bare class.

Chapter 5. Water accounting

The analysis could not be carried out for entire basin because the images do not completely cover by the area. The hydrological boundary from the confluence of Khageri and East Rapti rivers is considered as the hydrological domain for analysis. As stated earlier, the Rapti sub-basin or simply sub-basin indicates the hydrological boundary of the confluence between the East Rapti river and the Khageri river. Three sub-watersheds, the Rajaiya, the Manahari and the Lothar (**Figure 2.5**) are selected for water accounting analysis at the catchment scale. The process explained by Molden & Sakthivadivel (1999) is followed with slight modification according to the data availability. The analysis is carried out on the basis of long-term average data for the case of an average year in the sub-basin.

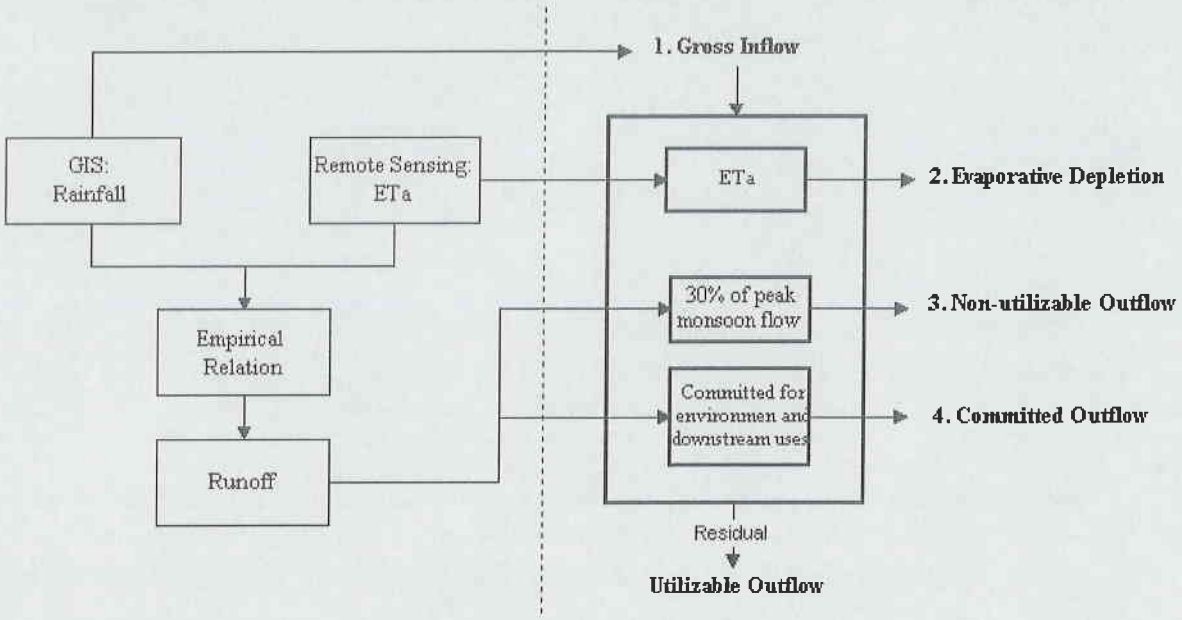

Figure 5.1: Geo-information procedures for quantifying the water accounts.

5.1. Water accounting components

Gross inflow: Sum of rainfall and inflow from Kulekhani hydropower is considered as gross inflow. The water balance closure term is considered due to the uncertainty in the spatial patterns of the rainfall. This quantity is also included in the gross inflow to close the water account.

Storage change: Since the computation is based on long term average data, the annual change in storage is considered zero.

Net inflow: Net inflow is calculated as sum of gross inflow and storage change.

Outflows: The river runoff at the out let of the sub-basin is further divided as follows:

***Committed outflow*:** The Royal Chitwan National Park is located at the tail-end of the basin. IWMI-Nepal (2000b) allocated a flow of 15 $m^3 s^{-1}$ at the outlet of the basin (entire basin) as requirement to

maintain environmental and touristic activities in the park. This figure was estimated based on the assumption that at least flow must take place in a width of 50 m and a depth of 1 m flowing with a velocity of 30 cm s^{-1}. A flow of 15 m^3 s^{-1} is equivalent to 473 Mm^3 per year. The same figure is considered in this analysis. It is assumed that the flow is contributed proportionately according to area. A volume 473 Mm^3 y^{-1} from entire basin is equivalent to 0.1522 Mm^3 km^{-2}. This multiplication factor is used to estimate contribution to the committed outflow from each catchment for the environmental requirement. At the sub-basin scale analysis, another committed outflow 12.5 Mm^3 is allocated for irrigation as the Khageri irrigation system tap water from the Khageri river to irrigate the tail-end part of the basin. This average figure is estimated as an average of 5 years flow data at the head works of the Khageri irrigation system, reported in IWMI (1998).

Uncommitted outflow: Though the outflow should have two values, one at present level of development and another is at optimum level of development. In this study, the outflow left over of committed outflow is considered as uncommitted outflow. The uncommitted outflow further classified into utilizable and non-utilizable. An assumption is made to quantify non-utilizable outflow. During the monsoon season, some portion of the flow cannot be tapped by general means of development. So, 30% of the peak monsoon flow (June to September) is considered *non-utilizable outflow*. The rest is categorized as *utilizable outflow*.

Available water: Available water is defined as the amount of water available to use in the sub-basin level without unsustainable withdrawal from storage. In this analysis, the difference between net inflow and both committed and non-utilizable outflows is considered as available water.

Process depletion: Water depleted by crops (ETa agriculture), domestic uses, animal uses and industrial uses are considered as process depletion. ETa from built up area is considered as the ETa from the home gardens. So, this is also categorized as process depletion. The non-ET depletions are very low. The depletion by domestic use, animal use and industrial use are computed for entire basin (Appendix 8). The domestic use and animal use are distributed proportionately by the catchment area. The Hetauda industrial district comes under Rajaiya catchment, thus 50% of the total industrial depletion is accounted in this catchment. No industrial depletion is accounted in the Manahari and the Lothar catchments.

Non-process beneficial depletion: Forest and grassland are important for environmental protection. Thus the water depleted by forest and grassland was considered as beneficial. Most of the Bush (Shrubs) lands are detected within the National Park area which is the main habitat of the endanger specie, the Rhino. In mountainous area the land cover class bush also includes all grazing lands, which is beneficial. So, evapotranspiration from bush land also considered non-process beneficial depletion.

***Non-process non-beneficial depletion*:** The evaporation from bare land, sand and gravel riverbed, water body are not beneficial for human activities. They are categorized to non-process non-beneficial depletion. ET from the unclassified area in the image is also included in this class.

5.2. Water accounting indicators

Three water accounting indicators are selected to explain the performance of water uses in the sub-basin.

- Depleted fraction of available water is selected to explain how much water available for use was depleted,
- Process fraction of available water is used to indicate how much water available was depleted by process uses and
- Beneficial utilization of available water indicates how much of the available water was depleted beneficially by both process and non-process uses.

5.3. Results

The water accounting results are presented as **Figure 5.2** to **Figure 5.5** and the detail results are given in **Table 5.1** along with the water accounting components for selected catchments. The values presented in the flow diagrams are in Million m^3 [Mm^3]. The computed indicators are listed in **Table 5.2**.

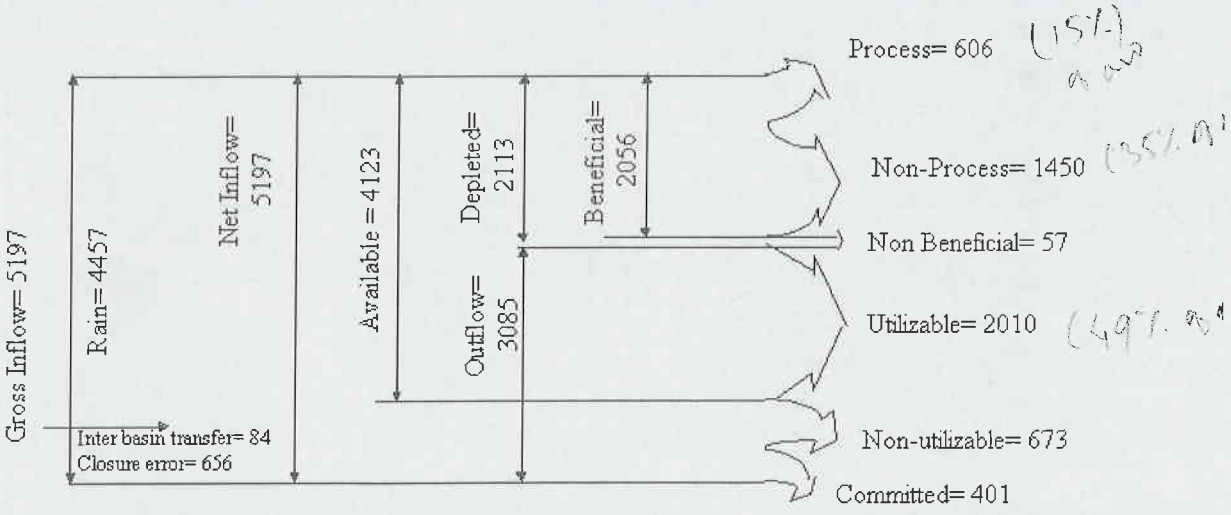

Figure 5.2: Flow diagram showing water accounting results for the Rapti sub-basin.

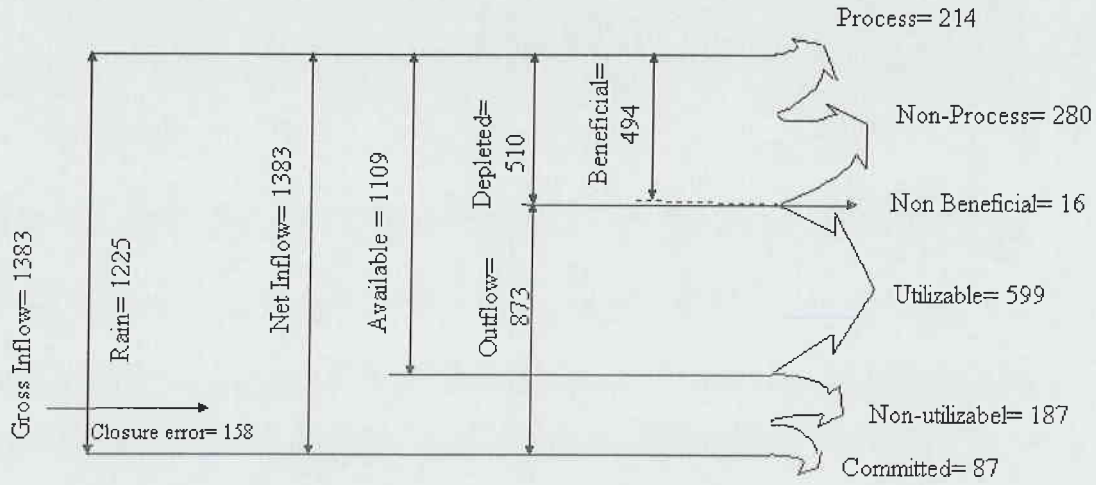

Figure 5.3: Flow diagram showing water accounting results for the Rajaiya catchment.

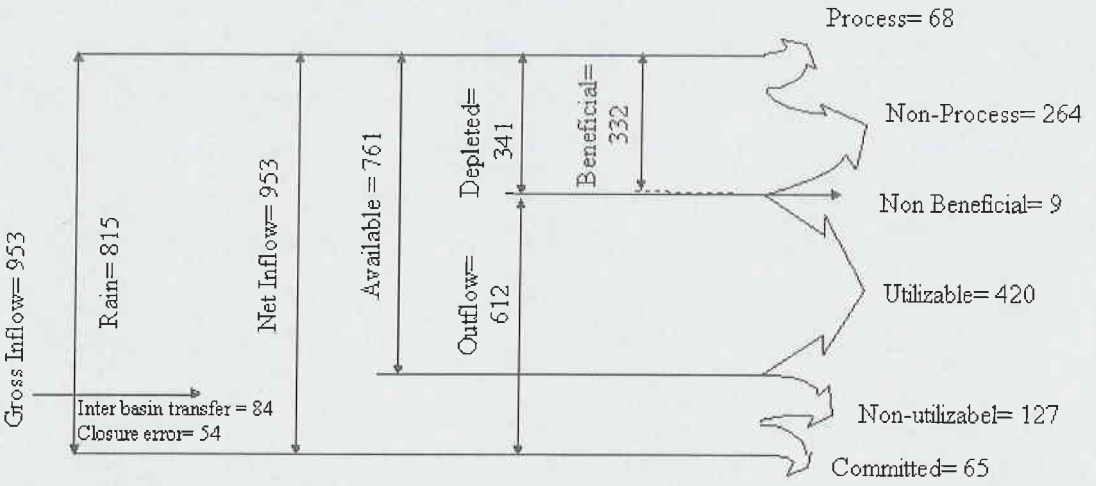

Figure 5.4: Flow diagram showing water accounting results for the Manahari catchment

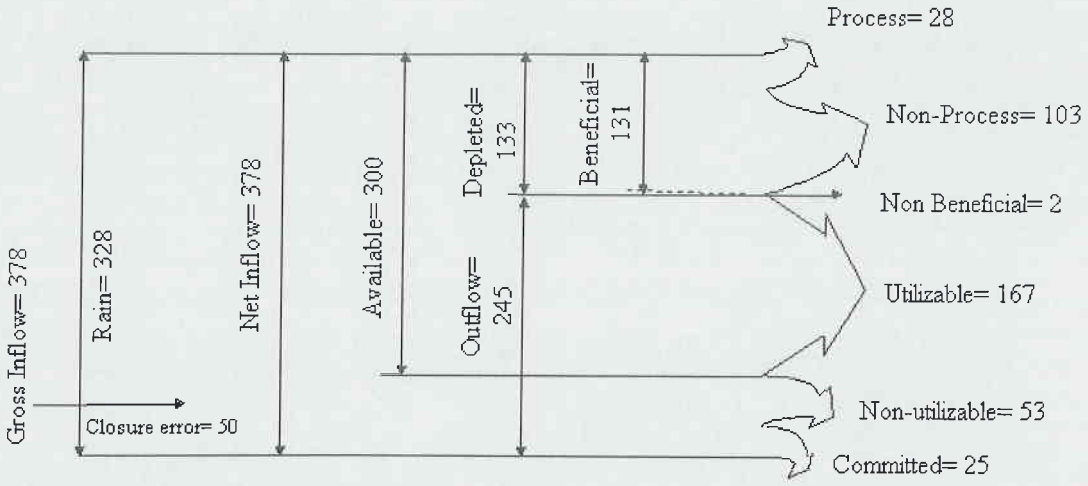

Figure 5.5: Flow diagram showing water accounting results for the Lothar catchment

Table 5.1: Water accounting components at different spatial scales in the Rapti sub-basin in (Mm^3)

Year of accounting: Average year (Long term average)

Description	Rapti Sub-basin (2217 km^2)		Selected Catchments					
			Rajaiya (570 km^2)		Manahari (429 km^2)		Lothar (167 km^2)	
	Total	Parts	Total	Parts	Total	Parts	Total	Parts
Gross Inflow	**5197.4**		**1382.4**		**952.8**		**378.4**	
Rainfall		4457.7		1224.9		815.2		328.2
Inter basin transfer (from Bagmati Basin)		83.9		0.0		83.9		0.0
Closure error		655.8		157.5		53.7		50.1
Storage change	**0.0**		**0.0**		**0.0**		**0.0**	
Net Inflow (NI)	**5197.4**		**1382.4**		**952.8**		**378.4**	
Depletion	**2112.6**		**510.0**		**341.0**		**133.2**	
Process	*606.1*		*213.3*		*67.9*		*28.0*	
ET cultivated land		597.8		210.9		66.6		27.5
Domestic uses		4.5		1.1		0.9		0.3
Animal use		2.1		0.5		0.4		0.2
Industrial uses		0.2		0.1		0.0		0.0
ET home garden		1.6		0.5		0.0		0.0
Non-process, beneficial	*1449.9*		*280.3*		*264.1*		*103.0*	
ET Forest		1396.4		277.8		262.6		102.2
ET bush, grass		53.5		2.5		1.4		0.8
Non-process, non-beneficial	*56.6*		*16.4*		*9.1*		*2.3*	
Outflow	**3084.9**		**873.0**		**611.8**		**245.1**	
Committed (CO)	*401.4*		*86.8*		*65.3*		*25.4*	
Committed for environment		*337.4*		*86.8*		*65.3*		*25.4*
Committed for irrigation (khageri)		*64.1*		*0.0*		*0.0*		*0.0*
Uncommitted	*2683.3*		*786.3*		*546.5*		*219.7*	
Utilizable		2010.4		599.1		419.6		167.3
Non-utilizable (NUO)		672.9		187.1		126.9		52.5
Available water (NI-CO-NUO)	**4123.0**		**1108.6**		**760.6**		**300.5**	

Table 5.2: Water accounting indicators at different spatial scales in the Rapti sub-basin

Indicator	Definition	Rapti Sub-basin	Catchments		
			Rajaiya	Manahari	Lothar
Depleted fraction of available water (DFAW)	TD/AW	0.51	0.46	0.45	0.44
Process fraction of available water (PFAW)	PD/AW	0.15	0.19	0.09	0.09
Beneficial utilization of available water or basin efficiency (BU or BE)	Db/AW	0.50	0.45	0.44	0.44

The water accounting analysis demonstrated that only 51% of the available water is depleted within the domain of the Rapti sub-basin, the remaining 49% of available water is flowing out of the sub-basin as utilizable outflow. As utilizable outflow takes place throughout the year from the sub-basin, it is still an "open basin". On the catchment scale, slightly smaller part of available water is depleted within the domain than in the sub-basin.

The process fraction of available water is found 15% for the sub-basin, which indicates only a small portion of available water is depleted by the human intended processes. A slightly higher value (19%) is found in Rajaiya. This is due to the fact that the Rajaiya catchment comprises Hetauda town as well as the Hetauda industrial area. It explains why the process fraction is slightly higher in Rajaiya catchment than in others, whereas the process fraction of available water is amounted to only 9% in Manahari and Lothar. This indicates that only a small portion of available water is depleted by processes for human consumption like irrigation, drinking water, industrial uses etc. in the East Rapti river sub-basin.

The beneficial utilization of available water indicates how much available water is depleted by both process and non-process beneficial uses. In the sub-basin the beneficial utilization of available water is 50%, the non-beneficial consumption accounts for only 1% and a bulk of the consumptive use is by forest, which is considered beneficial. This indicates that there is still 49% of available water, which can be used for beneficial purposes. The beneficial utilization is slightly lower in the selected catchments. There is no great difference in beneficial depletion among the catchments.

From the water accounting indicators it can be concluded that there is no great difference in the water use performances among the catchments. Values of depleted fraction and beneficial utilization are close in all catchments. However a difference is observed in values for process fraction. Based on the process fraction values, the Rajaiya catchment is performing better than the Manahari and Lothar.

It can be concluded from the water accounting analysis of the sub-basin that there is high potential to increase the beneficial depletion in the sub-basin. An utilizable outflow of 2058 Mm^3 per year is leaving the sub-basin and this flow can be diverted for irrigation. The East Chitwan area (**Figure 4.11**) is the one of the potential areas for irrigation development. Most of the northern part of the area is not served by existing irrigation facilities and there is more irrigation demand in the southern part also. During the winter season, a large area in the East Chitwan valley is covered by lentile and oil-

seed crops, which are mainly non-irrigated. This implies that there is still higher irrigation demand in the East Chitwan valley. And the available utilizable outflow can be used to fulfil this demand.

At present there is no any storage reservoir to tap the available utilizable outflow in the East Rapti river. A proposal was made to divert the river water for irrigation in the past, but this was not implemented for unknown reasons. One of the main reasons may be the depth of water to be maintained for National Park activities. Everybody seems to agree that a minimum flow is to be maintained for flora and fauna of the park, to feed to the wild life and to cater for touristic activities. Present study shows that the evapotranspiration in the National Park is higher than in other parts and the reference coefficient is close to one for this area (**Figure 4.13**). This implies that the flow requirement in the river is mainly for non-ET requirements such as maintaining aquatic life in the river, touristic activities (boating in the river) and to feeding wild life. It is necessary to analyse carefully, how much flow is needed in the river to fulfil these non-ET requirements, before making a meaningful development plan for the basin's available water resources.

Another possible area is to exploit the ground water storage in the sub-basin. The analysis of rainfall runoff indicated that the river flow is mainly due to the base flow during the dry months. More than 90% of the annual rainfall occurs in six months of monsoon period (May to Oct) and July and August received nearly 50% of annual rainfall. In other six months, the rainfall is very low and does not contribute to surface runoff. However there is sizable flow in the river, which is due to the base flow. This indicates there is potential to tap the ground water in the sub-basin. Because of the close interaction between dry weather flow and ground water storage, it is necessary to investigate and understand the interaction between the river flow and ground water storage.

Chapter 6. Conclusions

6.1. Remote sensing for water accounting

The growing competition for water between various users is leading to increased conflict. To meet the future demand of these competing users, an understanding is needed on how much water is available, is being used and depleted by various users in a river basin. But, the complexity of interaction between various users is difficult to understand. Water accounting is one of the tools to help to generate such understanding.

Evaporative depletion is the one of the key components in water accounting. The difficult topography in the mountainous catchments made the assessment of ET more complex as ET varies significantly according to surface steepness and orientation in mountain environment. The results achieved in this study confirm that the spatial patterns of evapotranspiration can be assessed by the SEBAL remote sensing technique. A mountain radiation model was deemed necessary to dealing with sloping surfaces. SEBAL needs only wind speed and radiation data (sunshine hours) as input to compute actual evapotranspiration. If these data are not available, the IWMI Water and Climate Atlas can be used. Use of a DEM for slope and aspect correction for solar radiation and a lapse correction on surface temperature provides opportunity to apply SEBAL in mountainous catchment. The average annual ETa in the East Rapti river basin is 987 mm y^{-1}. The mountainous catchments (Manahari and Lothar) depleted less water per unit area by evapotranspiration than other catchments due to their sloping terrain. The highest mean annual ETa of 1144 mm y^{-1} is found in the Royal Chitwan National Park area.

Land cover mapping is another important application of remote sensing. For the mountainous catchment, a simple method of band ratio between red and near infrared bands (band 3 and 4 in Landsat-7) can be used to distinguish general land cover classes. By overlaying SEBAL derived ETa with the land cover map, the evaporative depletion by land cover type can be quantified. In the East Rapti basin, the agricultural land evaporates an average rate of 960 mm y^{-1} whereas a higher mean annual ETa of 1029 mm y^{-1} is found in the forests.

Another important component of water accounting analysis is the outflow. A high statistical relationship (r^2=0.97) between rainfall surplus and river runoff is found for the East Rapti river basin. There is no flow measurement station available at the outlet of the entire basin. A simple approach of rainfall surplus was applied to estimate river runoff.

The evaporative depletions and outflows are the major components of the water accounting analysis. The water accounting analysis in the East Rapti basin showed that only 51% of available water is depleted in the basin. The remaining 49% of available water is leaving the basin. As there is utilizable outflow throughout the year, the basin is still an "open" basin. This indicates there is a high potential for further development of the water resources in the basin. The beneficial utilization showed that only 50% of the available water is depleted by beneficial uses such as agriculture (ET crop), environmental conservation (ET forest), domestic and industrial uses. Out of remaining 50% of the available water only about 1% is currently used by non-beneficial uses (e.g. ET bare land, sand and gravel river

bed) whereas the rest is flowing out of the basin. The utilization of water resources can be improved if this water can be diverted for irrigation to the East Chitwan area (**Figure 4.11**), mainly the northern part of the valley.

One main aspect to give attention to are the costs. The main costs involved in this study are the costs of three Landsat-7 images. The Lansat-7 images are available for US$ 600 per scene. The new ASTER radiometer could be used instead of Landsat-7, which is relatively cheaper (US$ 55) as well as better in spatial and radiometric resolution. Another cost factor is the software requirement to process satellite data. In the present analysis, all the analysis related to remote sensing and GIS application are carried out in ILWIS environment. ILWIS is much cheaper but more limited than other remote sensing softwares like ERDAS imagine. Next cost component is the professional skilled manpower involvement. A few months of young professional and a couple of weeks of an expert's involvement can easily perform this kind of analysis. This shows that the remote sensing method applied in this study is cost effective unlike traditional ground base methods, which are time consuming and data demanding.

6.2. Recommendation for further research

- The water balance on an annual basis is not closed and the water balance closure term is about 12% of the rainfall. This closure term needs more attention in the future.
- The rainfall patterns in the basin indicate that there is micro-climate effect on rainfall in the area, which causes significant uncertainty in the total rainfall estimation of the catchment. The uncertainties of spatial patterns of rainfall distribution have to be analysed further.
- The dry season flow is mainly contributed by the sub-surface storage, which implies that there is a strong storage effect. This complex sub-surface storage mechanism needs to be understood better by a few simple "fitting" parameters.
- In the present analysis, the solar radiation is corrected for surface steepness and orientation. The shadow effect is not incorporated yet. The shadow plays a significant role on ecological processes like evapotranspiration and carbon assimilation of natural vegetation. The effect of shadows on evapotranspiration process is to be analysed.
- The Royal Chitwan National Park is the one of the main attractions in the basin. An analytical study should be carried out to quantify the actual flow requirement in the East Rapti river to fulfil the non-ET requirements for the National park activities before making a meaningful development plan to use the available water resources in the basin.

References

Allen, R. G., Pereira, L. S., Dirk Raes, D., & Smith, M. (1998). *Crop evapotranspiration : guidelines for computing crop water requirements.* Rome, Italy.: FAO irrigation and drainage paper ; 56. http://www.fao.org/docrep/X0490E/x0490e00.htm.

Allen, R. G., & Tasumi, M. (2000, January 6, 2003). *Appendix B: Algorithms for applying SEBAL to sloping or mountainous areas. Application of the SEBAL methodology for estimating consumptive use of water and stream flow depletion in the Bear River basin of Idaho through remote sensing.* [PDF Format]. Idaho Department of Water Resource. http://www.idwr.state.id.us/gisdata/ET/final_sebal_page.htm. Retrieved, 2002, from the World Wide Web:

Allen, R. G., Willardson, L. S., & Fredriksen, H. D. (1997). *Water use definitions and their use for assessing the impacts of water conservation.* Proceedings of the ICID Workshop: "Sustainable Irrigation in Areas of Water Scarcity and Drought", Oxford, England, 11-12 September, 1997, J.M. deJager, L.P. Vermes, R. Ragab (eds).

ASCE-Manuals. (1996). *Hydrology handbook/prepared by the Task Committee on Hydrology Handbook of Management Group D of the American Society of Civil Engineers.* (2nd ed.). (ASCE manuals and reports on engineering practice; no. 28): The American Society of Civil Engineers.

Basnyat, D. B. (2001). *River basin approach to water resources planning and management. Paper presented at a one-day workshop at the Department of Irrigation, Kathmandu, Nepal. 31 August 2001.*

Bastiaanssen, W., & Chandrapala, L. (2003). Water balance variability across Sri Lanka for assessing agricultural and environmental water use. *Agricultural Water Management, 58*(2), 171-192.

Bastiaanssen, W. G. M. (1998). *Remote sensing in water resources management: The state of the art.* Colombo, Sri Lanka: International Water Management Institute.

Bastiaanssen, W. G. M. (2000). SEBAL-based sensible and latent heat fluxes in the irrigated Gediz Basin, Turkey. *Special Issue, hydrological models and field data. Journal-of-Hydrology-Amsterdam. 2000, 229*(1-2), 87-100.

Bastiaanssen, W. G. M., & Bandara, K. M. P. S. (2001). Evaporative depletion assessments for irrigated watersheds in Sri Lanka. *Irrig Sci, 21*, 1-15.

Bastiaanssen, W. G. M., Menenti, M., Feddes, R. A., & Holtslag, A. A. M. (1998). A remote sensing surface energy balance algorithm for land (SEBAL): 1. Formulation. *Journal of Hydrology, 213*(1-4), 198-212.

Bastiaanssen, W. G. M., Mobin-ud-Din Ahmad, & Chemin, Y. (2002). Satellite surveillance of evaporative depletion across the Indus Basin. *WATER RESOURCES REASEARCH, Vol. 38*(No. 12, 1273), 9-1 to 9-10.

Bastiaanssen, W. G. M., Molden, D. J., & Makin, I. W. (2000). Remote sensing for irrigated agriculture: examples from research and possible applications. *Agricultural Water Management, 46*, 137-155.

Brutsaert, W. (1982). *Evaporation into the atmosphere.*: D.Reidel Publishing Co. Dordrecht, Holland. 300p.

Brutsaert, W., & Sugita, M. (1992). Application of self-reservation in diurnal evolution of the surface budget to determine daily evaporation. *J. Geophys.*(Res. 97(D170, 18 377-18 382.).

de Bruin, H. A. R. (1987). *From Penman to Makkink. In: Hooghart, J.C. (Ed.), Proceedings and information: TNO Committee on Hydrological Research, vol. 39. Gravenhage, The Netherlands, p. 5-31.*

Doorenbos, J., & Pruitt, W. O. (1977). *Guidelines for predicting crop water requirements: FAO Irrigation and Drainage Paper 24.* Rome: Food and Agriculture Organization of the United Nations.

Droogers, P., & Allen, R. G. (2002). Estimating reference evapotranspiration under inaccurate data conditions. *Irrigation and Drainage Systems, 16*(1), 33-45. http://www.environmental-center.com/magazine/kluwer/irds/33.pdf.

Harazono, Y., Kim, J., Miyata, A., Choi, T., Yun, J. I., & Kim, J. W. (1998). Measurement of energy budget components during the International Rice Experiment (IREX) in Japan. *Hydrol Process 12:2081-2092.*

IWMI. (1998). *Comparative performance assessment in 7 selected schemes in Nepal. Part A.*: International Water Management Institute, Colombo, Sri Lanka; Research and Technology Development Branch (RTDB), DOI, Kathmandu, Nepal and Ford Foundation, Delhi, India.

IWMI. (2000, 29 January 2003). *WORLD WATER & CLIMATE ATLAS* . International Water Management Institute. Retrieved, 2003, from the World Wide Web: http://www.cgiar.org/iwmi/WAtlas/atlas.htm

IWMI-Nepal. (2000a). *Initial assessment of the existing physical resource base and institutional arrangements in East Rapti river basin Nepal.* Kathmandu, Nepal: Research and Technology Development Branch (RTDB)/DOI, Institute of Agriculture and Animal Science (IAAS), and International Water Management Institute (IWMI).

IWMI-Nepal. (2000b). *Water accounting for East Rapti river basin of Nepal.* Kathmandu, Nepal: Research and Technology Development Branch (RTDB)/DOI, Institute of Agriculture and Animal Science (IAAS), and International Water Management Institute (IWMI).

Jackson, R. D., Reginato, R. J., & Idso, S. B. (1977). Wheat canopy temperature: a practical tool for evaluating water requirements. *Wat. Resour. Res., 13*, 651-656.

Jhorar, R. K. (2002). *Estimation of effective soil hydraulic parameters for water management studies in semi-arid zones: integral use of modelling, remote sensing and parameter estimation.* Unpublished Doctoral Thesis, Wageningen University, Wageningen, the Netherlands. ISBN 90-5808-644-5.

Joshi, C. M. (2001). *Invasive banmara, Chromolaena odorata: Spatial detection and prediction.* Unpublished MSc, ITC, Enschede, the Netherlands.

Keller, A., & Keller, J. (1995). *Effective Efficiency: A Water Use Concept for Allocating Freshwater Resources.* (Water Resources and Irrigation division Discussion Paper 22). Arlington, VA, US: Winrock International.

Kelliher, F. M., Leuning, R., Raupach, M. R., & Schultze, E. D. (1995). Maximum conductances for evaporation from global vegetation types. *Agriculture and Forest Meteorology, 73*, 1-16.

Kustas, W. P., & Norman, J. M. (1996). Use of remote sensing for evapotranspiration monitoring over land surfaces. *IAHS Hydrol. Sci. J., 41 (4)*, 495-516.

Lacroix, M., Kite, G., & Droogers, P. (2000). *Using datasets from the Internet for Hydrological modeling: An example from the Kucuk Menderes Basin, Turkey.* (Research Report 40). Colombo, Sri Lanka: International Water Management Institute.

Lookingbill, T. R., & Urban, D. L. (2003). Spatial estimation of air temperature differences for landscape-scale studies in montane environments. *Agriculture and Forest Meteorology, 114 (2003)*, 141-151.

Meijerink, A. M. J., de Brouwer, J. A. M., Mannaerts, C. M., & Valenzuela, C. R. (1994). *Introduction to the use of geographic information systems for practical hydrology* (Vol. ITC Publication ; 23). Enschede, The Netherlands: ITC.

Molden, D. (1997). *Accounting for Water Use and Productivity* (SWIM Paper 1). Colombo, Sri Lanka: International Water Management Institute.

Molden, D., & Sakthivadivel, R. (1999). Water accounting to assess use and productivity of water. *International Journal of Water Resources Development, 15*(1-2), 55-71.

Molden, D., Sakthivadivel, R., & Habib, Z. (2001). *Basin-level use and productivity of water: Examples from South Asia.* (Research Reprot 49). Colombo Sri Landa: International Water Management Institute.

Morse, A., Allen, R. G., Tasumi, M., Kramber, W. J., Trezza, R., & Wright, J. L. (2001, December 15, 2001.). *Final Report: Application of the SEBAL Methodology for Estimating Evapotranspiration and Consumptive Use of Water Through Remote Sensing* [PDF Format]. Idaho Department of Water Resources. University of Idaho, Department of Biological and Agricultural Engineering. Retrieved, 2002, from the World Wide Web: http://www.idwr.state.id.us/gisdata/ET/final_sebal_page.htm

NIPPON_Koei. (1989). *Final report on disaster prevention master plan in Upper Rapti river basin: Main Report*: His Majesty's Government of Nepal, Second Kulekhani Hydroelectric Project. NIPPON Koei Co., Ltd. Consulting Engineer, Tokyo, Japan.

Schaake, J. C., Koran, V. I., Duan, Q. Y., Mitchell, K., & Chen, F. (1996). Simple water balance model for estimating runoff at different spatial and temporal scales. *J. Geophys.*, Res. 101: 7461-7475.

Seckler, D. (1996). *The New Era of Water Resources Management: From 'Dry' to 'Wet' Water Savings* (Research Report 1). Colombo, Sri Lanka: International Water Management Institute.

Seckler, D., Amarasinghe, U., Molden, D. J., De Silva, R., & Barker, R. (1998). World water demand and supply, 1990-2025: scenarios and issues. *Research Report 19.*

Shuttleworth, W. J., Gurney, R. J., & Hsu, A. Y., Ormsby, J.P. (1989). *FIFE: the variation in energy partitioning at surface flux sites, remote sensing and large scale global processes. Proceedings at the Baltimore Symposium IAHS publication no. 186, IAHS Press, Oxfordshire, p. 67-74.*

TAHAL-Consulting. (2002). *Institutional development of department of hydrology and meteorology. Technical report no. - 4: Meteorological study.* Kathmandu, Nepal: His Majesty's Government of Nepal (HMG/N). Ministry of Science and Technology. Department of Hydrology and

Meteorology (DHM). TAHAL Consulting Engineers Ltd. in association with GEOCE, ARMS and CEMAT. (Preliminary Draft).

Tasumi, M., Allen, R. G., & Bastiaanssen, W. (2000, January 6, 2003). *Appendix A: The theoretical basis of SEBAL. Application of the SEBAL methodology for estimating consumptive use of water and stream flow depletion in the Bear River basin of Idaho through remote sensing.* [PDF Format]. Idaho Department of Water Resource. Retrieved, 2002, from the World Wide Web: http://www.idwr.state.id.us/gisdata/ET/final_sebal_page.htm

Walter, I. A., Allen, R. G., Elliott, R., Jensen, M. E., Itenfisu, D., Mecham, B., Howell, T. A., Snyder, R., Brown, P., Echings, S., Spofford, T., Hattendorf, M., Cuenca, R. H., Wright, J. L., & Martin, D. (2000). *ASCE's standardized reference evapotranspiration equation*: National irrigation symposium. Proceedings of the 4th Decennial Symposium, Phoenix, Arizona, USA, November.

Appendices

Appendix 1: SEBAL Procedure

1. Visible Remote Sensing

a. Spectral Reflectance and Albedo:

The planetary reflectance of a band has been computed as (NASA, 1998):

$$r_p = \frac{\pi \cdot L_\lambda \cdot d^2}{E_{sun_\lambda} \cdot Cos\theta} \qquad [-] \qquad (1)$$

Where; L_λ is the spectral radiance [$Wm^{-2}\ sr^{-1}\mu m^{-1}$], d is the Earth-Sun distance [AU], $E_{sun\lambda}$ is the solar spectral irradiance [$Wm^{-2}\ \mu m^{-1}$] and θ is the solar incident angle.

The digital numbers (DN) recorded in images can be converted to spectral radiance as (NASA, 1998):

$$L_\lambda = \left[L\min + \frac{L\max - L\min}{254}(DN - 1) \right] \qquad [Wm^{-2}\ sr^{-1}\mu m^{-1}] \qquad (2)$$

Where, L_{min} and L_{max} are the post-calibration spectral radiances, which are generally given in the meta-data file (header files) of the image or can be downloaded from (NASA, 1998).

Table 1: The solar spectral irradiances [$Wm^{-2}\ \mu m^{-1}$] for Landsat 7 (NASA, 1998):

Band	1	2	3	4	5	7
Solar spectral irradiance	1970	1843	1555	1047	227.1	80.53

Albedo at the top of the atmosphere (r_{toa}):

The surface albedo at the top of the atmosphere is calculated by the spectral reflectance of each band calculated above by assigning the proper weight for the each band.

$$r_{toa} = \sum c_{p_i} \cdot r_{p_i} \qquad [-] \qquad (3)$$

Where, r_{toa} is albedo at top of the atmosphere, $c_{p_i} = \frac{E_{suni}}{\sum E_{suni}}$ is weighting coefficient for band i (i = 1 to 5 and 7), r_{p_i} is the spectral reflectance at band i.

Surface albedo (r_o)

There are three differences between radiation (accordingly albedo) at the earth's surface and at the top of the atmosphere. The incoming radiation is higher at the top of the atmosphere and lower in the land surface because a portion of incoming radiation is absorbed or reflected by air. The amount of absorption or decrement due to air is taken in to account by atmospheric transmittance (τ_{sw}). The correction for atmospheric interference is generally based on detailed information of the state of the atmosphere (temperature, humidity and wind velocity at different altitude). In absence of these data the broad band surface albedo can be derived from broad band albode at the top of the atmosphere by following equation (Bastiaanssen *et al.*, 1998):

$$r_o = \frac{r_{toa} - r_{path\_radiance}}{\tau_{sw}^2} \qquad [-] \qquad (4)$$

Where, $r_{path\_radiance}$ is albedo path radiance and τ_{sw}^2 is the two-way transmittance.

Usually, $r_{path\_radiance}$ has a value between 0.025 and 0.04 (Tasumi *et al.*, 2000). In this study, 0.04 has been accepted for $r_{path\_radiance}$.

The one-way transmittance assuming clear sky condition has been predicted as follows (Tasumi *et al.*, 2000).

$$\tau_{sw} = 0.75 + 2x10^{-5} \cdot z \qquad [-] \qquad (5)$$

Where, z is elevation above sea level [m]

b. Vegetation Indices:

The Normalize Difference Vegetation Index (NDVI) is a measure of the amount and vigor of the surface vegetation and has been calculated by reflectance in near infrared and red ban of visible spectrum as follows:

$$NDVI = \frac{r_4 - r_3}{r_4 + r_3} \qquad [-] \qquad (6)$$

Where, r_4 and r_3 are the reflectance at near infrared and red bands of visible spectrum respectively.

Soil Adjusted Vegetation Index (SAVI) has been computed as:

$$SAVI = \frac{(1 + L_1)(r_4 - r_3)}{L_1 + r_4 + r_3} \qquad [-] \qquad (7)$$

Where; L_1 is the non-dimensional correction factor, which ranges from 0 to 1. The most typically used value for intermediate vegetation cover is $L_1 = 0.5$ (Parodi, 2000).

c. Surface Emissivity (ε_0):

The emissivity of an object is the ratio of the energy radiated by that object at a given temperature to the energy radiated by a blackbody at the same temperature. In SEBAL surface emissivity was estimated using NDVI by an empirically derived method (Bastiaanssen *et al.*, 1998):

$$\varepsilon_o = 1.009 + 0.047 \cdot \ln(NDVI) \qquad [-] \qquad (8)$$

The relation is only valid for NDVI values greater than 0.16. Therefore, an adjustment has been made for NDVI less than 0.16. NDVI less than 0.16 (positive) is normally bare soil, for this value of NDVI, emissivity has been set to 0.92 and for NDVI less than 0 (normally water surface), the emissivity has been set to 1 (Gieske & Timmerman, 2002).

2. Thermal Remote Sensing

a. Surface Temperature

The brightness temperature was computed from the spectral radiance at thermal band (10.4-12.4 μm) by the equations (NASA, 1998):

$$T_b = \frac{K_2}{\ln\left(\frac{K_1}{L\lambda} + 1\right)} \quad [K] \tag{9}$$

Where, K_1 and K_2 are constants (for ETM+: K_2 = 1282.71 and K_1 = 669.09), $L\lambda$ is spectral radiance at band 6.

Then the surface temperature has been computed from the brightness temperature as:

$$T_o = \frac{T_b}{\varepsilon_o^{0.25}} \quad [K] \tag{10}$$

There are two thermal bands in Landsat ETM+, one operates in low gain (Band61) and another in high gain (Band 62). The histogram of both are analysed and Band 62 shows better distributive than Band 61 in all cases. Further assessment was made by computing brightness temperature for both bands and the results shows very much close to each other. Finally, Band 62 has been accepted for computation of surface temperature in all three images, as histogram of band 62 shows slightly more distributive than that of band 61.

b. DEM corrected apparent temperature

During the estimation of sensible heat flux in coming step, an estimation of the surface to air temperature different is needed. In SEBAL dT_a is estimated as a function of surface temperature. However the surface temperature that is used needs to be uniformly adjusted to a common reference elevation for accurate prediction of dT_a. Otherwise, high elevations that appear to be "cool" may be interpreted as having high evapotranspiration. Therefore a "lapsed" (an artificial) surface temperature map was made for purposes of computing surface-to-air temperature differences by assuming the rate of decrease in surface temperature by the orographic effect is the same as that for a typical air profile using the equation (Tasumi *et al.*, 2000):

$$T_{o\_dem} = To + 0.0065 \cdot \Delta z \quad [K] \tag{11}$$

Where, Δz is the difference of a pixel's elevation from the datum [m]. The datum was selected from the valley plain near Jhawani station having elevation 181 m.

3. Surface Energy Balance

The net radiation actually receives/loos from the land surface is positive during daytime and negative during nighttime. Some of the net energy is used to evaporate soil water, some energy is used to heat the air, and the rest of the net energy is stored in the ground (or water body). The surface energy balance can be expressed by following expression:

$$R_n = \lambda E + H + G_o \qquad [Wm^{-2}] \tag{12}$$

Where, λE is the latent heat flux [Wm^{-2}], H is the sensible heat flux [Wm^{-2}] and Go is the soil heat flux [Wm^{-2}]

a. Net Radiation

The net radiation is calculated from the incoming and outgoing all wave radiation fluxes as follows:

$$Rn = (1 - r_o)K^{\downarrow} + (L^{\downarrow} - L^{\uparrow}) - (1 - \varepsilon_o) \cdot L^{\downarrow} \qquad [W\ m^{-2}] \tag{13}$$

Where, $K^{\downarrow}$ is incoming short wave radiation [Wm^{-2}], $L^{\downarrow}$ & $L^{\uparrow}$ are incoming and outgoing longwave radiation respectively [Wm^{-2}], r_o is the surface reflectance [-] and εo is the surface emissivity.

In equation (13) the last term $[(1 - \varepsilon_o) \cdot L^{\downarrow}]$ is subtracted to account the surface reflectance of incoming long wave radiation.

The incoming shortwave radiation was computed as:

$$K^{\downarrow} = Gsc \cdot \cos\theta \cdot dr \cdot \tau_{sw} \qquad [W\ m^{-2}] \tag{14}$$

Where, Gsc is the solar constant [1367 Wm^{-2}], $\cos\theta$ is the cosine of solar zenith angle, dr is the inverse square relative distance Earth-Sun in astronomical unit, and τ_{sw} is the one-way transmittance

The incoming longwave radiation for cloud-free condition has been computed by following equation (Bastiaanssen *et al.*, 1998):

$$L^{\downarrow} = 1.08 \cdot (-\ln \tau_{sw})^{0.265} \cdot \sigma \cdot T_{oref}{}^{4} \qquad [W\ m^{-2}] \tag{15}$$

Where, σ is the Stefan Boltzman constant; and T_{oref} is the surface temperature at a reference point.

The reference point is generally selected at a well-watered pixel so that surface temperature and air temperature are similar (Tasumi *et al.*, 2000).

The out going long wave radiated was computed by following equation:

$$L^{\uparrow} = \varepsilon_o \cdot \sigma \cdot T_o^4 \qquad [\text{W m}^{-2}] \tag{16}$$

Where, ε_o is the surface emissivity [-], T_o is the surface temperature [K]

b. Soil heat flux

The soil heat flux is driven by a thermal gradient in the uppermost topsoil. In SEBAL, the soil heat flux is estimated empirically, considering the effects of surface heating, soil moisture and intercepted solar radiation. The soil heat flux has been estimated by the equation (Parodi, 2000):

$$G_o = R_n \cdot \left\{ \frac{(T_o - 273)}{r_o} \cdot \left[0.0032 \cdot (c_1 \cdot r_o) + 0.0062 \cdot (c_1 \cdot r_o)^2\right] \cdot (1 - 0.978 \cdot NDVI^4) \right\} [\text{W m}^{-2}] \tag{17}$$

Where, c_1 is a factor to convert the instantaneous values of albedo to daily averages (c_1 = 1.1).

c. Sensible heat flux

The basic equation to estimate aerodynamic transfer of heat to air is as follows:

$$H = \frac{\rho_a \cdot C_p}{r_{ah}} \cdot dT_a \qquad [\text{W m}^{-2}] \tag{18}$$

Where, ρ_a is air density which is a function of atmospheric pressure (computed process is outlined in following chapter); C_p is the air specific heat at constant pressure (1004 $\text{Jkg}^{-1}\text{K}^{-1}$); r_{ah} is aerodynamic resistance to heat transport; and dT_a is the vertical difference in air temperature between layers $z = z_{oh}$ and $z = z_{ref}$.

The main difficult (comparatively) part of SEBAL procedure is to estimate sensible heat flux. SEBAL compute the sensible heat flux by some iterative process assuming two extreme evaporating surfaces, driest and wettest pixel. SEBAL assumes laten heat flux zero at dry pixel and sensible heat flux zero at wettest pixel.

As the sensible and latent heat fluxes interact with the momentum fluxes, the heat fluxes cannot be solved explicitly if the momentum flux is unknown. It is therefore, first assumed that the buoyancy effect on the momentum flux is negligible, which is incorrect but allows the determination of the local scale friction velocity from the wind speed at the blending height and of the estimated local surface roughness length for momentum transfer (Bastiaanssen, 2000):

$$\frac{1}{u_*} = \frac{\ln\left(\frac{z_b}{z_{om}}\right)}{k \cdot u_b} \qquad [\text{s m}^{-1}] \tag{19}$$

Where, u_* [ms^{-1}] is the local scale friction velocity, u_b [ms^{-1}] is the average wind speed at blending height b [= 100 m considered in this study]; k is von Karman's constant; and z_{om} [m] is local surface roughness for momentum transport.

To solve above equation at least one wind speed observation is necessary within or close to the study area for the image date. But, there is no wind speed observation data available for the study area. So, u_{100} (average wind speed at blending height of 100m) necessary to solve above equation was estimated from the logarithmic wind profile using the average wind speed for the corresponding month from IWMI climatic atlas for the pixel corresponding to Jhawani rainfall station. The wind speed at blending height is considered to be constant over all pixels in the image. The local scale z_{om} were computed as 0.123 times average vegetation height around the station. The average vegetation heights for October image were taken as 0.75 m and for rest images taken as 0.5 m. These heights were considered corresponding to the crop season during the image dates. The Jhawani staition is located in the rice field (observed during the field visit) and the October is the about the end of Paddy season and rest is correspond to wheat season.

The surface roughness for momentum transport has been computed as function of SAVI by the following equation (Bastiaanssen, 2000):

$$z_{om} = \exp(-5.809 + 5.62SAVI) \qquad [\text{m}] \tag{20}$$

The aerodynamic resistance to heat transport r_{ah} has been computed as follows:

$$r_{ah} = \frac{1}{k \cdot u_*} \ln\left\{\frac{z_{ref}}{z_{oh}}\right\} \qquad [\text{s m}^{-1}] \tag{21}$$

Where, u_* is fiction velocity; k is von Karman's constant (0.41); Z_{ref} [m] is the upper integration limit for the eddy diffusivity for heat transport to which rah applies and z_{oh} [m] is the surface roughness length to heat transport. The reference height is taken as z_{ref} = 3 m, which is less than the pixel size by a factor of 10 (Bastiaanssen, 2000).

The temperature difference dT_a required to predict H were predicted assuming that dT_a has a linear relation to T_{o_dem}.

$$dT_a = a + b \cdot T_{o\_dem} \qquad [\text{K}] \tag{22}$$

Where, a and b are constants.

The estimation of constants a and b follows some iteration process. First, two extreme evaporating pixels (wet and dry pixel) were selected. This was done by assessing T_{o_dem} with the help of scatter plots of NDVI verses T_{o_dem} and r_o verses T_{o_dem}. In general the wettest pixel has high NDVI and low surface temperature indicating high evapotranspiration and dry pixel has medium albedo and high surface temperature indicating no evapotranspiration. The DEM corrected surface temperature corresponds to selected wet pixel and dry pixel have been noted as T_{o_wet} and T_{o_dry} respectively. Both the dry and wet pixels were selected from the flat valley area to avoid uncertainty due to mountain effect. The wet pixel is selected from the swampy forest area with high NDVI and low temperature among the surrounding pixels. And the dry pixel selected from the dry sandy riverbed with high T_{o_dem} within the area, medium albedo and less (but positive) NDVI.

In the wet pixel SEBAL assumes sensible heat flux zero. Sensible heat flux for dry pixel was estimated by solving equation **(18)** in inverse mode. Using these two extreme sensible heat fluxes, the linear constants a and b were predicted. The iterative steps for buoyancy correction on sensible het flux at dry pixel were carried out in Excel spreadsheets.

Then the first estimate of sensible heat fluxes were computed by equation **(18)** assuming zero stability correction factors; which was used to obtain the integrated stability correction using Monin Obukhov's similarity hypothesis.

First estimate of Monin-Obukhov stability length L [m] is estimated by the equation (Tasumi *et al.*, 2000):

$$L = -\frac{\rho_a Cp \cdot u_*^3 T_{o\_dem}}{k \cdot g \cdot H} \qquad [\text{m}] \qquad (23)$$

This Monin_Obukhov stability length allows to estimate stability correction factor for buoyancy effects on the momentum flux ψ_m and the stability correction factor for heat flux ψ_h.

$$\psi_m = 2\ln\left(\frac{1+x_m}{2}\right) + \ln\left(\frac{1+x_m^2}{2}\right) - 2ARCTAN(x_m) + 0.5\pi \qquad [-] \qquad (24)$$

and

$$\psi_h = 2\ln\left(\frac{1+x_h^2}{2}\right) \qquad [-] \qquad (25)$$

Where, x_m and x_h are defined as

$$x_m = \left(1 - 16\frac{z_{blend}}{L}\right)^{0.25} \qquad [-] \qquad (26)$$

$$x_h = \left(1 - 16\frac{z_{ref}}{L}\right)^{0.25} \qquad [-] \qquad (27)$$

Which allows second and improved estimation of u_* and r_{ah}; from improved equations of **(19)** and **(21)** respectively.

$$\frac{1}{u_*} = \frac{\ln\left(\frac{100}{z_{om}}\right) - \psi_m}{k \cdot u_{100}} \qquad [\text{s m}^{-1}] \qquad (28)$$

and,

$$r_{ah} = \frac{\ln\left\{\frac{z_{ref}}{z_{oh}}\right\} - \psi_h}{k \cdot u_*} \qquad [\text{s m}^{-1}] \qquad (29)$$

Using these improved estimate of u_* and r_{ah}, a second estimate of H was estimated by equation **(18)**. The loops of equations **(18)** to **(29)** are to be repeated until convergence in sensible heat fluxes is met. Bastiaanssen, (2000) suggested that five iterations are good enough to get satisfactory result.

d. Latent heat flux

The latent heat flux λE [Wm^{-2}] can be computed as residual term of the energy balance equation **(12)** using the values for R_n, G_o and H. This λE represents the instantaneous evapotranspiration at the time of the satellite overpass.

The instantaneous evaporative fraction Λ, was computed as:

$$\Lambda = \frac{R_n - G_o - H}{R_n - G_o} \qquad [-] \qquad (30)$$

Where, R_n, G_o and H are instantaneous net radiation, soil heat flux and sensible heat flux respectively all are in Wm^{-2}.

4. Evapotranspiration

The ultimate goal of whole SEBAL process is to compute daily evapotranspiration. Following Shuttleworth *et al.*, (1989), the instantaneous evaporative fraction was considered similar to its 24 h counterpart (Brutsaert *et al.*, 1992), which was used to compute the actual 24 h evaporation from instantaneous latent heat fluxes (Bastiaanssen, 2000):

$$ET_{24} = \Lambda R_{n24} \qquad [Wm^{-2}] \qquad (31)$$

Where, ET24 is the 24 hours actual evaporation, R_{n24} is the 24 hours net radiation.

The 24 hours net radiation can be computed according to de Bruin (1987), where surface albedo is assumed to be similar to the surface albedo during the morning overpass:

$$R_{n24} = (1 - r_o) \cdot \tau_{sw24} \cdot K_{a24}^{\downarrow} - 110\tau_{sw24} \qquad [Wm^{-2}] \qquad (32)$$

Where, r_o is the surface albedo, $K_{a24}^{\downarrow}$ is the 24 hours incoming extraterrestrial solar radiation and τ_{sw24} is the daily atmospheric transmittance.

References:

Bastiaanssen, W. G. M. (2000). SEBAL-based sensible and latent heat fluxes in the irrigated Gediz Basin, Turkey. Special Issue, hydrological models and field data. Journal-of-Hydrology-Amsterdam. 2000, 229(1-2), 87-100.

Bastiaanssen, W. G. M., Menenti, M., Feddes, R. A., & Holtslag, A. A. M. (1998). A remote sensing surface energy balance algorithm for land (SEBAL): 1. Formulation. Journal of Hydrology, 213(1-4), 198-212.

de Bruin, H. A. R. (1987). From Penman to Makkink. In: Hooghart, J.C. (Ed.), Proceedings and information: TNO Committee on Hydrological Research, vol. 39. Gravenhage, The Netherlands, p. 5-31.

Gieske, A., & Timmermans, W. (2002). ITC Lecture Note: Satellite Hydrology.

NASA. (1998, November 8, 2002). Landsat7 Science Data Users Handbook. Landsat Project Science Office. http://ltpwww.gsfc.nasa.gov/IAS/handbook/handbook_htmls/chapter11/chapter11.html. Retrieved January 14, 2003, from the World Wide Web:

Parodi, G. N. (2000). AHVRR Hydrological Analysis System: Algorithms and theory - Version 1.0.

Tasumi, M., Allen, R. G., & Bastiaanssen, W. (2000, January 6, 2003). Appendix A: The theoretical basis of SEBAL. Application of the SEBAL methodology for estimating consumptive use of water and stream flow depletion in the Bear River basin of Idaho through remote sensing. [PDF Format]. Idaho Department of Water Resource. Retrieved, 2002, from the World Wide Web: http://www.idwr.state.id.us/gisdata/ET/final_sebal_page.htm

5: Calibration Sheets for estimation of linear constants a and b to estimate dTa:

a. 24 October 2001

Image Date:	24-Oct-01			Julian Day:		297										
Read from calculated maps:			Steps:	psim	psih	ustar	rah	dtmax	b	a	L	Xh	xm	psi-h	psi-m	
To-wet	294.83		1	0.000	0.000	0.086	248.861	52.114	3.000	-884.557	-0.238	3.772	9.053	4.060	5.604	
To-dry	312.2		2	5.604	4.060	0.196	59.016	12.359	0.711	-209.768	-2.794	2.065	4.894	1.935	3.518	
Rn-dry	312.9		3	3.518	1.935	0.133	125.926	26.370	1.518	-447.593	-0.873	2.735	6.544	2.889	4.475	
G-dry	73.18		4	4.475	2.889	0.156	92.448	19.359	1.115	-328.598	-1.409	2.433	5.806	2.483	4.074	
Zom-dry	0.0045		5	4.074	2.483	0.146	105.955	22.188	1.277	-376.609	-1.142	2.561	6.119	2.659	4.248	
Displ-dry	0.0001		6	4.248	2.659	0.150	99.974	20.936	1.205	-355.350	-1.249	2.506	5.983	2.584	4.174	
u-blend	2.107		7	4.174	2.584	0.148	102.517	21.468	1.236	-364.390	-1.202	2.529	6.041	2.616	4.206	
hmax	239.72		8	4.206	2.616	0.149	101.417	21.238	1.223	-360.478	-1.222	2.519	6.016	2.602	4.192	
dT	17.37		9	4.192	2.602	0.148	101.890	21.337	1.228	-362.158	-1.213	2.524	6.027	2.608	4.198	
			10	4.198	2.608	0.149	101.686	21.294	1.226	-361.434	-1.217	2.522	6.023	2.606	4.195	
air_den	1.14		11	4.195	2.606	0.149	101.774	21.312	1.227	-361.746	-1.215	2.523	6.025	2.607	4.196	
cp	1004.16		12	4.196	2.607	0.149	101.736	21.304	1.227	-361.612	-1.216	2.522	6.024	2.606	4.196	
k	0.41		13	4.196	2.606	0.149	101.752	21.308	1.227	-361.669	-1.216	2.522	6.024	2.606	4.196	
g	9.81															
zblend	100				Row	Col		**a**	**-361.669**							
zref	3			Dry	**901**	**544**		**b**	**1.227**							
zoh	0.00045			Wet	**788**	**384**		hmax	239.720							
Reference station: Jhawani																
u2 m/s]	0.75	m/s														
h	1	m	Average vegetation height around the station													
d	0.6667	m	2/3 *h													
Zom	0.123	m	0.123 (vegetation height in m, around the meteostation)													
Zref	2	m														
Zblend	100	m	blending height is 100m assumed													
Ublend	2.107	m/s														
air_den	1.14	kg/m3	from air_den map													

b. 27 December 2001

Image Date:	27-Dec-01			Julian Day:		361										
Read from calculated maps:			Steps:	psim	psih	ustar	rah	dtmax	b	a	L	Xh	xm	psi-h	psi-m	
To-wet	287.84		1	0.000	0.000	0.048	440.037	103.199	6.912	-1989.613	-0.036	6.044	14.521	5.864	7.328	
To-dry	302.77		2	7.328	5.864	0.185	37.301	8.748	0.586	-168.656	-2.045	2.224	5.290	2.179	3.768	
Rn-dry	324.5		3	3.768	2.179	0.078	204.309	47.915	3.209	-923.775	-0.151	4.223	10.140	4.485	6.010	
G-dry	46.61		4	6.010	4.485	0.123	83.804	19.654	1.316	-378.915	-0.592	3.010	7.210	3.230	4.806	
Zom-dry	0.005		5	4.806	3.230	0.094	142.385	33.393	2.237	-643.788	-0.264	3.677	8.824	3.965	5.513	
Displ-dry			6	5.513	3.965	0.109	106.166	24.898	1.668	-480.024	-0.413	3.290	7.890	3.554	5.119	
u-blend	1.165		7	5.119	3.554	0.100	125.732	29.487	1.975	-568.491	-0.319	3.508	8.415	3.790	5.345	
hmax	277.89		8	5.345	3.790	0.105	114.304	26.807	1.796	-516.820	-0.369	3.384	8.115	3.657	5.217	
dT	14.93		9	5.217	3.657	0.102	120.691	28.305	1.896	-545.700	-0.340	3.454	8.285	3.733	5.290	
			10	5.290	3.733	0.104	117.030	27.446	1.838	-529.148	-0.356	3.414	8.188	3.690	5.249	
air_den	1.18		11	5.249	3.690	0.103	119.099	27.932	1.871	-538.501	-0.347	3.437	8.243	3.714	5.272	
cp	1004.16		12	5.272	3.714	0.103	117.920	27.655	1.852	-533.173	-0.352	3.424	8.212	3.700	5.259	
k	0.41		13	5.259	3.700	0.103	118.588	27.812	1.863	-536.194	-0.349	3.431	8.230	3.708	5.267	
g	9.81															
zblend	100				Row	Col		**a**	**-536.194**							
Zref	3			Dry	**875**	**559**		**b**	**1.863**							
Zoh	0.0005			Wet	**780**	**384**		hmax	277.890							
Reference station: Jhawani																
u2 m/s]	0.52	m/s														
h	0.5	m	Average vegetation height around the station													
d	0.33333333	m	2/3 *h													
Zom	0.0615	m	0.123 (vegetation height in m, around the meteostation)													
Zref	2	m														
Zblend	100	m	blending height is 100m assumed													
Ublend	1.165	m/s														

c. 1 March 2001

Image Date:	1-Mar-02			Julian Day:		60									
Read from calculated maps:			Steps:	psim	psih	ustar	rah	dtmax	b	a	L	Xh	xm	psi-h	psi-m
		dT													
To-wet	291.88	0.00	1	0.000	0.000	0.096	222.908	59.884	4.635	-1352.853	-0.252	3.719	8.925	4.007	5.553
To-dry	304.8	24.76	2	5.553	4.007	0.216	54.073	14.526	1.124	-328.172	-2.859	2.054	4.866	1.918	3.499
Rn-dry	377		3	3.499	1.918	0.148	113.396	30.464	2.358	-688.211	-0.917	2.703	6.464	2.847	4.433
G-dry	66.77		4	4.433	2.847	0.173	84.023	22.573	1.747	-509.945	-1.459	2.413	5.756	2.454	4.045
Zom-dry	0.0045		5	4.045	2.454	0.162	95.805	25.738	1.992	-581.450	-1.192	2.534	6.054	2.623	4.213
Displ-dry	0.0001		6	4.213	2.623	0.166	90.633	24.348	1.885	-550.063	-1.299	2.482	5.926	2.551	4.141
u-blend	2.352		7	4.141	2.551	0.164	92.817	24.935	1.930	-563.314	-1.252	2.504	5.980	2.582	4.172
hmax	310.23		8	4.172	2.582	0.165	91.879	24.683	1.910	-557.626	-1.272	2.495	5.957	2.569	4.159
dT	12.92		9	4.159	2.569	0.165	92.279	24.790	1.919	-560.050	-1.263	2.499	5.967	2.574	4.164
			10	4.164	2.574	0.165	92.108	24.745	1.915	-559.014	-1.267	2.497	5.963	2.572	4.162
air_den	1.15		11	4.162	2.572	0.165	92.181	24.764	1.917	-559.457	-1.265	2.498	5.964	2.573	4.163
cp	1004.16		12	4.163	2.573	0.165	92.150	24.756	1.916	-559.268	-1.266	2.498	5.964	2.572	4.163
k	0.41		13	4.163	2.572	0.165	92.163	24.759	1.916	-559.348	-1.266	2.498	5.964	2.573	4.163
g	9.81														
zblend	100			Row	Col			a	-559.348						
zref	3		Dry	900	541			b	1.916						
zoh	0.00045		Wet	761	344			hmas	310.230						
Reference station: Jhawani															
u2 m/s]	1.05	m/s													
h	0.5	m	Average vegetation height around the station												
d	0.3333	m	2/3 *h												
Zom	0.0615	m	0.123 (vegetation height in m, around the meteostation)												
Zref	2	m													
Zblend	100	m	blending height is 100m assumed												
Ublend	2.352	m/s													
air_den	1.15	kg/m3	from air_den map												

Appendix 2: ILWIS Scripts for estimation solar radiation in mountainous terrain

a. Slope and Aspect Maps Preparation

Parameters:

%1 Pixel size of DEM (Raster Image)
%2 Filename of DEM

Script:

```
        //Latitude Longitude maps//
lati {dom=VALUE.dom;vr=-90.00000:90.00000:0.00001} :=iff(%2, crdy(transform(mapcrd(DEM), latlon)), 0)
long {dom=VALUE.dom;vr=-180.00000:180.00000:0.00001} :=iff(%2, crdx(transform(mapcrd(DEM), latlon)), 0)
        //Horizontal gradient map//
dx.mpr{dom=Value.dom;vr=-1000.0:1000.0:0.01} := MapFilter(%2,DFDX.fil,Value.dom)
        //Vertical gradient map//
dy.mpr{dom=Value.dom;vr=-1000.0:1000.0:0.01} := MapFilter(%2,DFDY.fil,Value.dom)
        //Slope map in degree//
SlopeDeg.mpr {dom=Value.dom;vr=0.0:100.0:0.1} :=RADDEG(ATAN((Hyp(dx,dy))/%1))
        //Aspect map: 0 indicates directed towards North and angle in clock wise direction towards north//
Aspect.mpr {dom=Value.dom;vr=0.0:360.0:0.1} :=RADDEG(ATAN2(dx,dy)+pi)
        //Aspect map corrected for flat surface: 361 indicated flat area//
Aspect_corrected.mpr {dom=Value.dom;vr=0.0:361.0:0.1} :=ifundef(Aspect, 361)
        //Correction for according to Allen's reprot to fit the method//
Aspect_new.mpr {dom=Value.dom;vr=-180.0:181.0:0.1} :=Aspect_corrected - 180
        /// 0.1 Intermediate files for slope/aspect correction//
SIN_Slope {dom=VALUE.dom;vr=-1.00:1.00:0.0001}:= SIN(SlopeDeg*pi/180)
COS_Slope {dom=VALUE.dom;vr=-1.00:1.00:0.0001}:= COS(SlopeDeg*pi/180)
SIN_Aspect {dom=VALUE.dom;vr=-100.00:100.00:0.0001} := SIN(Aspect_new*pi/180)
COS_Aspect {dom=VALUE.dom;vr=-100.00:100.00:0.0001} := COS(Aspect_new*pi/180)
```

b. Estimation of Instantaneous Extraterrestrial Radiation:

Parameters:

%1	–	Local Standard time
%2	–	Julian day no.
%3	–	Standard meridian
%4	–	File name of DEM

Functions: DA, DE

a. DA

```
Function dayangle(Value a) : Value
Begin
  Return 0.01721420632*(a-1);
End;
```

b. DE

```
Function de(Value a) : Value
Begin
  Return (0.006918-0.399912*cos(a)+0.070257*sin(a)-0.006758*cos(2*a)+0.000907*sin(2*a)-
0.002697*cos(3*a)+0.00148*sin(3*a));
End;
```

Scripts:

```
        /// day angle
DA_map {dom=VALUE.dom;vr=-10.00000:10.00000:0.0001} := ifnotundef(%4, DA(%2))
        /// Solar declination of the day
Delta {dom=VALUE.dom;vr=-10.00000:10.00000:0.0001} := ifnotundef(%4, DE(DA_map))
        ///Longitude correction = Lc in minutes
Lc {dom=VALUE.dom;vr=-100.00000:100.00000:0.00001} := 4*(%3-Long)
```

```
        /// Local apparent time or solar time (hr min sec)
LAT {dom=VALUE.dom;vr=-100.00000:100.00000:0.00001} := %1-Lc/60 +ET(DA_map)/60
        ///hour angle map w in degree: norning negative afternoon positive, noon zero
w {dom=VALUE.dom;vr=-1000.00000:1000.00000:0.00001} := 15 * (LAT-12)
        //Cosine of the Incidence angle (Idaho, Appendix A, page 49: ERDAS field guide p383 "Lambertian
Reflectance Model".)
P1 := SIN(Delta)*SIN(lati*pi/180)*COS_Slope
P2 := SIN(Delta)*COS(lati*pi/180)*SIN_Slope*COS_Aspect
P3 := COS(Delta)*COS(lati*pi/180)*COS_Slope
P4 := COS(Delta)*SIN(lati*pi/180)*SIN_Slope*COS_Aspect
P5 := COS(Delta)*SIN_Slope*SIN_Aspect

Cos_theta_temp1 := P1-P2+P3*COS(w*pi/180)+P4*COS(w*pi/180)+P5*SIN(w*pi/180)
COS_theta {dom=VALUE.dom;vr=-10.00:10.00:0.0001} :=iff(Cos_theta_temp1<0.1, 0.1, Cos_theta_temp1)

Kexo_temp {dom=VALUE.dom;vr=-1.00000:10000.00000:0.0001} := 1367*dr*COS_theta
Kexo {dom=VALUE.dom;vr=0.0000:2000.0000:0.0001} :=iff(Kexo_temp>1367, 1367, Kexo_temp)
```

c. Main Scrip to Estimate Daily Solar Radiation:

Parameter:

%1 - Time step (value)

Script: Step0_5 (file name of this script)

```
w%1 {dom=VALUE.dom;vr=-10.00:10.00:0.0001} :=ifnotundef(ws, (-pi+%1*0.5*pi/12))
Cos_theta_temp1 {dom=VALUE.dom;vr=-10.00:1.00:0.0001} := P1-P2+P3*COS(w%1)+P4*COS(w%1)
+P5*SIN(w%1)
Cos_theta_temp2 {dom=VALUE.dom;vr=-10.00:10.00:0.0001} :=iff(Cos_theta_temp1<0.1, 0.1, Cos_theta_temp1)
Cos_theta_temp3 {dom=VALUE.dom;vr=-10.00:10.00:0.0001} := iff((w%1<-ws)or(w%1>ws), 0, Cos_theta_temp2)
Cos_theta_final {dom=VALUE.dom;vr=-100.00:100:0.0001} :=Cos_theta_Pre+ Cos_theta_temp3
Cos_theta_Pre :=Cos_theta_final

del w%1.* -force
```

d. Script to run main script <Step0_5> for 48 time steps:

```
Cos_theta_Pre {dom=VALUE.dom;vr=-10.00:1000.00:0.0001} :=ifnotundef(ws, 0)
P1 := SIN(Delta)*SIN(lati*pi/180)*COS_Slope
P2 := SIN(Delta)*COS(lati*pi/180)*SIN_Slope*COS_Aspect
P3 := COS(Delta)*COS(lati*pi/180)*COS_Slope
P4 := COS(Delta)*SIN(lati*pi/180)*SIN_Slope*COS_Aspect
P5 := COS(Delta)*SIN_Slope*SIN_Aspect

run   Step0_5    1
run   Step0_5    2
.....
.....
run   Step0_5    46
run   Step0_5    47
run   Step0_5    48

Ra24 {dom=VALUE.dom;vr=0.00:10000.00:0.0001} :=(0.5/24) * 1367 *dr*Cos_theta_final
```

Appendix 3: Rainfall and temperature model constants

a. Rainfall model constants

Month	A	B	C	D	R^2
Jan	-0.002	12.7	6.18	-858.5	0.26
Feb	0.002	23.2	7.01	-1219.1	0.62
Mar	-0.011	168.5	66.36	-10239.1	0.83
Apr	0.001	113.2	46.86	-7034.9	0.89
May	0.018	-162.6	-35.87	7663.8	0.26
Jun	0.020	-405.8	-88.10	18951.9	0.32
Jul	-0.019	-355.7	-28.46	12766.4	0.56
Aug	-0.039	-424.4	47.27	8170.3	0.87
Sep	-0.044	-351.9	52.78	5548.9	0.89
Oct	-0.001	-157.7	-32.52	7182.7	0.86
Nov	0.004	-70.5	-13.04	3056.4	0.92
Dec	-0.004	48.2	17.62	-2799.0	0.27

b. Temperature model constants

	Coefficient for T_{max}					Coefficients for T_{min}				
Month	A	B	C	$D*10^{-3}$	R^2	A	$B*10^{-2}$	$C*10^{-2}$	$D*10^{-4}$	R^2
Jan	-90.95	1.77	0.78	-5.80	0.93	40.20	-75.00	-11.30	-38.20	0.76
Feb	-78.62	1.57	0.74	-6.70	0.96	41.23	-68.10	-12.60	-41.10	0.78
Mar	-27.08	0.82	0.44	-7.00	0.96	63.94	-97.60	-25.20	-42.30	0.79
Apr	45.63	0.07	-0.13	-7.40	0.97	144.42	-209.10	-79.40	-44.40	0.82
May	70.32	0.38	-0.52	-6.90	0.95	141.49	-164.70	-86.00	-53.30	0.93
Jun	-6.63	1.61	-0.02	-6.40	0.93	90.36	-77.80	-51.20	-51.80	0.98
Jul	-85.39	2.29	0.67	-5.80	0.90	41.20	-10.70	-14.40	-51.30	0.99
Aug	-86.21	2.04	0.77	-5.80	0.92	37.19	-2.80	-12.10	-51.10	0.98
Sep	-76.17	2.05	0.63	-5.90	0.93	45.90	-32.80	-13.90	-52.70	0.98
Oct	-39.44	1.31	0.43	-6.30	0.95	79.39	-130.90	-26.30	-51.00	0.93
Nov	-41.99	1.12	0.49	-6.30	0.95	77.99	-132.70	-31.20	-42.00	0.80
Dec	-52.17	1.18	0.53	-5.50	0.94	61.18	-114.40	-21.80	-38.00	0.73

Appendix 4: Original Hargreaves (1985) and Modified Hargreaves (2002) equations for estimating ETo

To overcome the problem with scarce meteorological data the Hargreaves (1985) method presented a simple equation to estimate ETo. This method use only temperature as input from the meteorological data. Hargreaves, 1994 recommend this equation for general use because of its simplicity and the accuracy of estimates (Hargreaves, 1994). The Hargreaves (1985) equation is as follows:

$$ETo = 0.0023 * 0.408 \cdot Ra \cdot (T_{avg} + 17.8) \cdot TD^{0.5} \qquad [\text{mm d}^{-1}] \qquad (1)$$

Where, Ra is the extraterrestrial radiation [$MJm^{-2}d^{-1}$], T_{avg} is the average daily temperature [°C] (Average of T_{max} and T_{min}) and TD is the Temperature difference.

This method very much simpler and less data demanding than the PM equation but major drwback of this method is that it overestimate ETo in humid area (Droogers and Allen, 2002). To overcome this problem, recently, Droogers and Allen (2002) revised the Hargreaves (1985) equation using global Water and Climate Atlas published by International Water Management Institute (IWMI). They introduced an additional term of monthly precipitation in the original Hargreaves (1985) equation. The Modified Hargreave equation according to Droogers and Allen (2002) is as follows:

$$ETo = 0.0023 * 0.408 \cdot Ra \cdot (T_{avg} + 17.8) \cdot (TD - 0.0123P)^{0.5} \quad [\text{mm d}^{-1}] \qquad (2)$$

Where, P is the precipitation in mm per month.

References

Droogers, P., and R.G. Allen. 2002. Estimating reference evapotranspiration under inaccurate data conditions. Irrigation and Drainage Systems 16:33-45. http://www.environmental-center.com/magazine/kluwer/irds/3.pdf

Hargreaves, G.H. 1994. Defining and using reference evapotranspiration. Journal of Irrigation and Drainage Engineering, ASCE 120:1132-1139. http://www.aquarien.com/sptutor/fieldb1/sld006.htm

Walter, I.A., R.G. Allen, R. Elliott, M.E. Jensen, D. Itenfisu, B. Mecham, T.A. Howell, R. Snyder, P. Brown, S. Echings, T. Spofford, M. Hattendorf, R.H. Cuenca, J.L. Wright, and D. Martin. 2000. ASCE's standardized reference evapotranspiration equation National irrigation symposium. Proceedings of the 4th Decennial Symposium, Phoenix, Arizona, USA, November.

Appendix 5: Cloud detection

Out of three investigated images in this study, the images taken on 24 October 2001 and 1 March 2002 contain some clouds contaminated pixel within the study area. These are detected based on the bi-spectral response histograms. The algorithms used to create cloud-masking image is based on the response in the visible and the thermal infrared part of the electromagnetic spectrum. The histogram of visible band (band 3) and the thermal infrared bands (band 6) were examined. Cloudy pixels mainly have high response (reflectivity) in the visible wavelength range and a rather low response in the thermal infrared part.

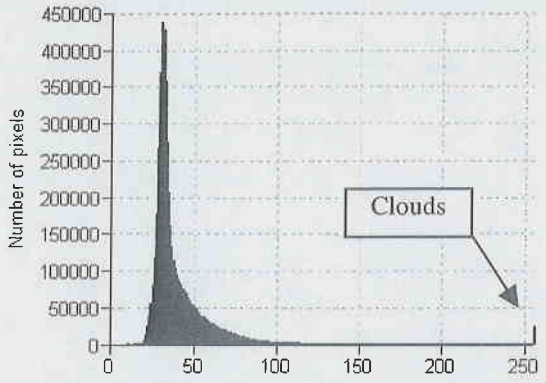

a. Histogram of band 3 – 24 October 2001

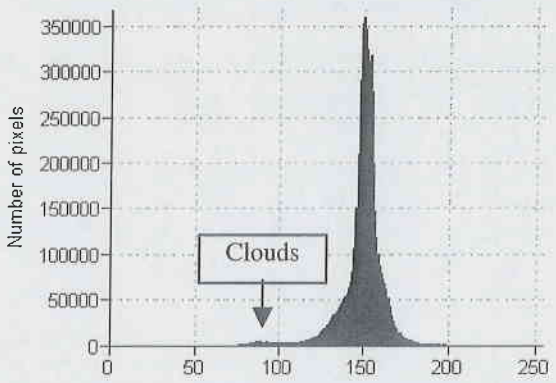

b. Histogram of band 6 – 24 October 2001

By examining band 3 and band 6 the bi-spectral thresholds are fixed for each image. In the histogram of visible spectrum (band 3 was used in this study) the high response (high DN values) corresponds to clouds whereas in the thermal infrared spectrum (Band 6) low response corresponds to cloud. A certain pixel having high response in the visible spectrum and at the same time a low response at the thermal infrared spectrum is supposed to be cloud contaminated. The thresholds have been determined for every individual image by examining their respective histograms. As soon as a pixel scores on both thresholds (i.e. $DN_{vis}>T_{vis}$ and $DN_{th}<T_{th}$)[1], the pixel was assign a value 1, otherwise assigned value 0. This cloud map, 1 indicating clouds and 0 indicating non-clouds used to masked out the cloud contaminated pixels from the corresponding image.

Reference:

Timmermans, W. 1995. Remote sensing evapotranspiration. Ir Thesis. Delft University of Technology, Faculty of Civil Engineering, Department of Hydrology, Delft 1995.

[1] DN_{vis} – DN value in visible spectrum (band 3) DN_{th} – DN value in thermal infrared spectrum (band 6)
T_{vis} – threshold value in band 3 T_{th} –threshold value in band 6

Appendix 6: Monthly water balance components [Mm^3]:

Description	Jan	Feb	Mar	Apr	May	Jun	Jul	Aug	Sep	Oct	Nov	Dec	Year
Rapti Sub-basin (2217 km^2)													
Inflow (Rainfall)	31.0	35.5	62.1	130.8	350.2	713.8	1208.1	1026.3	660.6	168.5	26.6	44.3	4457.8
Inflow (Kulekhani)	9.4	9.7	11.5	12.4	11.5	2.9	2.7	3.7	5.4	7.5	3.4	3.7	83.8
Qin	40.4	45.2	73.6	143.2	361.7	716.7	1210.8	1030.0	666.0	176.0	30.0	48.0	4541.6
Depletion (ETa)	88.7	104.2	166.2	212.8	239.4	252.7	243.8	235.0	206.1	161.8	108.6	88.7	2108.0
Runoff	83.0	74.3	57.9	53.2	129.2	321.2	622.9	739.6	559.4	282.0	92.4	74.3	3089.4
Qout	171.7	178.5	224.1	266.0	368.6	573.9	866.7	974.6	765.5	443.8	201.0	163.0	5197.4
Rest term	-131.3	-133.3	-150.5	-122.8	-6.9	142.8	344.1	55.4	-99.5	-267.8	-171.0	-114.9	-655.8
30% of Monsoon peak outflow						96.4	186.9	221.9	167.8				673.0
Rajaiya (570 km^2)													
Inflow (Rainfall)	8.0	9.1	14.3	33.6	94.6	192.1	322.1	289.6	193.2	49.0	8.6	10.8	1225.0
Qin	8.0	9.1	14.3	33.6	94.6	192.1	322.1	289.6	193.2	49.0	8.6	10.8	1225.0
Depletion (ETa)	20.0	23.4	38.2	48.5	56.6	63.3	61.6	59.0	52.4	39.8	25.8	20.4	509.0
Runoff	23.0	21.3	17.1	16.9	38.8	89.5	168.2	204.2	161.9	83.2	27.8	21.1	873.0
Qout	43.0	44.7	55.3	65.4	95.4	152.8	229.8	263.2	214.3	123.0	53.6	41.5	1382.0
Rest term	-35.0	-35.6	-41.0	-31.8	-0.8	39.3	92.3	26.4	-21.1	-74.0	-45.0	-30.7	-157.5
30% of Monsoon peak outflow						26.9	50.5	61.2	48.6				187.2
Manahari (429 km^2)													
Inflow (Rainfall)	6.0	8.2	15.0	30.1	65.7	127.1	220.2	184.6	115.9	28.8	3.9	9.9	815.4
Inflow (Kulekhani)	9.4	9.7	11.5	12.4	11.5	2.9	2.7	3.7	5.4	7.5	3.4	3.7	83.8
Qin	15.4	17.9	26.5	42.5	77.2	130.0	222.9	188.3	121.3	36.3	7.3	13.6	899.2
Depletion (ETa)	15.9	16.7	24.9	31.0	35.7	40.8	39.9	38.6	35.4	26.5	19.0	16.4	340.8
Runoff	17.3	16.5	16.5	19.2	33.3	64.2	117.3	138.4	103.1	52.1	18.5	15.4	611.8
Qout	33.2	33.2	41.4	50.2	69.0	105.0	157.2	177.0	138.5	78.6	37.5	31.8	952.6
Rest term	-17.8	-15.3	-14.9	-7.7	8.2	25.0	65.7	11.3	-17.2	-42.3	-30.2	-18.2	-53.7
30% of Monsoon peak outflow						19.2	35.2	41.5	30.9				126.8
Lothar (167 km^2)													
Inflow (Rainfall)	2.6	2.5	3.2	8.5	23.1	46.7	88.6	81.8	54.0	13.3	1.4	2.5	328.2
Qin	2.6	2.5	3.2	8.5	23.1	46.7	88.6	81.8	54.0	13.3	1.4	2.5	328.2
Depletion (ETa)	6.5	6.7	9.7	12.0	13.7	15.4	15.1	14.7	13.5	10.8	7.9	6.7	132.7
Runoff	6.1	6.1	5.2	5.4	11.0	23.3	46.0	58.6	47.0	24.1	7.5	5.2	245.6
Qout	12.6	12.8	14.9	17.4	24.7	38.7	61.1	73.3	60.5	35.0	15.5	11.9	378.4
Rest term	-10.0	-10.3	-11.7	-8.9	-1.6	8.0	27.5	8.5	-6.5	-21.7	-14.0	-9.4	-50.1
30% of Monsoon peak outflow						7.0	13.8	17.6	14.1				52.5

Appendix 7: Accuracy matrices of land cover classification

a. Accuracy matrix – 24 October 2001

	Paddy	Water	Maize	Wet Riverbed	Bush	Sand/ Gravel	Clear Paddy Field	Bare	Grass	Built-up area	Forest dense	Forest Sparse	ACCURACY
Paddy	126	0	10	0	0	0	0	3	0	0	0	0	0.91
Water	0	127	0	2	0	0	6	0	0	0	0	0	0.94
Maize	0	0	139	0	0	0	0	0	1	0	0	3	0.97
Wet riverbed	0	12	0	39	0	8	0	0	0	30	0	0	0.44
Bush	12	0	0	0	42	10	0	8	0	0	0	0	0.58
Sand/Gravel	0	0	0	2	0	130	0	0	0	0	0	0	0.98
Clear Paddy Field	4	0	0	0	0	0	89	6	0	0	0	0	0.9
Bare	0	0	0	0	0	0	12	59	0	0	0	0	0.83
Grass	1	0	0	0	5	0	0	5	28	0	0	0	0.72
Built-up	89	0	3	0	0	0	16	5	0	65	0	0	0.37
Forest dense	0	0	7	0	0	0	0	0	0	0	121	28	0.78
Forest sparse	0	0	13	0	0	0	0	0	1	0	0	39	0.74
RELIABILITY	0.54	0.91	0.81	0.91	0.89	0.88	0.72	0.69	0.93	0.68	1	0.56	

Average Accuracy = 76.25 %
Average Reliablity = 79.40 %
Overall Accuracy = 76.88 %

b. Accuracy Matrix - 1 March 2001

	Bare	Built-up area	Bush	Cultivated	Forest	Grass/ grazing	Sand/ Gravel	Water	ACCURACY
Bare	44	2	15	17	1	0	0	0	0.56
Built-up area	7	26	0	0	0	0	0	0	0.79
Bush	0	0	1	0	2	0	0	0	0.33
Cultivated	0	1	17	121	0	4	0	0	0.85
Forest	0	0	11	0	104	0	0	0	0.9
Grass/grazing	0	0	0	1	0	5	0	0	0.83
Sand/Gravel	0	2	0	0	0	0	75	0	0.97
Water	0	0	0	0	0	0	0	60	1
RELIABILITY	0.86	0.84	0.02	0.87	0.97	0.56	1	1	

Average Accuracy = 77.95 %
Average Reliability = 76.53 %
Overall Accuracy = 84.50 %

Appendix 8: Depletions

a. Evaporative depletion by catchment [Mm^3]

1. Rapti sub-basin

	Area		ETa	
Landuse	[km^2]	%	[mm/year]	Mm^3
Forest	1407.7	63.5	992	1396.4
Cultivated	632.6	28.5	945	597.8
Grass_grazing	7.3	0.3	945	6.9
Bush	44.7	2.0	1042	46.6
Sand_Gravel	42.5	1.9	733	31.1
Bare	43.6	2.0	519	22.6
Builtup	1.7	0.1	944	1.6
Water	1.5	0.1	1205	1.8
Unclassified	35.1	1.6	80	2.8
Sum	2217	100		2107.6

2. Rajaiya

	Area		ETa	
Landuse	[km^2]	%	[mm/year]	Mm^3
Forest	298.7	52.4	930	277.8
Cultivated	236.2	41.4	893	210.9
Grass_grazing	0.0	0.0	831	0.0
Bush	2.7	0.5	910	2.5
Sand_Gravel	12.1	2.1	731	8.9
Bare	11.7	2.0	560	6.5
Builtup	0.6	0.1	935	0.5
Water	0.2	0.0	1180	0.2
Unclassified	8.0	1.4	90	0.7
Sum	570	100		508.1

3. Manahari

	Area		ETa	
Landuse	[km^2]	%	[mm/year]	Mm^3
Forest	317.4	73.9	828	262.6
Cultivated	78.8	18.4	845	66.6
Grass_grazing				
Bush	1.9	0.5	740	1.4
Sand_Gravel				
Bare	16.4	3.8	482	7.9
Builtup				
Water				
Unclassified	14.8	3.4	77	1.1
Sum	429	100		339.7

4. Lothar

	Area		ETa	
Landuse	[km^2]	%	[mm/year]	Mm^3
Forest	122.2	73.3	836.37	102.2
Cultivated	31.1	18.6	885.35	27.5
Grass_grazing				
Bush	1.0	0.6	818.21	0.8
Sand_Gravel				
Bare	5.3	3.2	318.79	1.7
Builtup				
Water				
Unclassified	7.2	4.3	78.5	0.6
Sum	167	100		132.7

b. Depletion by Domestic, Animal and Industrial uses.

1. Domestic Water Consumption in East Rapti Basin

	Makwanpur	Chitawan	Water used	Total water consumed	Depletion Fraction	Process Consumption
			(l/head/day)	[Mm^3/year]		[Mm^3/year]
Total no of VDC	23	31				
Total Population (VDC)	185824	314293	45	8.21	0.5	4.11
No of Minucipality	1	2				
Total Population (Muni.)	68482	127114	60	4.28	0.5	2.14
Total	254306	441407		12.50		**6.25**

Note: The water use rate and depleted fraction were taken from IWMI 2000.

2. Industrial Water Use in East Rapti basin (IWMI, 2000)

S.N.	Category	No. of Industries	Average Consumption (l)	Total Consumption (l)	Fraction Depleted	Process Depletion (Mm^3)
1	Brewery	2	69,738,224	139,476,448	0.15	0.02
2	Bottlers Nepal	1	146000000	146,000,000	0.25	0.04
3	Cement & Lime	3	577,064	1,731,192	0.16	0.00
4	Concrete & Hume Pipe	6	2,440,775	14,644,650	0.25	0.00
5	Dairy	1	23,018,000	23,018,000	0.02	0.00
6	Feed Industry	11	280,000	3,080,000	0.25	0.00
7	Food Industry	8	11,041,268	88,330,143	0.5	0.04
8	Leader & Bone	2	16,798,455	33,596,909	0.5	0.02
9	Metal Base Industries	7	264,477	1,851,336	0.1	0.00
10	Paints and Chemicals	7	9,569,273	66,984,909	0.25	0.02
11	Plastic	11	988,572	10,874,292	0.25	0.00
12	Textile & Synthetics	4	8,710,569	34,842,277	0.2	0.01
13	Tobacco	1	2,360,616	2,360,616	0.05	0.00
14	Vegetable Gee Industry	1	34,598,000	34,598,000	0.5	0.02
15	Wood Works & Furniture	10	1,157,039	11,570,387	0.5	0.01
16	Others	55	1,402,489	77,136,907	0.1	0.01
	Total	130		690096064.5		**0.18**

3. Water depleted by Animals in the East Rapti river basin (IWMI 2000)

Type of Animal	Total numbers	Water requirement lit/day/no	Yearly water requirement lit.	Depletion fraction	Water use [M. m^3]
Cattle	111220	60	2435717160	0.5	1.22
Buffalo	99770	90	3277436206	0.5	1.64
Sheep Goat and Pigs	122655	5.5	246229912.5	0.5	0.12
Fowl & Duck	155559	0.5	28389517.5	0.5	0.01
Total water use (Mm^3) =					**2.99**

807.